Republic of Iraq

Ministry of Higher Education and Scientific Research

University of Babylon

College of science for women

Chemistry Department

Role of Synthesized Alginate/Bentonite Impregnated TiO_2 Beads Nanocomposite: as a Recyclable Adsorbent Surface for Removal of Pollutants and Biological Activity

A Thesis Submitted
to the Council of the College of Science for Women, University of Babylon as a Partial Fulfillment of the Requirements for the Degree of Master of Chemistry

By

Zainab Dhyaa Mohammed Saeid Al-hattab

B.Sc. Chemistry, College of Science, Babylon University, 1999-2000

Supervised by

Asst. Prof. Dr. Aseel Mushtaq Aljeboree

2022 A.D **1444A.H**

Supervisor Certification

I certify that this thesis entitled

Role of Synthesized Alginate/Bentonite Impregnated TiO2 Beads Nanocomposite: as a Recyclable Adsorbent Surface for Removal of Pollutants and Biological Activity .

Was prepared under my supervision at the University of Babylon / College of Science for Women as a partial Requirement for the degree of Master in Chemistry Science .

Signature
Dr. Aseel Mushtaq Kadum
Scientific Order: Asst. Prof.
Address:
University of Babylon / College of
Science for Women
Date: / /2022

Recommendation of Head of Chemistry Department

According to the available recommendation, I forward this thesis for Discussion.

Signature of Chemistry Department
Dr/ Hazim Yahya Mohammed
Scientific order: Asst. Prof.
Address: Head of Chemistry Department
University of Babylon / College of
Science for Women
Date: / /2022

Dedicationts

To whom who honored me carry his name is my father, may god have mercy on him.

To the light of my eyes and my way, the joy of life my mother, may god have on her, whose prays and words the companion of brilliance and excellence.

To the supporters : my husband , my sisters and my loved ones, my son and daughter

to everyone one who taught me a letter and supported me even with smile you have this humble effort .

Researcher

Acknowledgments

Praise be to Allah, Lord of the worlds. Praise be to Allah, who helped me and gave me the strength, patience, and endurance to complete this thesis.

I would like to thank and appreciate my supervisor Assistant Professor ***Dr. Aseel Mushtaq Aljeboree*** , for her suggestions and support, definitely without her continuous advice and valuable guidance, the research work could not be completed.

I also would like to extend my sincere thanks and appreciation to professor **Dr. Ayad Alkaim** for his continuous support and encouragement.

I also express my thanks and gratitude to the deanship of the college of science for the women's department of chemistry, and all other lecturers who helped me and gave their valuable comments to make my thesis in good form.

Finally, I would like to express my sincere thanks and appreciation to the members of my family, especially, my dear father who did not skimp on me and encouraged me until I reached this stage.

Summary

In this work, an eco-friendly, simple, stable new adsorbent adsorption properties based on clay and biopolymer was successfully designed via a combination of a simple cross-linking way, a new clay-based composite beads adsorbent made by incorporating clay into sodium alginate (Bentonite clay/alginate beads) followed by impregnation TiO_2NPs and ($CaCl_2.2H_2O$) to give (sodium alginate - Bentonite - TiO_2NPs) (SA-Bn-TiO_2 NPs) hydrogel to removal of three pollutants (Congo red CR dye , Amoxilluin AMX drug ,and 4-chloro phenol CPH) . TiO_2 nanoparticles were prepared by thermal hydrolysis (hydrothermal method) by using titanium(IV) bis (ammoniumlactate) dihydroxide (TALH), and ammonium hydroxide (NH_4OH) . The morphology and structure of the TiO_2 NPs, Bentonite clay, SA-Bn and SA-Bn-TiO_2NPs hydrogel were investigated utilizing Ultraviolet-Visible Spectroscopy (UV–Vis), Fourier Transform Infrared (FT-IR) , Thermo gravimetric analysis (TGA) , Field Emission Scanning Electron Microscopy (FE-SEM) ,Transmission Electron Microscopy (TEM) , Energy Dispersive X-Ray (EDX) and X-ray Diffraction Spectroscopy (XRD).

The practical experiments included calculation of the maximum wavelength and study optimum condition of the effect of adsorption parameters are :effect of contact time, effect of adsorbent dose, effect of pH solution, effect of temperature solution, adsorbent regeneration experiments (Desorption), comparative adsorption between different surfaces to removal three pollutant, removal of laboratory sample aqueous Pollutants , amoxilluin (AMX) drug Loading , In vitro drug release , biological activity bacterial test and treating Mice Wounds Using a Surface Prepared from SA-Bn-TiO_2 NPs hydrogel .

The results of the adsorption study show that percentage of removal increases with the increase of the weight of the surfaces; and contact time. The optimized value of agitation time is 1 hr. after which the adsorption becomes constant. The best results of the percentage of removal have been attained in pH 6.6, but in pH 4 there is a very small amount of removal; The Freundlich and Langmuir models are also introduced. It has been found that all results follow the Freundlich model in the presence of Three pollutant .

Comparative between (SA-Bn-TiO_2 NPs, SA-Bn, and TiO_2 NPs) surfaces as adsorbents. The best results of the percentage of removal (E%) of three pollutant (Congo red CR dye , Amoxilluin AMX drug and 4chlorophenol CPH) arrange in order increasing (SA-Bn-TiO_2 NPs > SA-Bn > TiO_2 NPs), The good results of the percentage of removal (E%) of SA-Bn-TiO_2 NPs , 92,451%, and 87.56% and 82.56 for CR, AMX and CPH at the same order .

Kinetics adsorption models of three pollutant on SA-Bn-TiO_2 NPs was studied by using three kinetic models. The classification of the kinetic models according to the simulation of the adsorption study is pseudo first order< Psuedo-second order > Chemisorption. and calculated thermodynamic parameter suggested that a endothermic and spontaneous process .

Recyclability and desorption studies indicated the best recycling performance of the prepared composite. Based on the results, the prepared SA-Bn-TiO_2NPs can be useful as a promising, eco-friendly , cost-effective, and efficient material for dyes decontamination .Studies was carry out utilizing several desorption agents at various concentration (0.01, 0.05, 0.1 N) include H_2SO_4, NaOH, H_3PO_4 , HCl , HNO_3, ethanol

, acetone and water. The SA-Bn-TiO_2NPs was regeneration with 100% by using water .

The release of amoxicillin (AMX) drug was studied in conditions similar to the human body in terms of acidity and temperature. drug release of 62% and 42% , in the first 1 hr was observed for AMX drug . The cumulative release of AMX in 3 h was 68%, 44% from pH=7.5 and pH 1.2 at the same order.

The results showed that the surface SA-Bn-TiO_2 NPs and SA-Bn have antibacterial activity against the Gram-negative bacteria compared to the gram-positive bacteria with an inhibition area (20 mm),. More than TiO_2NPs and clay where the results showed that it has very little antibacterial activity against two types of bacteria .

It was studied, treating rat wounds with a surface prepared from SA-Bn-TiO_2NPs, which was observed within two to seven days, according to the results, there is complete healing of the mice and the return of the skin to its natural color. This is due to the fact that SA-Bn-TiO_2 NPs have high effective efficiency in treating and healing mice. It is considered environmentally friendly, non-toxic, and also considered anti-inflammatory. In addition, there is biocompatibility with mammalian cells.

List of Contents

List of Tables

List of Figures

List of Abbreviations

Shorten	Full name
T	Absolute temperature
Abs	Absorbance
pH	Acidic function
q_e	Amount of adsorbate per unit weight of adsorbent at equilibrium
B.D.H	British Drug Houses
BET	Brunauer-Emmett-Teller
ΔH	Change of enthalpy
ΔS	Change of entropy
Conc.	Concentration
R^2	Correlation coefficient
K_e	Distribution coefficients
EDX	Energy Dispersive X-Ray
K_{eq}	Equilibrium constant
C_e	Equilibrium dye concentration
FE-SEM	Field emission scanning electron microscopy
FT-IR	Fourier Transform Infrared
K_f	Freundlich constant
ΔG	Gibbs free energy
Q	Heat of adsorption
C_o	Initial Concentration
k_L	Langmuir constant
M	Mass of adsorbent
Q_m	Maximum adsorbed
X_m	Maximum adsorption

Shorten	Full name
q_m	Maximum Adsorption Capacity
λ_{max}	Maximum wavelength
NP	Nanoparticles
PEI	Poly Ethylene Imine
E%	Removal percent
q_t	The amount of adsorbent at a given time
k_1	The pseudo-first-order rate constant
K_2	The pseudo-second-order rate constant
TGA	Thermal gravimetric analysis
T	Time
TEM	Transmission electron microscopy
UV–Vis	Ultraviolet-Visible Spectroscopy
R	Universal gas constant
XRD	X-ray diffraction spectroscopy

Chapter One

Introduction

1- Introduction

1-1 General Introduction

Pollution is the most widespread major problem that has caused a defect in the ecosystem, as well as a dangerous problem that threatens human life. Therefore, it is difficult to obtain clean water in the existence the ratio of water pollution that affects the human system is increased[1, 2] .The most hazardous compounds are heavy metals, oils, drug, phenol compound and dyes. Especially، Organic dyes are produced in many different local industries for example textile ,paper, plastic, leather, food, cosmetic, etc.[3-6].Textile dyes have a strong color even in extremely low concentrations. These Pollutions are non degradable, bioaccumulation in living organisms and stable toward light, biological and chemical treatments. Additionally , they display high biotoxicity and potential mutagenic and carcinogenic effects. The dye pollutions in water incline to preclude light penetration and therefore, affect photosynthesis considerably.[7] .Numerous dyes are difficult to remove from contaminated water solutions due to complex structure and synthesis. These Pollutions are not effectively removed by using traditional techniques. Numerous methods can be used to remove these Pollutions with high efficiency such as ion exchange, coagulation /flocculation, adsorption, chemical oxidation, ozone treatment, membrane filtration , sono-chemical and electrochemical methods, photo catalysis economical innovation because of its high effectiveness, naivety of design and simplicity of operation [8].

1-2 Dyes

Dyes is the most obvious indicator of water contamination. The release of colored wastewater of the streams not only moves their nature aesthetic but to interferes with the show of sunlight into streams and thus decreases photosynthetic action. Wastes from the industrial dye industry, pulp textile industry, and paper manufacturing are greatly colored . Synthetic dyes are extensively utilized in different textile dyes branches manufacturing, photography color, cosmetics, drug، plastic [9]. The find of even so little concentration of dyes in water decreases light penetration by the water surface, precluding photosynthesis of the flora aqueous. Various dyes, teratogenic, carcinogenic, mutagenic, and too toxic to beings human, bacteria, and types of fish. Therefore, the removal from water wastes becomes ecologically important[10] .

Generally, the dyes used in the textile industry are basic dyes, acid dyes, reactive dyes, direct dyes, azo dyes, mordant dyes, vat dyes, disperse dyes, and sulfur dyes, where azo derivatives dyes are the major class of dyes that are used in the industry today[11].

1-2-1 Congo Red

Congo red dye (CR)) is disodium;4-amino-3-[[4-[4-[(1-amino-4 sulfonatonaphthalen-2 yl)diazenyl]phenyl]phenyl]diazenyl]naphthalene-1-sulfonate (Figure 1-1), one of the well-known and used diazo dyes that contains two azo acids (-N=N-) and is a color carrier in its molecular structure. characterized by molecular stability, extreme toxicity and resistance to biodegradation. Congo dye is anionic in nature and its basis is benzidine. produced by some industries, including textiles, dyes, papers, printing, and others. Congo red dye toxic to many living organisms and a carcinogen, as it has a complex aromatic structure [12].

Adsorption techniques are used to remove (CR) from polluted water. Congo red dye offers wide uses in many industries such as textiles, papers, rubber, plastics and other industries. Congo red dye is one of the first industrial dyes that has the ability to dye cotton directly, and it is a sensitive dye .The change in the pH value ranges from (pH 4-11), as color is stable in the pH range and changes to blue in the acidic medium less than (pH < 4), and characterized by its physical-chemical, optical and thermal stability[١٣] . The Table(1-1) shows Physicochemical properties of the Congo red .

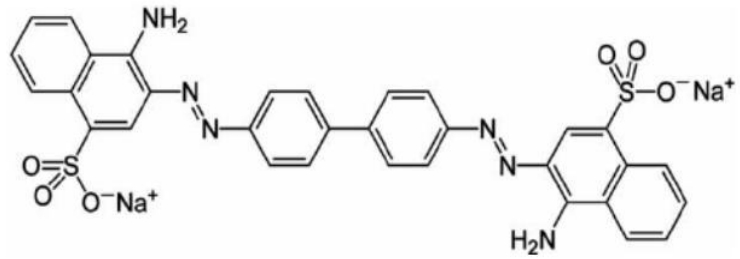

Figure (1-1): Chemical structure Congo red dye (CR) .

Table(1-1): Physicochemical properties of Congo red dye [12]..

Physicochemical properties	Congo red
Molecular formula	$C_{32}H_{22}N_6Na_2O6S_2$
Type of dye	Anionic
Molecular Weight	696.66 g/mol
Maximum wavelength (nm)	530
Color	Red
IUPAC	disodium;4-amino-3-[[4-[4-[(1-amino-4 sulfonatonaphthalen-2 yl)diazenyl]phenyl]phenyl]diazenyl]naphthalene-1-sulfonate

1-3 Pharmaceuticals compound

Pharmaceuticals products that are used for human health promotion, animal care and agriculture applications . Antibiotics are commonly used drugs for preventing or treat microbial infections [14]. They are released into water through wastewater treatment and pharmaceuticals plants [15]. Pharmaceuticals are represented as bio-accumulative contaminant compounds in the environment of aquatic or terrestrial ecosystems[16] . Oxidation processes are coasty and difficult for complete elimination of antibiotics. Adsorption as a physical technique, is the most suitable and efficient treatment option for removing Pharmaceuticals for its high efficiency, simplicity and economical[17] .

1-3-1 Amoxicillin

Amoxicillin (AMX) is a semi-synthetic β-lactam antibiotic belonging to the group of penicillins (Figure 1-2) consists of d-4-hydroxyphenylglycine side chain linked to 6-aminopenicillanic acid (6-APA) moiety. This molecule is relatively unstable both in aqueous solution and storage. Amoxicillin (AMX) have been widely used in human and veterinary medicine for the treatment of bacterial infections caused by Gram-negative and Gram-positive organisms[18]. However, AMX can cause some side-effects on human beings as other β-lactam antibiotics , various preparations of this drug either alone or combined with other ingredients are commercially available [19]. It can cause serious pollution problems.Some selected physicochemical properties of amoxicillin are shown in Table (1-2) .

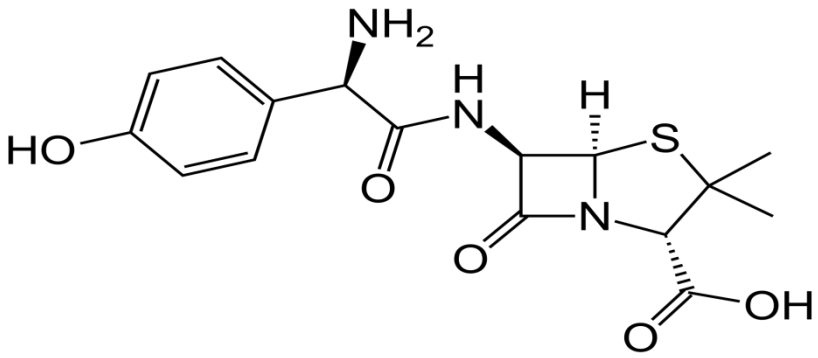

Figure (1-2): Chemical structure Amoxicillin (AMX) .

Table(1-2): Physicochemical properties of Amoxicillin [20]

Physicochemical properties	**Amoxicillin**
Molecular Formula	C_{16} H_{19} N_3 O_5S
Molecular weight(g/mole)	365.4
Solubility in water (mg/L)	3430
Melting point	194 °C
Boiling point	743.2°C at760 mm Hg
Acid dissociation constant (pKa)	2.4(carboxyl), 7.4(amine) and 9.6(phenol)

1-4 Phenolic compounds

Phenolic compounds are a group of small molecules characterized by their structures having an aromatic ring with one or more hydroxyl groups Based on their chemical structures, and acting as antioxidants. Phenolic compounds are highly toxic pollutants. They are widely used in tanning, dye, chemical, cosmetic and pharmaceutical industries [21, 22]. They come from different sources, like industrial wastewater, gasworks, paper mill, chemical plants, coking factory, pharmaceutical industry and solid castoff of coal tar[23] .

1-4-1 Chlorophenol

4-Chlorophenol and Other name p-Chlorophenol is an organic compound and one of three monochlorophenol isomers. Chemical formula ClC_6H_4OH, Molar mass128.56 $g.mol^{-1}$, colorless or white solid that melts easily and exhibits significant solubility in water as shown in Figure (1-3) . Chlorophenols are synthetic organic compounds that are used on a large scales in chemical industry including the production of pharmaceuticals, pesticides and dyes. They can find their way to the environment since they were detected at high concentrations in wastewater treatment plant (WWTP) and discharged effluents close to industrial activities[21] . Due to the toxicity and carcinogenic properties, the long term exposure to chlorophenols at high concentration levels was found to causeliver, kidney and neurological defects, and therefore, their removal from water sources becomes environmentally warranted. There are different physical and chemical technologies currently used for removal phenol and its derivative compounds from their aqueous solution like oxidation, adsorption and ion exchange [24] . Some selected physicochemical properties of 4-Chlorophenol are shown in Table (1-3) .

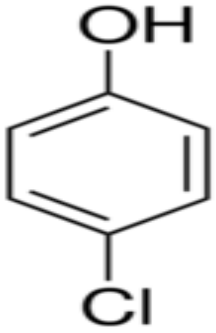

Figure (1-3): Chemical structure 4- Clorophenol.

Table(1-3): Physicochemical properties of 4-Chlorophenol[21]

Physicochemical properties	4-Chlorophenol
Molecular Formula	ClC_6H_4OH
Molecular weight(g/mole)	128.56
Solubility in water (mg/L)	27.1
Melting point	42.4 °C
Boiling point	217.2°C at 760 mm Hg

1-5 Clay minerals classification

Clay are natural adsorbent classified based on their difference in layered structure. The available classes of clay materials include smectites (montmorillonite, saponite), mica (illite), kaolinite, serpentine, pylophyllite (talc), vermiculite and sepiolite. The process by which adsorption takes place is as a result of net negative charge on the structure of minerals, and it's this negative charge that gives the clay mineral the capability to adsorb positively charged species[25] . Most of Their sorption properties depends their high surface area and high porosity. As mentioned earlier, naturally occurring adsorbents have received much concerns for their low cost in removing pollutants from contaminated water like natural clays that have many physical characteristics mainly, plasticity, hardness, cohesion in addition it contains silica, alumina, iron, calcium, and magnesium oxides and can be chemically modified to improve adsorption capacity. Figure(1-4) shows Grim's classification and lattice structure of clay minerals [26, 27].

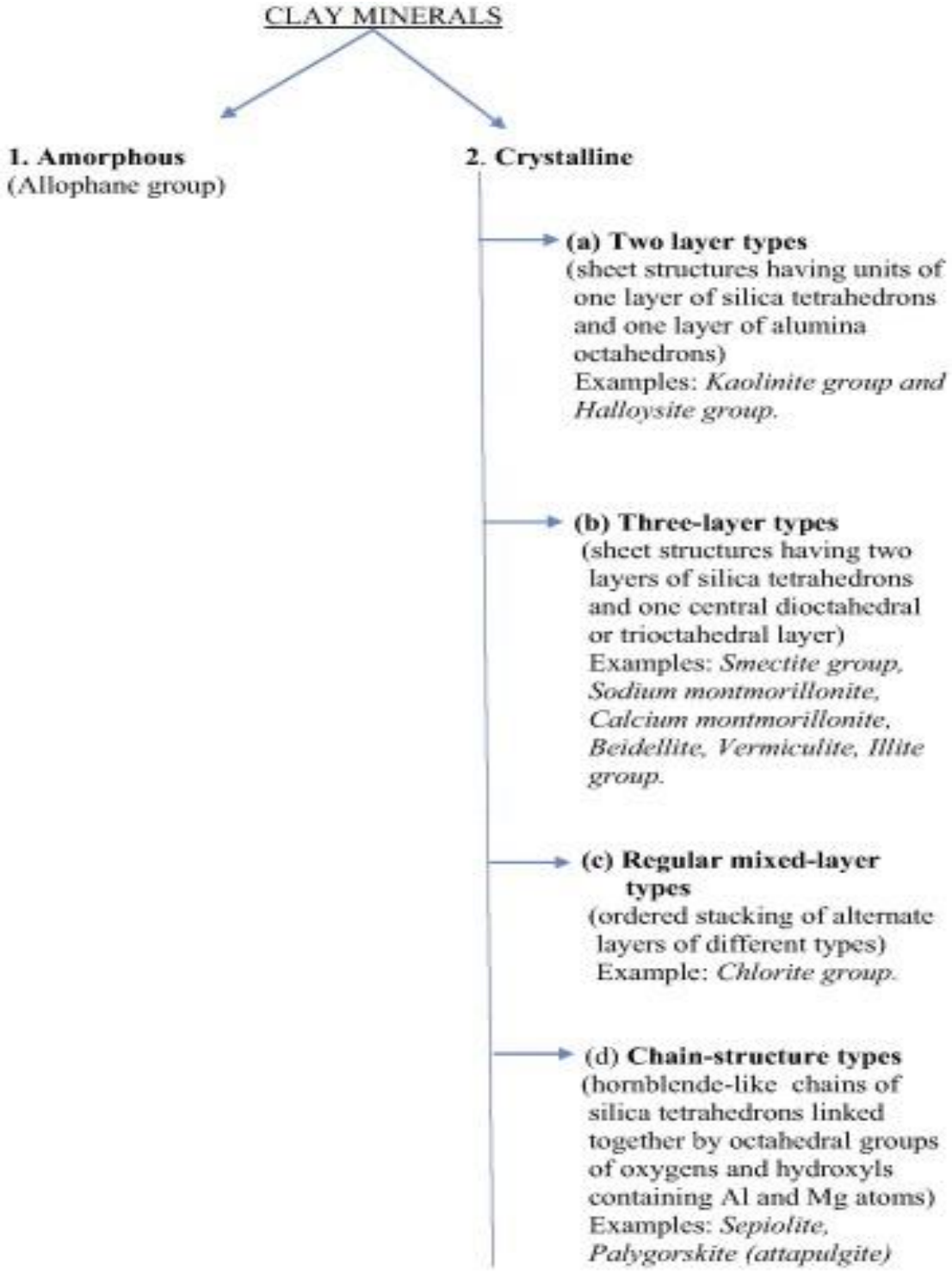

Figure (1-4): Clay minerals classification [٢٦]

1-5-1 Bentonite

Bentonite clay consists of two silica tetrahedral sheets and one central alumina octahedral sheet. The structural formula of Bentonite is defined as $Rx(H_2O)_4((Al_2{-}x,Mgx)_2[(Si,Al)_4O_{10}](OH)_2)$ that R is the exchangeable cations of alkali and alkali-earth metals between the layers . It has a cation-exchange capacity of about 70 to 110 meq/100 g of clay bentonite, [28] which has layered structure with cations such as Na^+ or Ca^{+2} shows promising and highly suitable application for the loading of an extensive range of biomolecules .After etching, bentonite exhibited highly improved characteristics, including those relation to cation exchange capacity and surface area Furthermore, bentonite, as a natural mineral, is eco-friendly, inexpensive, and accessible[29, 30] .

1-6 Hydrogel

Hydrogels are hydrophilic polymer chains that are cross linked to form gel structures that swell in aqueous solution and trap fluids for a long period without dissolving. Hydrogels may contain carboxylic, amine, imide, hydroxyl and sulfonyl groups in their 3D structure that are responsible for the hydrophilicity and swelling capacity[31]. Depending on the nature of the hydrogel, it can be classified based on various properties. can be based on whether they are synthetic (involves the use of synthetic monomers), natural (involves using biopoly mers) or a combination of synthetic and natural monomers resulting in a hybrid hydrogel [32].

1-6-1 Sodium Alginate

Sodium alginate (SA, Figure 1-5) is made up of poly-β-1, 4-D-mannuronic acid and α-1, 4-L-guluronic acid. The structure consists of carboxylic groups and hydroxyl groups, which can react with metal ions or crosslinking agents to form hydrogels. Alginate can be extracted from its salt forms by ion-exchange methods. Because of the presence of divalent ions, monovalent, water-soluble salts of alginates can transform into water-insoluble salts [33]. The COO and -OH functional groups on the alginate backbone will allow adsorption of cationic dye pollutants. However, sodium alginate just like other polysaccharides suffers from a lack of stability[34]. To enhance the stability of SA and its adsorption capacity, the biopolymer may be cross-linked with synthetic polymers into forming a hydrogel. This will allow their use as adsorbents without them dissolving in the adsorbate solution. The major disadvantage of polysaccharides as adsorbents is that they dissolve in water and have low mechanical stability. To resolve this problem, polysaccharides are cross-linked to form hydrogels, which do not dissolve in water [35].The most common method to prepare hydrogels from an aqueous alginate solution is to combine the solution with ionic cross-linking agents, such as divalent cations (i.e., Ca^{+2}).Calcium chloride ($CaCl_2$) is one of the most frequently used agents to ionic ally cross-link alginate [36].

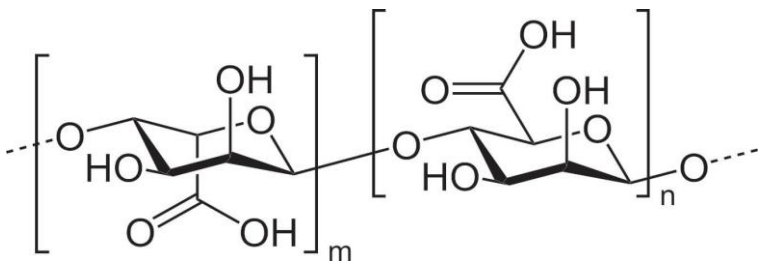

Figure (1-5): The chemical Structure of sodium alginate [36].

1-7 Titanium dioxide–based hydrogels .

Titanium dioxide (TiO_2) is a naturally occurring oxide of titanium. It exists in three crystalline phases, namely, brookite, anatase and rutile. The rutile phase is thermodynamically stable compared to the anatase and brookite phases, which are metastable. The advantages of TiO_2 are that it effective, contains electrochemical properties and is safe to produce .In addition, TiO_2 possesses antimicrobial and UV-protection properties. Applications of titanium dioxide include the use of a photocatalyst for water-dye degradation, and pharmaceuticals [37]. where adsorbent hydrogel incorporated with TiO_2 nanoparticles was used for removing pollutant from water. The group reported that incorporating TiO_2 nanoparticles improved the recovery of the hydrogel from the aqueous solution after the removal of pollutant . also , hydrogel was modified with TiO_2 for antimicrobial activity, Therefore, looking at these properties, the TiO_2 would be ideal for preparing hydrogels for adsorbing pollutant [38-40] .

1-8 Hydrothermal Process for Synthesis of Nanomaterials

This method involves the use of water as a catalyst and sometimes as a component of the formation of solids. This method is performed at high temperature (> 100 ° C) and high pressure (>1 atm). The synthesis of nanomaterials using this method depends on several variables such as temperature, process time, pressure, solvent type, and pH . Hydrothermal synthesis can be clarified as a method of synthesis of single crystals that depends on the solubility of metal in spicy water at high pressure [41].Where the process of growth of the crystals in a steel pressure vessel called an autoclave ,in which a nutrient is provided along with water. The

method is also particularly good for the growth of large good-quality crystals while keeping control over their composition [42] as shown in Figure (1-6).

Figure (1-6): Autoclave commonly used for hydrothermal synthesis .

1-9 Adsorption

The term adsorption points out to a process wherein a substance is concentrated ate solid surface from its liquid or gaseous ocean. It is a process whereby the mass transfers to the surface of the solids from its aqueous solution by attracting dissolved material to its surface [43].Adsorption is essentially a phenomenon that occurs on the surfaces and consists of two elements: the material that attaches to the hard surface, known as "adsorbent", and the compound that occurs on its surface adsorption, known as "adsorbate" .The adsorption can be classified into two categories based on the nature of the bonds between the molecules of the adsorbent and the surface[44] as shown in Table (1-4) .

Table 1-4: Properties of physisorption and chemisorptions [45].

Physisorption	Chemisorptions
Multilayer adsorption	Monolayer adsorption
Low degree of specificity	Depends on the reactivity of adsorbent and adsorbate substance
Desorption is possible	Desorption is impossible
Always exothermic (adsorb molecules keeps their identity) less than 40 kJ/mole	Exothermic, or endothermic chemical bonds forms (the energy involved can reach several hundreds of kJ/mole)
The system generally reaches thermodynamics equilibrium rapidly	Activation energy is involved and at low temperatures, the system may not reach equilibrium.

1-9-1 Factors Affecting on Adsorption Process

1-9-1-1 Effect of Initial Concentration

Adsorption capacity of dyes removal from aqueous solutions depends on the primary dye concentration. The effect of primary dye concentration depends on the direct relationship between dye concentration and active sites on the surface of the adsorbent material. In addition, we note the reduced efficiency of the dyes removal with increased primary dye concentration owing to the saturation of sites available on the surface of the adsorbent material [46].

1-9-1-2 Effect of Adsorbent mass

Adsorbent dosage is a very important factor for determining the capacity of the adsorbent material using different amounts of surface after all the conditions of the equilibrium time and the primary dye concentration are established. Where we note that, the percentage of removal of dyes increase with the increase adsorbent dosage owing to the increase of effective sites on the adsorbent surface [44].

1-9-1-3 Effect of Temperature

The effect of temperature on the adsorption process, we can determine whether the reaction is an endothermic or an exothermic reaction. adsorption efficiency increases with increasing temperature, the reaction is an endothermic reaction owing to increased mobility of dye molecules with increased adsorption sites active on adsorbent surfaces. Either when low adsorption efficiency with increasing temperature refers to an exothermic reaction due to the low adsorption forces between the dye molecules and the available sites because of the low amount of adsorption[47].

1-9-1-4 Effect of Solution pH

The pH factor is the most important factors in the process of adsorption, especially adsorption of dyes. Where the change of pH leads to a change in the degree of ionization of the dyes, the properties of the adsorbent surface and the speed of adsorption. pH of the aqueous solution can control the amount of electrostatic charges obtained from the ionized dye molecules [48].

1-9-1-5 Ionic Strength:

The ionic strength of the solution is one of the factors that control both electrostatic and non-electrostatic interactions between the adsorbate and the adsorbent surface. The solubility of ionic salts is affected in the adsorption process because when the ionic salts having solubility are better than the adsorbent substances caused an increase in adsorption, or decrease because the ionic salts caused interference on the surface adsorption [49].

1-10 Adsorption Isotherms:

Adsorption isotherms the amount that is adsorbed on the surface in terms of pressure (if gas) or concentration (if liquid) at a constant temperature[50]. The most important of these isotherms in the application are:

1-10-1 Langmuir Isotherm:

Assumes that the molecules are adsorbed on a fixed number of adsorption sites on the surface of the adsorbate material. These sites are equally energy-efficient, and each site can be occupied by only one molecule. These particles are not interfering with each other or with other molecules in the solutions. Thus, one layer of adsorbed particles will form on the surface of the adsorbate material. Langmuir isotherm can be expressed mathematically as follows[51]:

$$q_e = \frac{q_m K_a C_e}{1 + K_a C_e} \qquad (1\text{-}1)$$

Where Ce the residual concentration, qe ,qm is the adsorption capacity at equilibrium and the maximum adsorption capacity respectively, Ka Langmuir constant. The linear form of the equation of Langmuir isotherm is according to the following equation [52]:

$$\frac{C_e}{q_e} = \frac{C_e}{q_m} + \frac{1}{K_a q_m} \qquad (1\text{-}2)$$

1-10-2 Freundlich Isotherm:

The Freundlich equation is one of the most important used isotherms in the case of adsorption of solution. This model assumes that the surface of the adsorbate material is heterogeneous because of the different energy levels for adsorption sites, and adsorption does not reach saturation. The mathematical relationship of the Freundlich isotherm can be expressed as follows[53]:

$$q_e = K_f C_e^{\frac{1}{n}} \qquad (1\text{-}3)$$

K_f is a Freundlich constant and their values depend on the nature of the absorbent material, the surface, and the temperature. The linear form of Freundlich isotherm can be expressed as follows:

$$\log q_e = \log k_f + \frac{1}{n} \log C_e \qquad (1\text{-}4)$$

1-11 Release of Drug

The entrapped drug in hydrogels releases only when the water penetrates into the polymer networks and dissolves the drug. A drug solubilization is followed by diffusion through a network of fluid-filled pores and channels. In such cases, the control over the internal pore size, distribution, and connectivity would be useful for fine tuning formulation conditions and drug release kinetics [54].

The release kinetics often deviates from the expected one and is strongly influenced by a variety of parameters. These parameters include device

geometry, the physicochemical properties of the polymer matrix (molecular weight, swelling, crystallinity, and glass transition temperature), initial drug concentration profile, drug– matrix interactions, and osmotic pressure associated with drug solubility and its loading content [55] . The release of drug is closely related to the swelling characteristics of the hydrogels, which in turn, is a, key function of chemical architecture of the hydrogels as shown in Figure (1-7) .

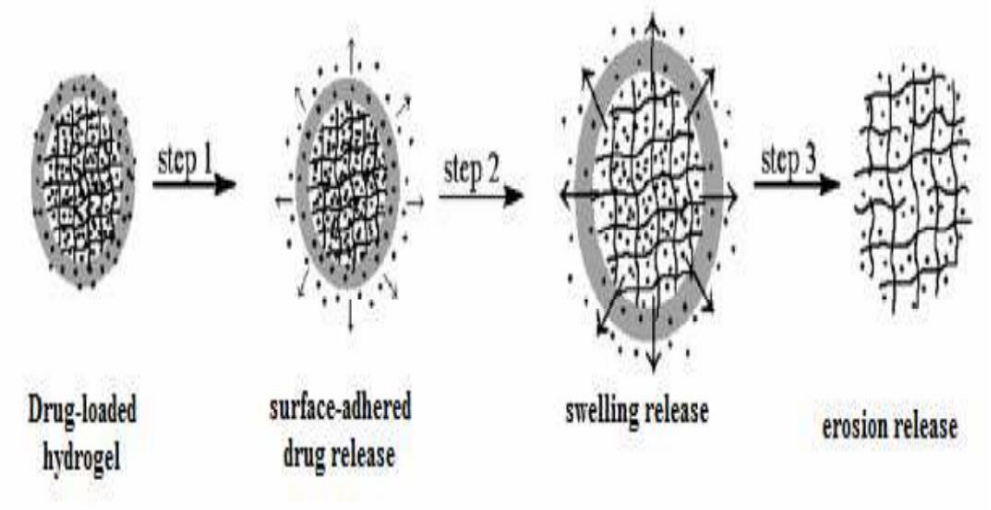

Figure(1-7): Drug release process for hydrogels [55].

1-12 Microorganisms

Microorganisms, the category of microbes includes a large group of living organisms including bacteria, fungi and algae. In this study, wear used two types of bacteria, like bacteria Gram-positive and bacteria Gram-negative .

1-**12-1** ***Escherichia coli***

Escherichia coli is a Gram-negative, facultative anaerobic, rod-shaped, coli form bacterium of the genus Escherichia that is commonly found in the environment, foods, and intestines of people and animals . Most E. coli strains are harmless, but some serotypes (EPEC, ETEC etc.) can cause serious food poisoning in their hosts, and are occasionally responsible for food contamination. Although most strains of E. coli are harmless, others can make you sick. Some kinds of E. coli can cause diarrhea, while others cause urinary tract infections, respiratory illness and pneumonia, and other illnesses [56].

1-12-2- ***Klebsiella pneumonia***

Klebsiella pneumonia is a Gram-negative, non-motile, encapsulated, lactose-fermenting, facultatively anaerobic, rod-shaped bacterium. It appears as a mucoid lactose fermenter on MacConkey agar. Klebsiella species are found everywhere in nature. This is thought to be due to distinct sublineages developing specific niche adaptations, with associated biochemical adaptations which make them better suited to a particular environment. They can be found in water, soil, plants, insects and other animals including humans. The species of Klebsiella are all gram-negative and usually non-motile. They tend to be shorter and thicker when compared to others in the family Enterobacteriaceae. The cells are rods in shape and generally measures 0.3 to 1.5 µm wide by 0.5 to 5.0 µm long. They can be found singly, in pairs, in chains or linked end to end. Klebsiella can grow on ordinary lab medium and do not have special growth requirements, like the other members of Enterobacteriaceae. The species are aerobic but facultatively anaerobic. Their ideal growth temperature is 35° to 37 °C, while their ideal pH level is about 7.2 [57].

1-12-3 *Staphylococcus aureus*

Staphylococcus aureus is a Gram-positive round-shaped bacterium, a member of the Firmicutes, and is a usual member of the microbiota of the body, frequently found in the upper respiratory tract and on the skin. It is often positive for catalase and nitrate reduction and is a facultative anaerobe that can grow without the need for oxygen. Although S. aureus usually acts as a commensal of the human microbiota it can also become an opportunistic pathogen, being a common cause of skin infections including abscesses, respiratory infections such as sinusitis, and food poisoning. Pathogenic strains often promote infections by producing virulence factors such as potent protein toxins, and the expression of a cell-surface protein that binds and inactivates antibodies[58, 59].

1-12-4 *Streptococcus pyogenes*

Streptococcus pyogenes, (colloquially named "group A *streptococcus*" (GAS)), is a Gram positive bacterial pathogen that can cause both non-invasive and invasive disease (iGAS), as well as nonsuppurative sequelae. This includes pharyngitis, scarlet fever, impetigo,cellulitis, type II necrotizing fasciitis, streptococcal toxic shock syndrome, acute rheumatic fever and post-streptococcal glomerulonephritis [60].

Group A streptococcus (GAS) is synonymous with Streptococcus pyogenes, the only species within this group of β-hemolytic streptococci. GAS is one of the leading pathogenic bacteria that infects children and adolescents, and is associated with a wide spectrum of infections and disease states. Worldwide, there are estimated to be >600 million cases of GAS pharyngitis ("strep throat") and>100 million cases of GAS pyoderma annually[61, 62] .

1-13 Literature Survey of application for removal of pollutants by using different surfaces:

The table below represents a comparison between the current work and previous research on the high ability of hydrogel to remove different types of pollutant . This was reported in Table(1-5):

Table (1-5): Removal of pollutant using different surfaces.

No.	Sorbent	Pollutant	T (°C)	pH	t (hr.)	Dose (g)	Q_e (mg/g)	E%	Co ($mg.L^{-1}$)	Ref.
1	SA-g-P(AAc-co-MA)/TiO_2	Brilliant green	25	6	1	0.05	1200	99.9	700	[63]
1	(AM-g-GO)hydrogel	Congo red	27	5	1	0.25	3002	96.6	50	[64]
2	Acrylamide/acrylate hydrogel.	Ammonia	25	-	1	0.1	3.6	82.3	50	[65]
3	Acrylamide/acrylate TiO2 composite.	Ammonia	25	-	1	0.1	5.9	95.3	50	[65]
4	(PAAm/Starch) hydrogel	Phenol	25	6	2	0.12	20.12	90	100	[66]
5	Chitosan/ Nano ZnO	Congo red	25	6	1	0.1	120	90	100	[67]
6	Chitosan/ Nano ZnO	Methylene blue	25	7	1	0.1	470	80	100	[67]
7	Alginate/carboxymethyl cellulose/TiO2	Methylene blue	25	7	2	0.15	600	93.3	50	[67]
8	Alginate/carboxymethyl cellulose/TiO2	Congo red	25	6	2	0.15	350	84.3	50	[67]
9	N-isopropyl acrylamide (NIPAM)	phenol	25	7	1	0.15	77.7	88.8	20	[68]
10	Polyacrylamide/ starch hybrid hydrogels	Phenol	25	2	6	0.1	20	60	50	[69]
11	Alginate/acid activated bentonite beads (A-AAB)	Crystal violet	25	8	3	0.2	582.4	92.39	100	[70]
12	Alginate/bentonite beads (AB)	Crystal violet	25	8	3	0.2	498.2	84.59	100	[70]
13	PAM/SH/clay hydrogels	Methylene blue	30	6	1	0.05	180	86	20	[71]
14	SA-g-PAA	Methyl violet	25	6	1	0.3	655	86.55	100	[72]

No.	Sorbent	Pollutant	T (°C)	pH	t (hr.)	Dose (g)	Q_e (mg/g)	E%	Co ($mg.L^{-1}$)	Ref.
15	SA-g-PAA/TiO2	Methyl violet	25	6	1	0.3	1156	98.2	100	[72]
16	Hydrogel-palm kernel shell	Phenol	25	2	6.8	0.1	19.6	-	50	[٧٣]
17	Alginate/Mauritanian clay	4-nitrophenol	25	5.5	24	0.5	176	96	20	[74]
18	(2-hydroxyethyl methacrylate/acrylamidopyridine) hydrogel	Phenol	25	2	7.5	0.1	26.45	-	100	[75]

1-14 Objectives:

This work aims to investigate the following:

1- Synthesize new adsorbent surface material (composite) containing sodium alginate (Bentonite clay/alginate beads) followed by impregnation TiO_2NPs and ($CaCl_2.2H_2O$) to removal of three pollutants (Congo red CR dye , Amoxilluin AMX drug ,and 4-chloro phenol CPH) .

2- Characterize the adsorbent surface by using different techniques X-ray diffraction(XRD), Field Emission Scanning Electron Microscopes (FE-SEM), Energy Dispersive X-Ray (EDX) Thermo-gravimetric analysis (TGA) ,Fourier–transform-infrared-spectroscopy(FTIR), and Transmission Electron Microscopy (TEM).

3- Study optimum conditions to estimate three pollutant .

4- Investigate the effectiveness of the SA-Bn-TiO_2 NPs to adsorb selected three pollutants (CR,AMX, and CPH) through adsorption processes.

5- The effects of contact time, adsorbent dosage, pH, temperature, during batch treatment methods.

6- Determine the applicability of Freundlich, and Langmuir approach to estimate design parameters characterizing the performance of the adsorption batch tests, and determine the adsorption constants of three pollutants onto hydrogel surfaces.

7- The thermodynamic parameters for three pollutants on the hydrogel surfaces.

8-Study the effect of adsorbent Regeneration , and In vitro drug release on the adsorption capacity.

9- Study the Removal of laboratory sample aqueous pollutants by using SA-Bn-TiO_2 NPs by using several pollutants.

10- The biological effect of the surface prepared from SA-Bn-TiO_2 NPs on a class of Gram-positive bacteria and Gram-negative bacteria . And it was clear from this study that the surface SA-Bn-TiO_2 NPs has high effectiveness in inhibiting negative and positive bacteria effectively.

Chapter Two

Experimental Part

Experimental Part

2-1 Instruments

There are several techniques were used in the current study, most of them are listed in table (2-1) .

Table (2-1): Instruments used in this research

No.	Instrument	Model	Company supplied	Location of current measurement
1	UV-Visible spectrophotometer, Double beam	PC 1650	Shimadzu, Japan	University of Babylon / College of science for women-Chemistry Department
2	UV-Visible spectrophotometer, Single beam	UV mini-1240	Shimadzu, Japan	University of Babylon / College of science for women-Chemistry Department
3	Field-Emission Scanning electron microscope (FE-SEM)	MIRA3	TESCAN ,Czechia Republic	University of Tehran
4	Transmission electron microscope (TEM)	912AB	Leo, Germany	University of Tehran
5	X-Ray diffraction (XRD)	D2 Phaser	Bruker AXS Gmbh, Germany	University of Tehran
6	1 Thermogravimetric analysis (TGA)	DTG-60	Shimadzu, Japan	University of Babylon / College of science for women-Chemistry Department
7	Energy Dispersion X-ray (EDX)	MIRA3	TESCAN ,Czechia Republic	University of Tehran
8	Shaker water bath	CL002	K&K Scientific, Korea	University of Babylon / College of science for women-Chemistry Department

9	Centrifuge	CL008	JANETZI - T5, Belgium	University of Babylon / College of science for women-Chemistry Department
10	Ultrasound bath	405 power sonic	Hwashin, Korea	University of Babylon / College of science for women-Chemistry Department
11	Oven	LDO-060e	Labtech, Korea	University of Babylon / College of science for women-Chemistry Department
12	pH meter	HI 83141	Hanna, Romania	University of Babylon / College of science for women-Chemistry Department
13	Autoclave and Stainless steel device	Binder	Germany	University of Babylon / College of science for women-Chemistry Department

2-2 Chemical Materials :

The chemical materials used in this study are shown in Table (2-2) :

Table (2-2): Materials used in the study, purity, and their manufacturers

No.	Material	Formula compound	Molecular weight (g/mol)	Purity (%)	Supplier
1-	Congo Red	$C_{32}H_{22}N_6Na_2O_6S_2$	696.66	98.9	Sigma-Aldrich
2-	Amoxicillin	$C_{16}\ H_{19}\ N_3\ O_5S$	365.4	99.7	SDI-Iraq
3-	4-Chlorophenol	ClC_6H_4OH	182.56	99.5	(B.D.H)
4-	Phosphoric acid	H_3PO_4	97.9	98.0	Sigma-Aldrich
5-	Nitric acid	HNO_3	98.9	98	Sigma-Aldrich
6-	Sodium hydroxide	NaOH	39.997	99.0	(B.D.H)
7-	Sodium alginate (SA)	$C_6H_9NaO_7$	216.12	99.0	Sigma-Aldrich
8-	Bentonite	$Rx(H_2O)_4((Al_2{-}x,Mgx)_2$ $[(Si,Al)_4O_{10}](OH)_2)$		99.0	Sigma-Aldrich
9-	Calcium chloride dehydrate	$CaCl_2$-$6H_2O$	147.995	99.0	Sigma-Aldrich
10-	Ethanol	C_2H_5OH	46.07	99.0	(B.D.H)
11-	Titanium (IV)bis(ammonium lactate)dihydroxide solution	$[CH_3CH(O-)CO_2NH_4]2Ti(OH)_2$	294.08	99.0	Sigma-Aldrich
12-	Ammonium hydroxide	NH_4OH	35.04	28*	(B.D.H)

13-	Methanol	CH_3OH	32.04	99.0	Sigma-Aldrich
14-	Hydrochloric acid	HCl	37.46	37.0*	Sigma-Aldrich
15--	Sulfuric acid	H_2SO_4	36.07	98*	Sigma-Aldrich

***(W/W)**

2-3 Synthesis of Nanoparticles :

2-3-1 Preparation of TiO_2 by Hydrothermal Synthesis

Titanium dioxide nanoparticles were prepared by thermal hydrolysis of titanium(IV) bis (ammoniumlactate) dihydroxide (TALH), and these experiment was carried out in a 150 mL teflon cup enclosed in a stainless steel autoclave (Berghof, DAB-3). In all experiments, 10 mL of titanium (IV) bis (ammoniumlactate) dihydroxide aqueous solution, in the presence of ammonium hydroxide (NH_4OH) concentration of ammonium hydroxide 0.1 N ,were mixed, followed by the addition of distilled water to reach the final volume of 100 mL. Then this solution was mixed very well for further 30 minutes. The resulting solution was transferred into the teflon cup . Afterward the teflon cup was sealed in the autoclave, which was closed and placed into an electric furnace held at 160 ℃ for 24 hr . Finally , the autoclave was cooled down to ambient temperature and the resulting powder was separated by centrifuge at 6000 rpm speed for several times (at least three times), washed with distal water at least for four times , and dried overnight in an oven at 60℃ .as appear in Scheme (2-1) .

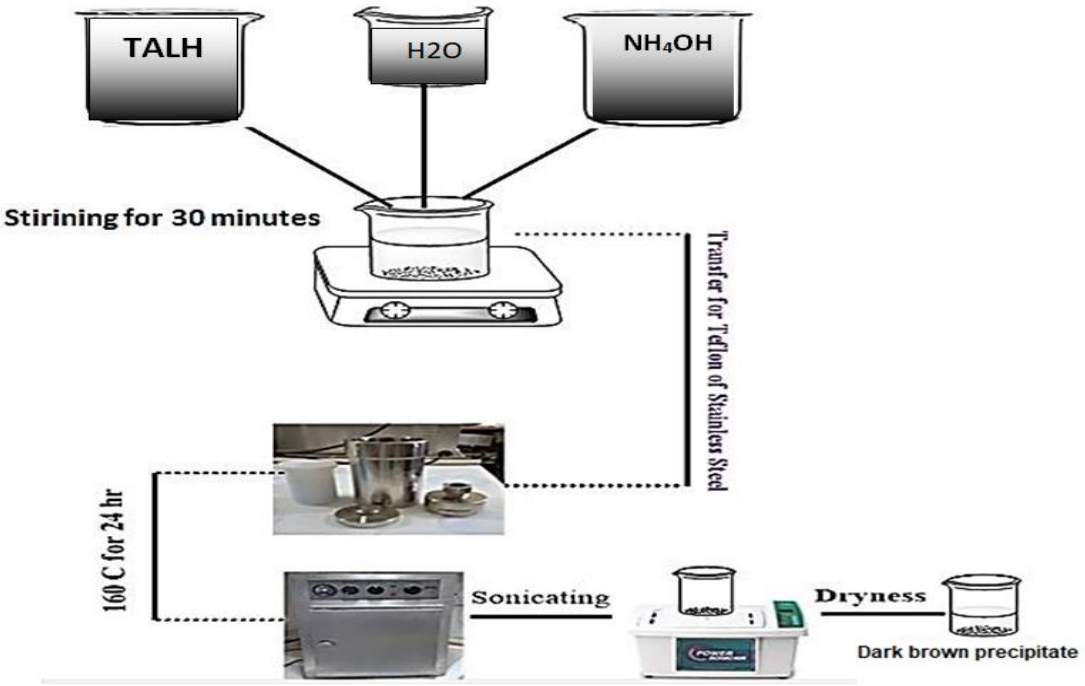

Scheme (2-1): Preparation of TiO_2 nanoparticles .

2-3-2 Preparation of the SA-Bn-TiO_2 NPs hydrogel beads

The SA-Bn-TiO_2 NPs were made up of a two-step way. First step, The homogeneous and transparent of the gel solution sodium alginate (SA) was prepared via dissolving 4 g of SA in 150 mL of distilled water for 2 h and stirring at (350 rpm) to guarantee dissolution total without any plums or air bubbles . at the same time, bentonite clay was prepared via dissolving 2 g of clay in 50mL distilled water and sonicated for 1hr to ensure the best dispersion. Then, it was little by little added to sodium alginate solution , followed via stirring for 2hr at 25 ^{o}C until the formation of a homo-geneous and gel well-dispersed. The second-step consists of adding drop-wise the resultant mixture out of a syringe needle by drop-drop in to a mixed solution saturated bath of TiO_2 NPs 0.5 % (w/v) and $CaCl_2.2H_2O$ 6% (w/v) and to ensure the cross-linking of the bio-polymer matrix and its surface impregnation with TiO_2 NPs all at once as shown in Scheme(2-2) .

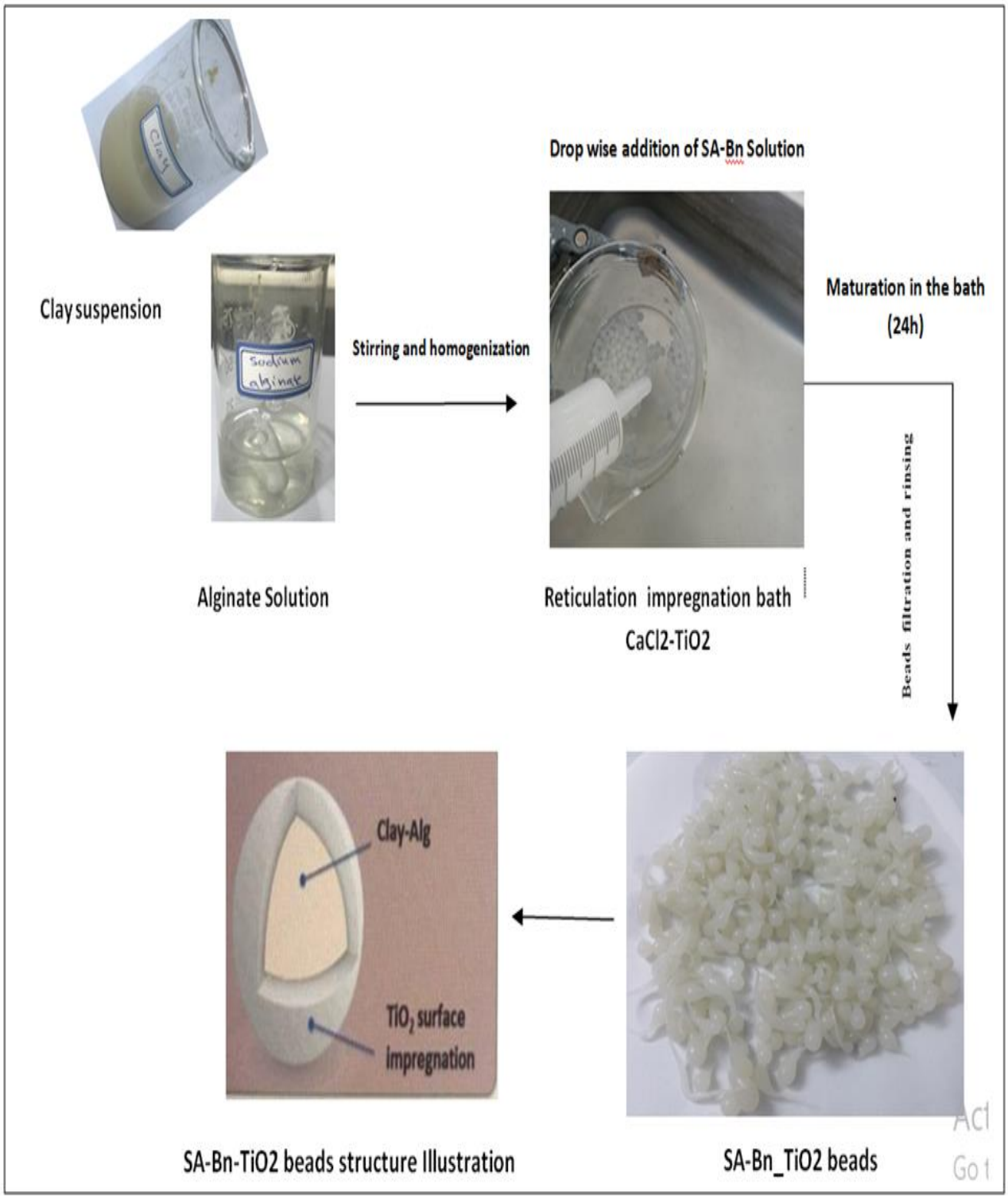

Scheme 2-2: Preparation of the SA-Bn-TiO_2 NPs hydrogel beads

2-4 Characterization and Measurements of The prepared Nanocomposites :

The samples were examined using transmission electron microscopy (TEM), Field emission scanning electron microscopy (FE-SEM), X-ray diffraction spectroscopy (XRD), Thermo gravimetric analysis (TGA), Fourier Transform Infrared (FT-IR) .

2-4-1 Ultraviolet-Visible Spectroscopy (UV–Vis) :

An important technique used to measure absorption and transmission for dye solution. Where 0.1 $mg.mL^{-1}$ of the composite are placed in the dye solution and then filled the quartz cells for measurements wavelength and concentration [76].

2-4-2 Fourier Transform Infrared (FT-IR) Analysis :

The vibrational motions of the chemically bound constituents of matter have frequencies in the infrared region. The oscillations induced by certain vibrational modes provide a means for the matter to couple with an impinge beam of infrared electromagnetic radiation and exchange energy with it when the frequencies are in resonance. Consequently, the molecular vibration will be excited by infrared frequency causing the energy of molecular vibration to increase. In the meantime, the electromagnetic radiation with a specific frequency will be absorbed by the molecule because the photon energy is transferred to excite molecular vibrations. FTIR spectra were recorded using the FTIR instrument (Shimadzu. 8400S) in the 4000-400 cm^{-1} frequency range. Dried absorbance (1 mg) was mixed with KBr powder (10 mg) in an agate mortar. The mixture was pressed into a pellet under 10 tons load for 2–4 min, and the spectrum was recorded immediately[17].

2-4-3 Field Emission Scanning Electron Microscopy (FE-SEM) :

FE-SEM is a powerful device that is used in characterizing sample morphology such as grain size, particle size, particle distribution, crystal defects, and surface structure. FE-SEM has several features like a large depth of field, higher resolution, and more control in the degree of amplification because it also uses electrons as the probe.[77].

2-4-4 Transmission Electron Microscopy (TEM) :

TEM is a microscopy technique that is used as a beam of electrons transmitted across an ultra-thin sample where the electrons are transformed into light and form an image. TEM provides information on phase composition, structure, and lattice defects [76].

2-4-5 Thermogravimetric analysis (TGA) :

The thermodynamic analysis is performed to determine the thermal stability of prepared nanomaterials and to determine the purity of these particles. The sample was heated from 10 °C to 800 °C and at a heating speed of 10 °C/min [78] .

2-4-6 X-ray Diffraction Spectroscopy (XRD) :

X-ray diffraction is a powerful nondestructive technique for characterizing crystalline materials. Provides information about the average spacing between layers or rows of atoms, the orientation of a single crystal or grain, the crystal structure of an unknown material, measures the size, shape, and internal stress of small crystalline regions. The crystalline properties of materials prepared using an X-ray deflection technique were studied using a single-wavelength light (1.5104nm) from the CuKα source using nickel as a filter. Where the range is taken from deviation angles (2Θ) in this measurement is between (5-80) degrees [79].

2-5 Removal of pollutants by using SA-Bn-TiO_2 NPs surfaces as Adsorbents :

2-5-1 Determination of optimum wavelengths (λmax) and Calibration curves of (Congo Red (CR) dye, Amoxicillin (AMX) drug and 4-Chlorophenol (CPH)) .

2-5-1-1 Congo Red

A Congo Red dye is a very well-known anionic dye that has a molecular formula ($C_{32}H_{22}N_6Na_2O_6S_2$), and molecular weight (696.66 g/mol); the dye is odorless red powder used for various purposes, also extensively used in textile dying and paper printing[80][80][80][80] .A stock solution (1000 mg L^{-1}) was prepared by dissolving (1.0 g) of dye in (1000 mL) D.W.

2-5-1-2 Amoxicillin

A Amoxicillin drug is a very well-known antibiotic that has a molecular formula ($C_{16}H_{19}N_3O_5S$), and molecular weight (365.4 g mol^{-1}); the drug is colorless powder used for various purposes, also extensively used human and veterinary medicine for the treatment of bacterial . A stock solution (1000 mg L^{-1}) was prepared by dissolving (1.0 g) of Amoxicillin in (1000 mL) D.W.

2-5-1-3 Chlorophenol

4-Chlorophenol CPH is a very well-known pollutant that has a molecular formula (ClC_6H_4OH), and molecular weight (128.56 g/mol); the 4-Chlorophenol is colorless or white powder used on a large scales in chemical industry including the production of pharmaceuticals, pesticides and dyes . A stock solution (1000 mg L^{-1}) was prepared by dissolving (1.0 g) of 4-Chlorophenol in (1000 mL) D.W.

To determine the maximum wavelength of the three pollutant (Congo Red (CR) dye, Amoxicillin (AMX) drug and 4-Chlorophenol (CPH)) the ultraviolet-visible absorption spectra of three pollutant solution were recorded within wavelengths of 200-800 nm. Where the maximum wavelength of the solution was determined from its highest absorption in the UV-Vis spectrum found at the wavelength λ_{max} CR= 495 nm , λ_{max} AMX= 272 nm, λ_{max} CPH= 270 nm in Figure (2-3), Figure (2-4), and Figure (2-5) .

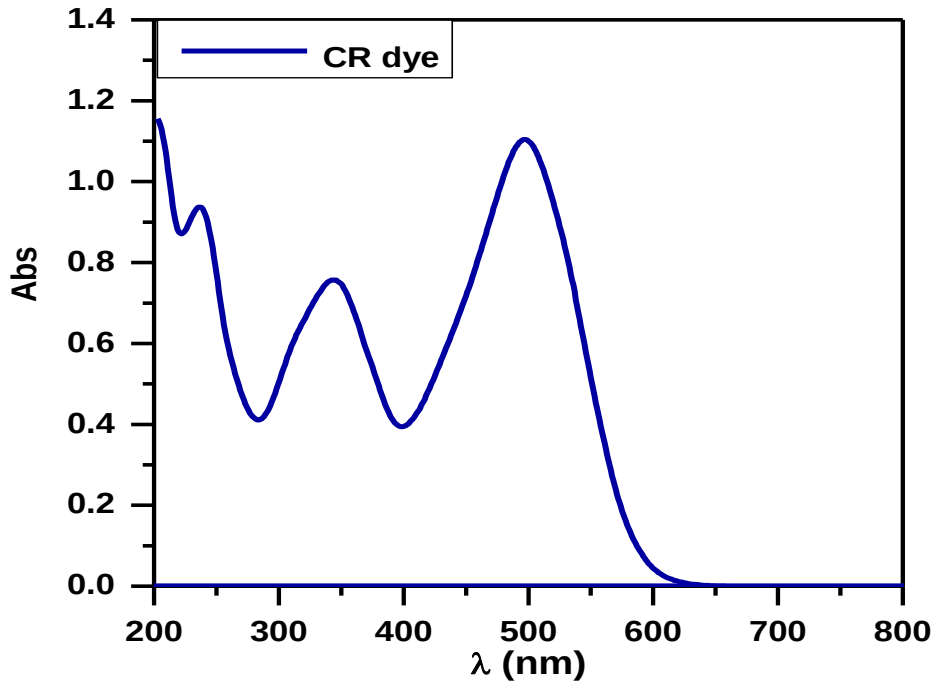

Figure(2-3): UV-Visible absorption spectra of Congo Red (CR) dye .

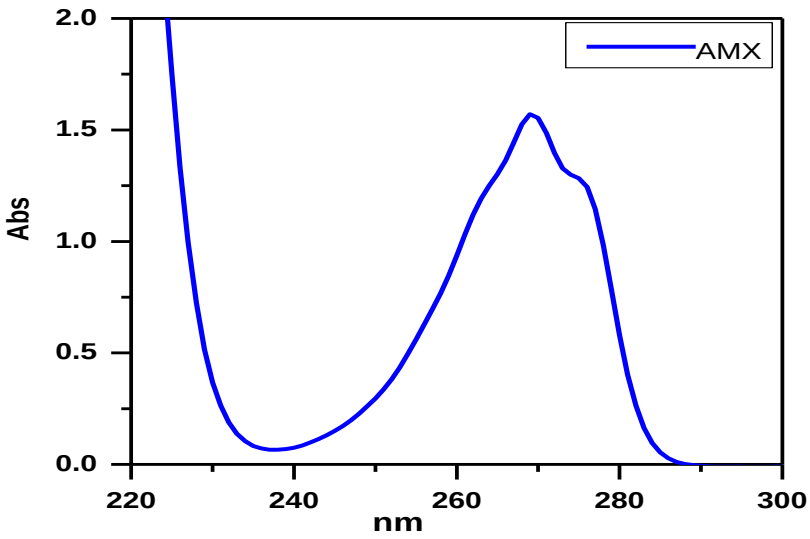

Figure(2-4): UV-Visible absorption spectra of Amoxicillin (AMX) drug .

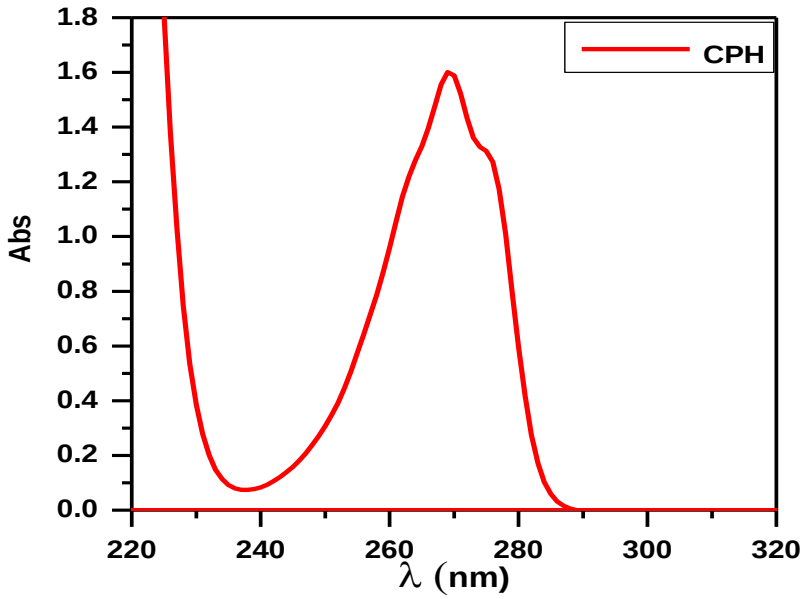

Figure(2-5): UV-Visible absorption spectra of 4-Chlorophenol .

The calibration curve of different concentration of each Congo Red(CR) dye, Amoxicillin (AMX) drug and 4-Chlorophenol (CPH)) were prepared in serial dilutions (2-100 mg/L). Absorbance was measured at the λ_{max} for each Congo Red dye, Amoxicillin (AMX) drug and 4-Chlorophenol (CPH)) and plotted against the concentration values of AMX and PHE (Figure 2-6), (Figure 2-7)and(Figure 2-8) .

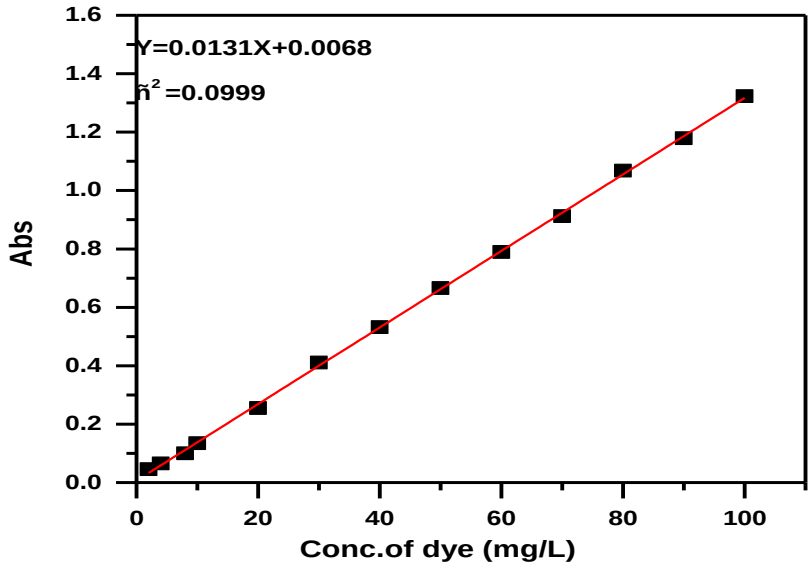

Figure (2-6): Calibration curve for Congo Red (CR) dye

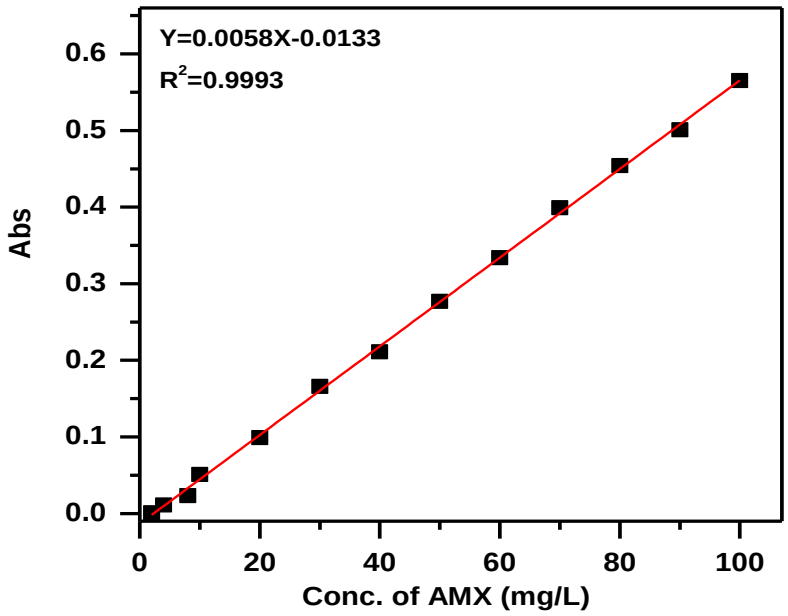

Figure (2-7): Calibration curve for Amoxicillin (AMX) drug

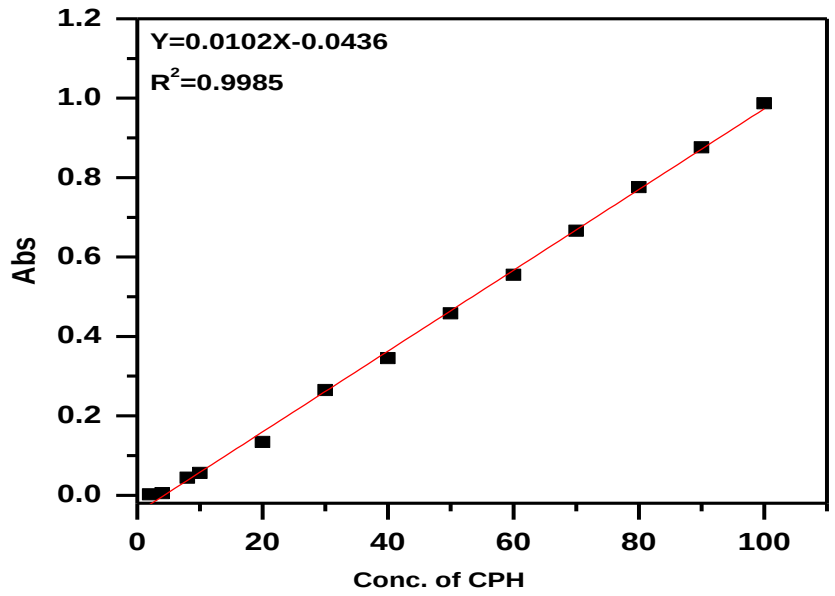

Figure (2-8): Calibration curve for 4-Chlorophenol (CPH)

In order to determine of the method, the solutions containing ten different concentrations. The measured detection limit LOD, limits of Quantitation's, LOQ, relative standard deviations percent (R.S.D%) and standard deviation (S.D.), (Table 2-3) [81].The limit of detection (LOD) for the proposed method was calculated using equation (2-1). The signal-to-noise ratio (S/N) obtained by standard addition quantification and subsequent extrapolation to a S/N of 3.[82, 83]

$$\text{LOD} = \frac{3\ \text{S.D}}{\text{b}} \qquad (2-1)$$

The limits of Quantitation's (LOQ) was experimentally calculated using equation (2-2) [82, 84] :

$$\text{LOQ} = \frac{10\ \text{S.D}}{\text{b}} \qquad (2\text{-}2)$$

S.D is the standard deviation(blank) and *b* is the sensitivity, namely the slope of the calibration graph.

Table (2-3): Statistics data of calibration for different concentrations of Congo Red (CR) dye, Amoxicillin (AMX) drug and 4-Chlorophenol (CPH))

Parameters	Proposed Method CR	Proposed Method AMX	Proposed Method CPH
λ_{max} (nm)	495	272	270
Beer's law limit (µg/ml)	2-100	2–100	2-100
Regression equation	(Y = m X + C) Y=0.0131+ 0.0068	(Y = m X + C) Y=0.0058X-0.0133)	(Y = m X + C) Y=0.0102X-0.0436)
Slope (m)	0.0131	0.0058	0.0102
Intercept (C)	0.0068	-0.0133	-0.0436
Correlation coefficient (r^2)	0.9996	0.9993	0.9985
Color	red	Colorless	Colorless
Detection limit LOD (µg/ml)	1.029×10^{-4}	1.027×10^{-4}	1.026×10^{-4}
limit of Quantitation LOQ (µg/ml)	102.96	102.724	102.647
% Relative Standard deviation (RSD%)	77.67	83.51	87.77
standard deviation (SD)	0.4496	0.1986	0.349
Molar absorptivity (L/mol.cm)	9.126×10^{3}	2.119×10^{3}	1.311×10^{3}
Sandal's sensitivity (µg/cm)	7.63×10^{-8}	0.172×10^{-6}	9.8×10^{-8}

2-6 Effect of different parameters on the adsorption process:

2-6-1 Effect of contact time:

100 mL of pollutants solution (100 mg.L^{-1}) With different time periods(2-120) minute is prepared and put in a conical flask with adsorbent concentration (0.05 g/100 mL) of SA-Bn-TiO2 NPs at 25°C and 220 rpm Shaking speed and kept separately in a shaker the water bath controlled temperature. Pollutant concentration to be estimated spectrophotometrically at the wavelength corresponding to maximum absorbance, λ_{max}, using a single beam UV-Visible spectrophotometer. The samples at different interval times are separated by the centrifugation process. The absorbance of the solution is then measured, the dye concentration is to be measured after (2- 120) minute until equilibrium is reached.

The adsorption capacity was calculated from equation (2-3): [46]

$$qe = \frac{(C_0 - C_e) * V_L}{m_g} \qquad (2-3)$$

Where: q_e = Amount of pollutant adsorbed per unit mass of adsorbent (mg/g).

C_o= Initial concentration (mg.L^{-1}).

C_e= Equilibrium concentration (mg.L^{-1}).

m = Dose of adsorbent (g).

V_L= is the volume of solution (L).

The percentage removal (E%) of the pollutants was calculated based on the reduction in absorbance at λ_{max} value of the pollutant as follows:[46]

$$E\ \% = \frac{C_{0-}C_e}{C_0} * 100 \qquad (2-4)$$

Where: C_0 and C_e are initial and equilibrium concentrations, respectively.

2-6-2 Effect of dose of adsorbent :

The study was carried out with different doses (0.005, 0.008,0.01, 0.025,0.04, 0.08, and 0.1) g for SA-Bn-TiO2 NPs .The concentrations of the samples were (100) mg.L-1. The solutions were kept in the shaker water bath at (220 rpm) about (1 hr.) at a fixed temperature 25 0C the remaining pollutant concentration in the aqueous phase is measured spectrophotometry for the chosen wavelength.

2-6-3 Effect of initial concentration of pollutant :

A series of different concentrations of 100 mL for pollutant has been used in this study (10,20,30,40,50,60,70,80 and 100) mg.L-1, was added to a conical flask (Erlenmeyer) in the presence of (0.05g/100 mL) of SA-Bn-TiO2 NPs at 25°C and 220 rpm Shaking speed these series were putting in a shaker water bath for 1 hr. , after that the supernatant was separated by centrifuge and measured the remaining concentration of pollutant in the aqueous phase is measured spectrophotometry for the chosen wavelength.

2-6-4 Effect of pH :

The effect of solution pH on the pollutant removal is examined by varying the initial pH solutions (3,4,5,6,8, and 11) using conical flasks (100 mL) container concentrations (100 mg.L-1) in 100 mL .The pH was adjusted by using (0.1N) HCl and/or (0.1N) sodium hydroxide (NaOH) and was measured using a pH meter. Then the amount of adsorbent surface (0.05 g/100 mL) of SA-Bn-TiO_2 NPs adsorbents was set on the conical flask.

The flasks were put inside the shaker water bath (220 rpm fixed throughout the study) maintained at 25 ^{o}C and the final concentration of dye was measured using the single beam UV-Vis spectrophotometer and the calibration plot of the pollutant after1 hr.

2-6-5 Effect of Temperature :

The adsorption experiments are performed at different temperatures (10, 20,30 and 40°C) in a thermostat water bath with a shaker. The effect of temperature was investigated with (0.05g) dose of adsorbent SA-Bn-TiO_2 NPs mixing with (100mL) aqueous solution of dye concentration (10-100) mg/L, and the sample was shaking at a period for (1 hr.) , then measured the remaining pollutant concentration in the aqueous phase is measured spectrophotometry for the chosen wavelength.

2-7 Adsorbent regeneration experiments:

Reusability to investigate the reusability of the adsorbent, 0.5g of SA-Bn-TiO_2 NPs adsorbent was added into 100 mL for each of three pollutant (CR,AMX, CPH) solution of concentration 500 mg/L at 30 ^{o}C temperature and pH of 6.0 to achieve saturated adsorption. The SA-Bn-TiO_2 NPs was regenerated in excess desorption studies were carried out using different desorption agents at different concentration (0.01, 0.05, 0.1 N) such as H_2SO_4, NaOH, H_3PO_4 , HCl , HNO_3, ethanol , methanol and water to regenerate anionic binding sites and finally washed with excess distilled water prior to use in the next adsorption cycle. An adsorption and desorption cycle was repeated six additional times using 100 mL of pollutant solution of concentration 500 mg/L at 25^{o}C temperature and pH of 6.0.

2-8 A Comparative adsorption between different surfaces

A sample of 100 mL of three pollutant concentration(100 $mg.L^{-1}$) are used in this study, then added to a conical flask (Erlenmeyer) in the presence of 0.05g from prepared (SA-Bn-TiO_2 NPs , SA-Bn, and TiO_2 NPs), and put in a shaker water bath for 1 hr., after that the supernatant was separated by centrifuge and measured the remaining concentration by using UV-Visible spectrophotometer for the chosen wavelength .

2-9 Removal of Pollutants (pharmaceutical) by Using SA-Bn-TiO_2

A laboratory sample 100mL of pharmaceutical pollutants containing (Amoxicillin (AMX), phenylephrine hydrochloride (PHE), Tetracycline (TC) , Paracetamol (PR) , Vitamin B6 (pyridoxine) Riboflavin (RF) with a riffle concentration were using in this study, then added to a conical flask (Erlenmeyer) in the presence of 0.05g from prepared SA-Bn-TiO_2 NPs, after that the mixture were putting in Shaker water bath for 1hr, after that the supernatant were separated by centrifuge and measured the remaining concentration by using UV-Visible spectrophotometer at the λ_{max} 272 nm for AMX drug .

2-9-1 Removal of Pollutants (Dyes) by Using SA-Bn-TiO_2 NPs

A laboratory sample 100mL of pharmaceutical pollutants containing (Congo red (CR), Crystal Violet (CV), Methylen Blue (MB) , Berlllint Blue (BB) , Direct yellow (DY) ,Reactive blue (RB) with a riffle concentration were using in this study, then added to a conical flask (Erlenmeyer) in the presence of 0.05g from prepared SA-Bn-TiO2 NPs, after that the mixture were putting in Shaker water bath for 1hr, after that the supernatant were separated by centrifuge and measured the remaining concentration by using UV-Visible spectrophotometer at the λmax 495nm for CR dye .

2-9-2 Removal of Pollutants (Dyes , pharmaceutical , and phenol compound) by Using SA-Bn-TiO_2 NPs

A laboratory sample 100mL of pollutants containing (Phenol (PH), 4-Clorophenole (CPH), Amoxicillin (AMX), phenylephrine hydrochloride (PHE), Tetracycline (TC) , Paracetamol (PR) , Vitamin B6 (pyridoxine) Riboflavin (RF) Congo red (CR), Crystal Violet (CV), Methylen Blue (MB) , Berllint Blue (BB) , Direct yellow (DY)) with a riffle concentration were using in this study, then added to a conical flask (Erlenmeyer) in the presence of 0.05g from prepared SA-Bn-TiO_2 NPs, after that the mixture were putting in Shaker water bath for 1hr, after that the supernatant were separated by centrifuge and measured the remaining concentration by using UV-Visible spectrophotometer at the λmax 495 nm for CR and λ_{max} 272 nm for each AMX and CPH at the same order

2-10 Amoxicillin drug Loading

About (0.5) gm of the SA-Bn-TiO_2 NPs is added to (100 ml) of the amoxicillin solution in concentration 500 mg/L and placed in a shaker device for a period of (1hr) at a temperature (30 ^{o}C), after that the surface is separated from the solution and the drug-loading SA-Bn-TiO_2 NPs is dried in an oven at a temperature (70 ^{o}C) and then ground to obtain the powder as appear in scheme 2-3 .

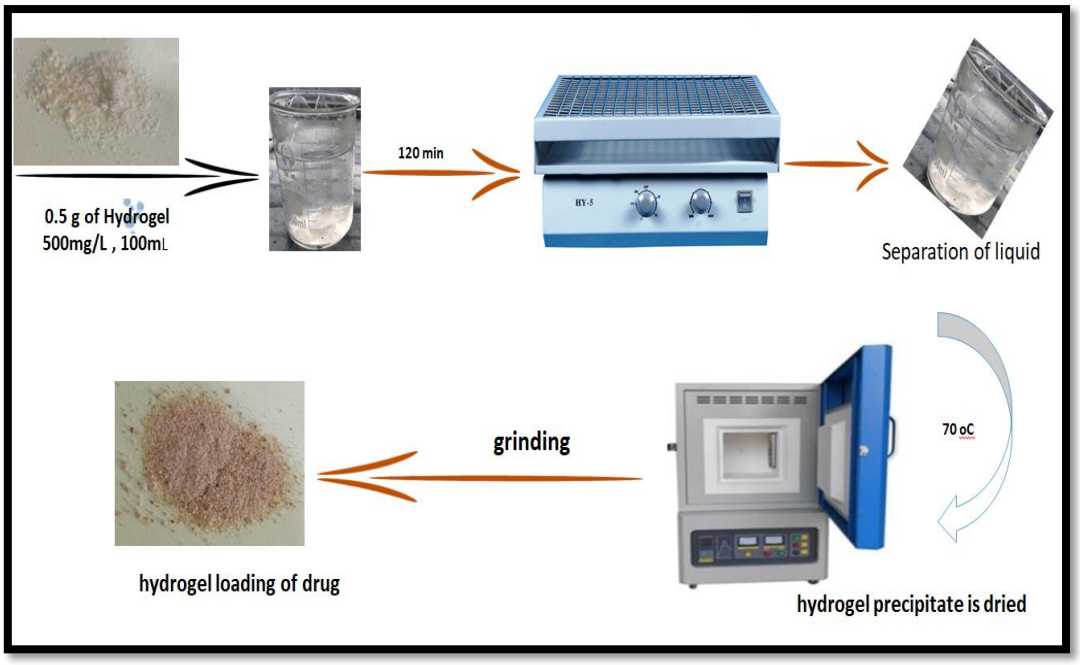

Scheme 2-3 : Amoxicillin drug Loading onto SA-Bn-TiO_2 NPs .

2-11 In vitro drug release

The effect of the hydrogel loaded with a drug in different acidic media, as the release of the drug at (pH 1.2) and (pH 7.5) was studied. Where (0.1gm) of the surface loaded with a drug was placed in (100ml) of different acidic media, and then placed in a shaker water bath , at a temperature (37 ^{o}C) in different time, the removal percentage and amount of drug release is calculated through the equations .

$$\text{Amount of drug release} = \frac{Ce\ V}{M} \qquad (2\text{-}5)$$

$$\text{Percentage drug release} = \frac{\text{amount of drug release}}{\text{amount of drug loading}} \times 100 \qquad (2-6)$$

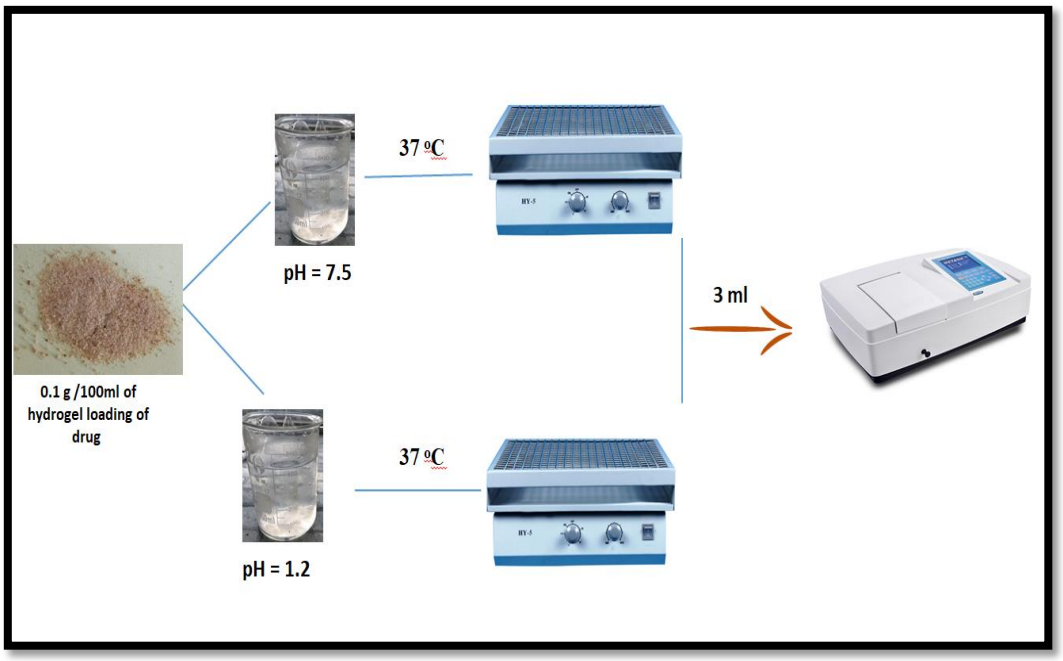

Scheme 2-4: In vitro drug release

2-12 Bacterial biological activity test

The two types of Gram-positive bacteria (*Staphylococcus aureus and Streptococcus epigenetics*) and Gram-negative bacteria (*E.coli, and Klebsiella spp*.), were obtained from the Department of Life Sciences / College of Science - University of Babylon. Hinton agar) and Mannitol salt agar as media for cultivation, isolation, and differentiation between positive and negative bacteria.

2-12-1 Preparation of standard solutions for bacteria

Mueller Hinton agar medium was prepared by dissolving (37 gm) of the culture medium in 1 liter of distilled water, then heating the mixture until the agar dissolved, then putting the culture medium in an autoclave at a temperature of 120 ^{o}C for 15 minutes). then pour the medium into sterilized glass dishes (Petri disk) at a rate of (15-20) milliliters per plate and left until solidification completes, then the dishes were placed in the incubator for (24 hrs.) at a temperature (37 ^{o}C) to make sure that there were no any contaminate it.

2-13 Treating Mice Wounds Using a Surface Prepared from SA-Bn-TiO_2 NPs

Mice were obtained from the animal house of the College of Veterinary Medicine at Al-Qadisiyah University, where the rats were wounded with a wound of medium depth and this wound was bandaged by loading (0.1 gm) of the surface prepared from the leaves of the castor plant and the rates of wound healing after surface loading were studied from (1-7) days depending on the superior surface properties on wound healing and the ability to deliver it to the inside of the wound.

Chapter Three

Result and discussion

3-Results and discussion

3-1 Physicochemical characterization of adsorbents surfaces

3-1-1 FTIR characterization for adsorbent/adsorbate

FTIR technique was used to analyses the surface functional groups responsible for three pollutant (CR, AMX, and CPH) adsorption. Adsorbent surfaces SA-Bn-TiO_2NPs and pollutant-loaded adsorbents samples after adsorption was placed in an oven at 65 ◦C for 4 h. Samples were made as pellet and then the infrared spectra of three pollutant CR, AMX and CPH on adsorbents before and after the adsorption process was recorded in the range 4000–400cm^{-1} on an Infrared spectrophotometer, FTIR, 8000, Shimadzu-Japan. Results are shown in figures (3-1),(3-2) and (3-3).

Illustrates the FT-IR spectra of the Bentonite clay , SA-Bn and SA-Bn-TiO_2NPs .The broadband around 3435 cm^{-1} and 2927 cm^{-1} is characteristic of the stretching of the –OH groups and the C–H stretching of the CH_2 groups, respectively. Starting by the SA-Bn, it clear that the characteristic bands of the polymer matrix are well depicted at 3300 cm^{-1} , 1600 cm^{-1} ,and 1409cm^{-1} assigned respectively to the stretching vibration of –O–H from the hydroxyl group , to C=O, and to symmetric COO− stretching vibrations .Bentonite clay shows typical infrared characteristic bands ; at 1009 cm^{-1} corresponding to Si-O-Si stretching vibration, at 918 cm^{-1} Al− OH vibrations, and at 450 cm^{-1} Si-O bending vibration [85, 86]. New characteristic adsorption band 1718 cm^{-1} , assigned to C=O stretching in the spectrum of SA-Bn-TiO2.with the addition of new bands at 1415 cm^{-1} attributed to the stretching vibrations of Ti-O-Ti bonds. Also teeth like peaks in the region around 450− 600 cm^{-1} of Ti-O bending are observed which confirms the impregnation of TiO_2 nanoparticles [72, 87, 88].

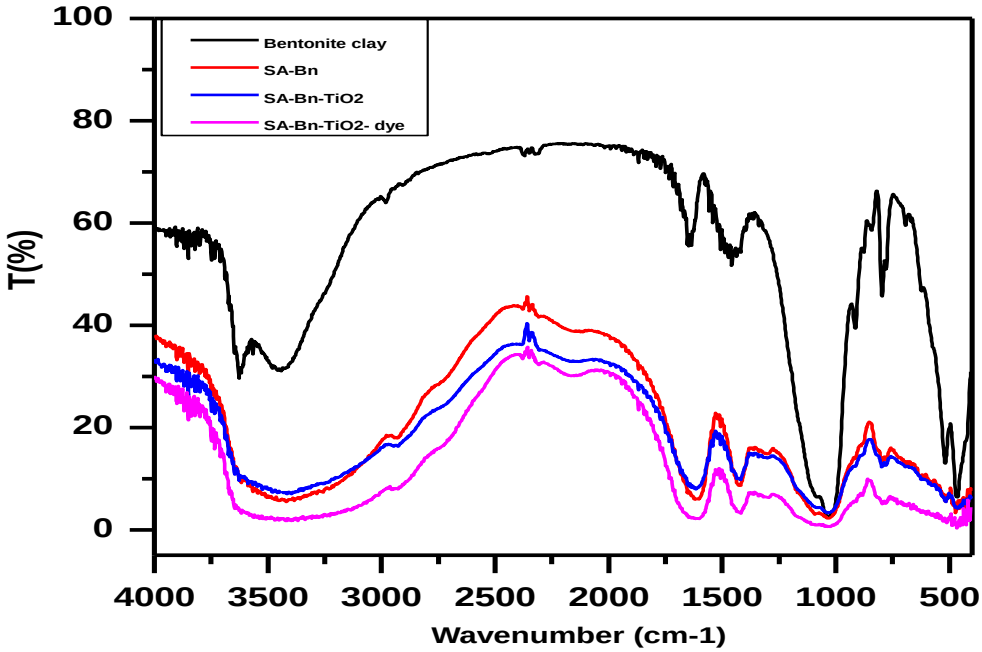

Figure (3-1) FT-IR spectra of SA-Bn-TiO_2 NPs surface before, and after adsorption of CR dye .

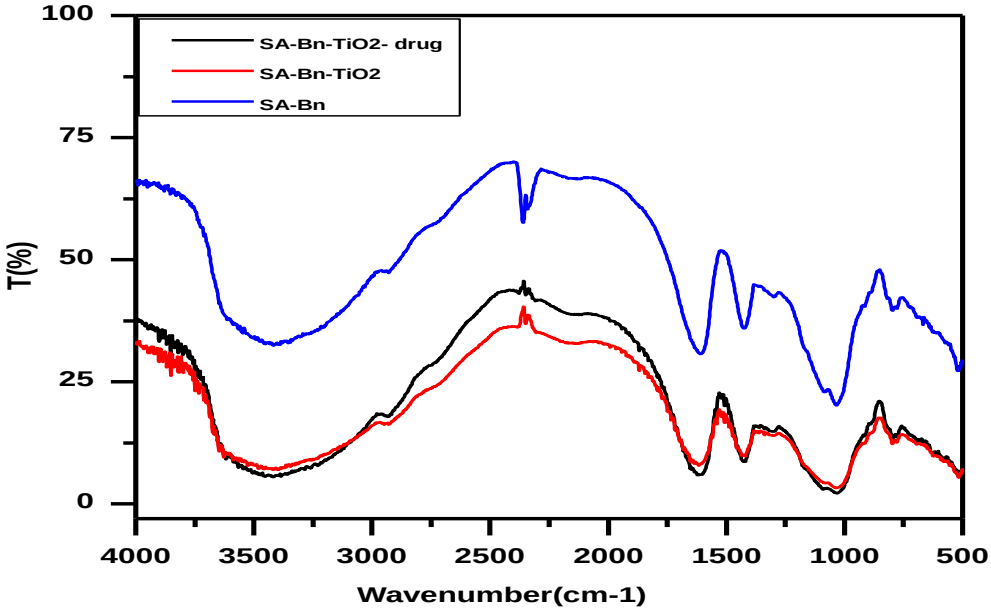

Figure (3-2) FT-IR spectra of SA-Bn-TiO_2 NPs surface before, and after adsorption of AMX drug .

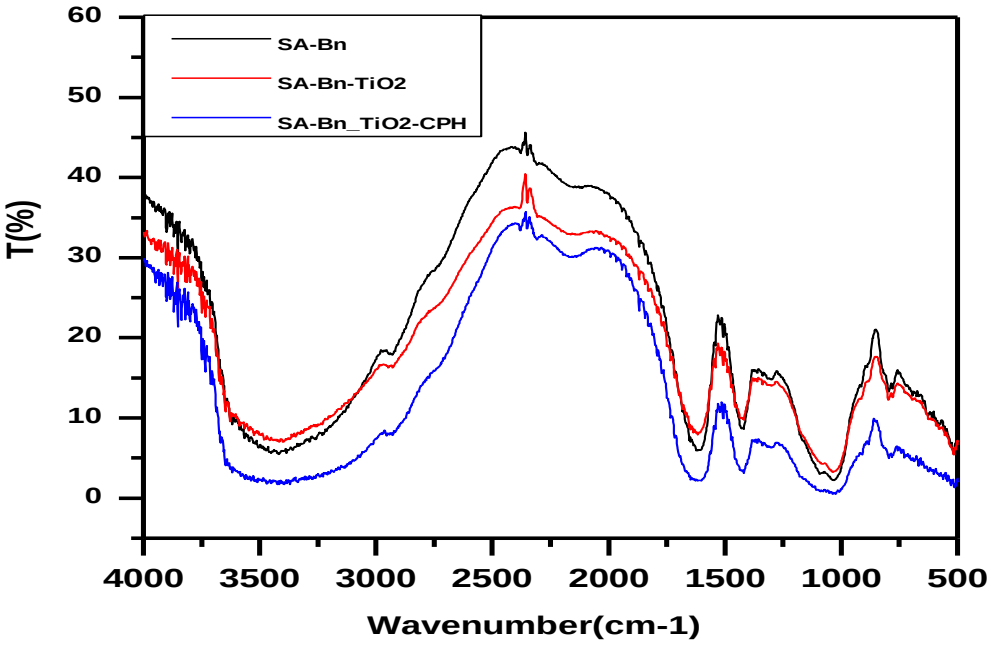

Figure (3-3) FT-IR spectra of SA-Bn-TiO_2 NPs surface before, and after adsorption of CPH .

3-1-2 FESEM characterization for adsorbent/adsorbate:

FE-SEM was utilized to study the morphology of the surface before and after adsorption and chemical modification (Figure 3-4 a)TiO_2 NPs , b)bentunite clay , c) SA-Bn , d) SA-Bn-TiO_2NPs). The surface morphology of SA-Bn is found to be smooth (Figure 3-4(c)), whereas, after grafting of SA-Bn on TiO_2 NPs, the surface morphology becomes rougher displayed the existence of holes and cavities with different sizes and shapes[89]. (Figure 3-4(d)).The introduction of TiO_2 NPs into SA-Bn increases the roughness of surface , which is desirable for the adsorption of CR dye. Enhanced the separation of the clay minerals into thin sheets, mainly Bentonite mineral due to its Ti–O–Ti structure (i.e., exfoliated clay); see Figure3-4 b). Further-more, TiO_2 NPs was observed as an aggregate of several nano-particles with dissimilar sizes below 100 nm

.Obviously, the physical combination between TiO_2 and Clay was clearly observed wherein the TiO_2 NPs were connected to the outer surface of clay and filled the cracks and holes of the SA-Bn sample [72].Therefore, the existence of spherical-like TiO_2 NPs could be considered as a support to enhance the uptake of three pollutant because of the improvement of the surface area of SA-Bn-TiO_2NPs . The internal pores can be seen in the morphology of SA-Bn-TiO_2 NPs, which favours the intraparticle diffusion of three pollutant as appear in figure 3-4 (e, f, g) , TiO_2 NP was sufficient to create well-developed pores with uniform distribution leading to large surface area and porous structure. The pores and surface of SA-Bn-TiO_2 NPs hydrogel were entirely occupied. Furthermore, this confirms the adsorption of three pollutant by SA-Bn-TiO_2 NPs [90].

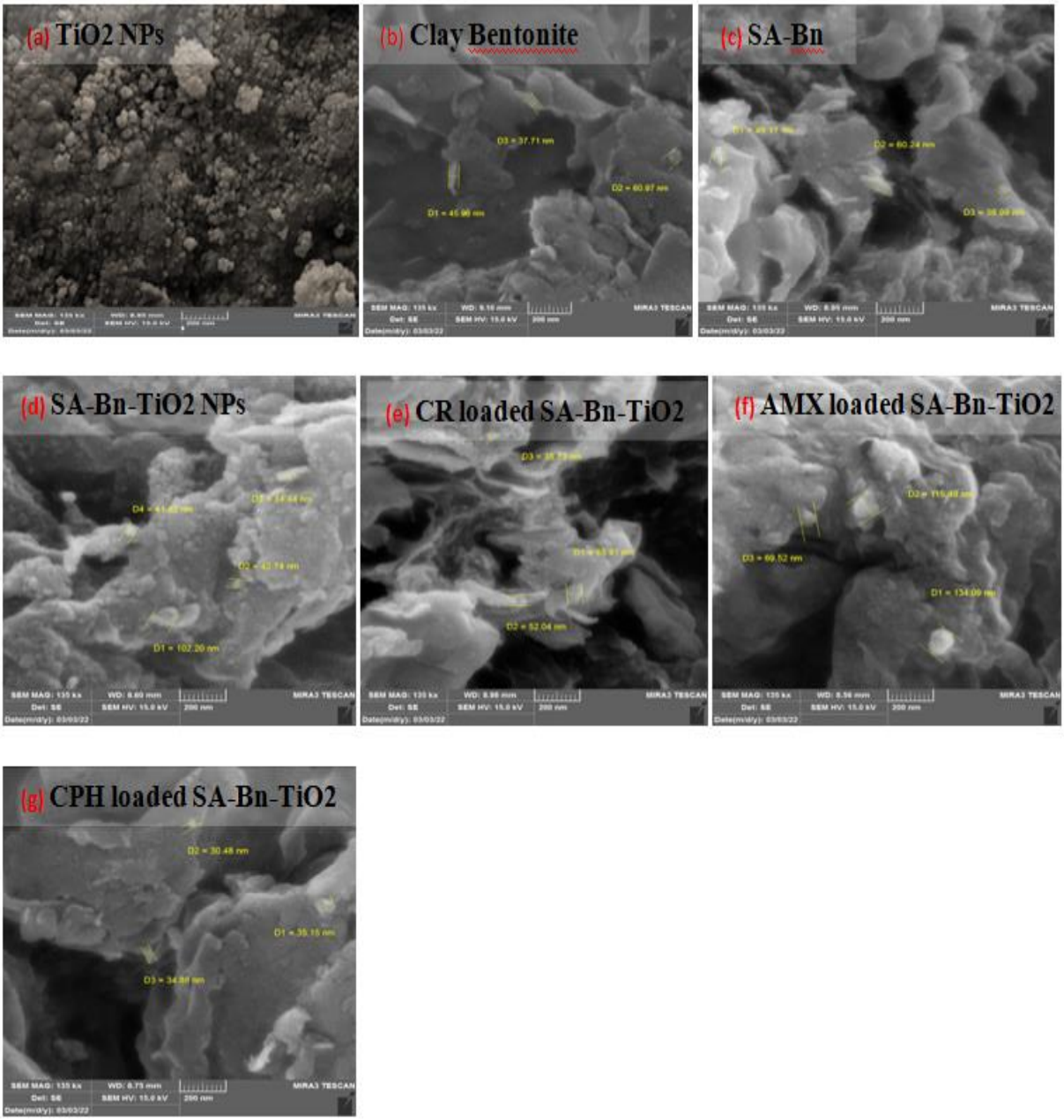

Figure 3-4. FE-SEM images of (a) TiO2 NPs, (b) Clay Bentonite (c) SA-Bn, (d) SA-Bn-TiO2 NPs, (e) CR loaded SA-Bn-TiO2 NPs, (f) AMX loaded SA-Bn-TiO2 NPs and (g) CPH loaded SA-Bn-TiO2 NPs

3-1-3 Transmittance Electron Microscopy (TEM) and Energy Dispersion X-ray (EDX)

Figure 3-5(a) shows image of TEM SA-Bn-TiO_2 NPs, where TiO_2 NP was observed embedded inside the SA-Bn-TiO_2 NPs hydrogel. too, incorporation of TiO_2NPs in to SA-Bn is supported via the presence of Ti and O peak in the EDX of SA-Bn as appear in figure 3-5 (b) . the synthesized nano-composite have elements O, C, Ti, Si Ca, Mg, and, Al, That indicates the presence of Bentunite clay onto SA-Bn-TiO2 NPs. values of the highest and lowest elements that existed in the modified SA-Bn-TiO_2 NPs by 42.4 wt.% and 0.5 wt.%, respectively[65].

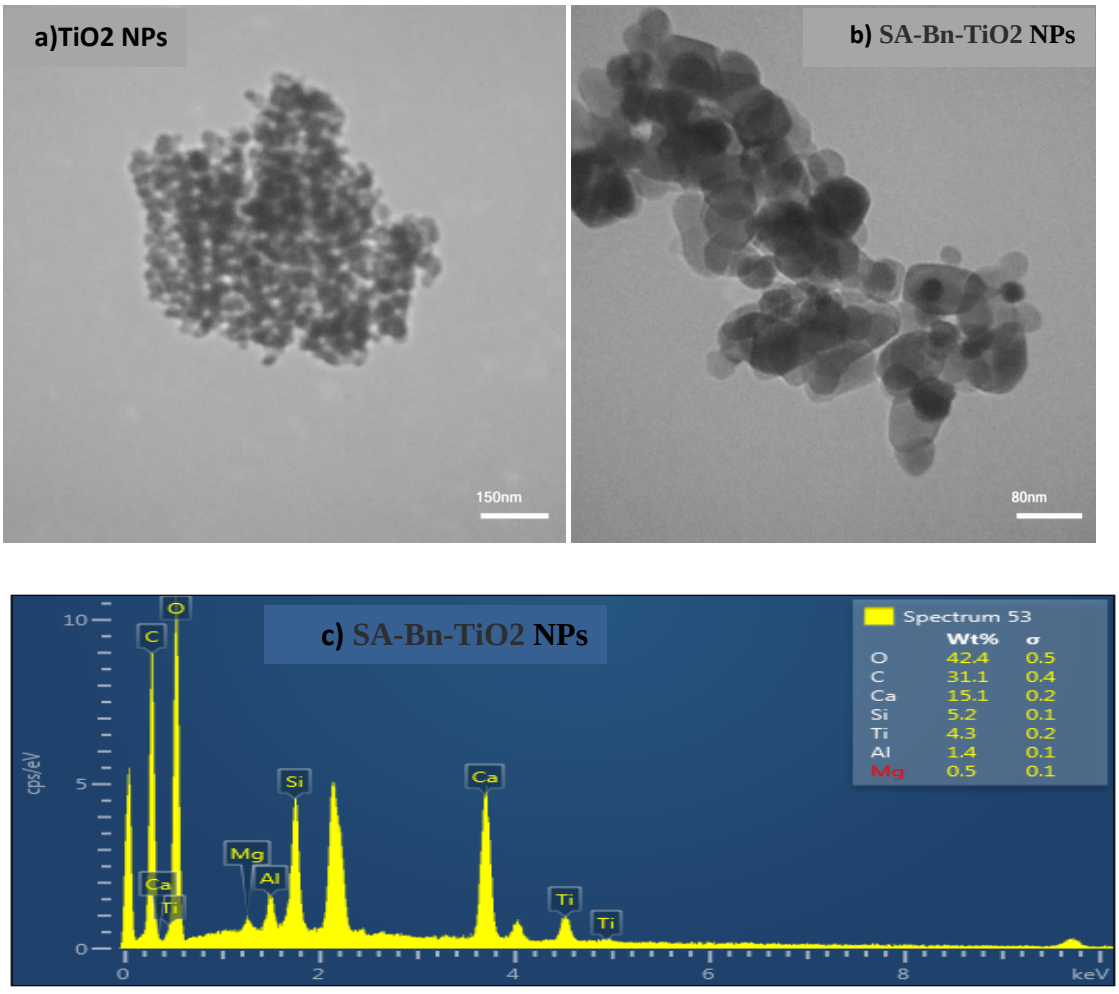

Figure 3-5. TEM images of a) SA-Bn-TiO2 NPs and (b) EDS of SA-Bn-TiO2 NPs.

3-1-4 Thermogravimetric analysis (TGA)

The thermal gravimetric analysis of the hydrogel was investigated. TGA curves of the Matrix SA-Bn, and SA-Bn-TiO_2NPs obtained at a heating rate of 5 ◦C/min up to 600 ◦C under a dry nitrogen flow is shown in (Figure 3-6 and Figure 3-7); one can see that the degradation process is different. It is well- known that any weight loss below 200 ◦C is due to the loss of unbound water, while the loss in the range of 200− 800 ◦C is mainly due to the organic matter degradation. By analyzing the thermograms of SA-Bn and SA-Bn-TiO_2NPs, it is quite clear that the incorporation of clay has an approving effect on the thermal stability of the biopolymer matrix since we have a decrease of the weight loss percentage. In fact, the virgin biopolymer lost about 88 % of its total weight, which implies that it is totally degraded up to 600 ◦C, unlike Alginate supported bentonite of which the total weight loss is of the order of 52.1 %. This means that there was a creation of a resistant path through the polymer matrix by clay to retard the decomposition process. Similarly, by examining the thermograms of SA-Bn and SA-Bn-TiO_2NPs composite, we can detect an enhancement in thermal stability attributed to the TiO_2 loading. It is very common that the nanocomposite's thermal degradation is affected by the presence of organic and inorganic materials at their surface. In fact, in our case the bonds at the biocomposite surface are originated from the interaction between Ti atoms and COO− biopolymer groups. The reduced size and increased area of TiO_2 nanoparticles on the surface of the hydrogel assure the good interactivity between them, which gives rise to more stable complexes. Thusly, the latter ameliorates the SA-Bn-TiO_2NPs thermal stability [91-94] .

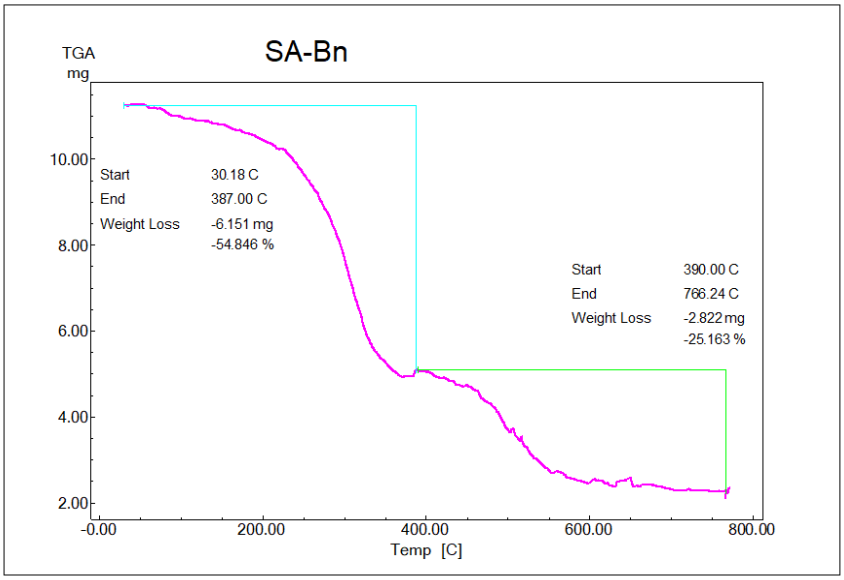

Figure 3-6:TGA curve of the SA-Bn .

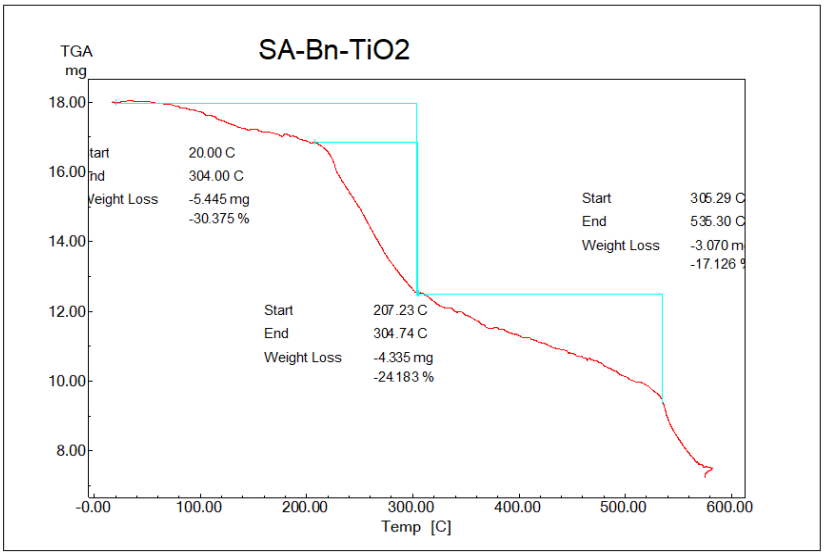

Figure 3-7:TGA curve of the SA-Bn-TiO_2 NPs .

3-1-5 X-Ray Diffraction (XRD)

The XRD pattern of nano-composite displays diffracting lines corresponding to a)TiO_2NPs ,b)SA-Bn-TiO_2, c)SA-Bn , and d)Bentonite clay , as shown in (Figure 3-8).The minor variations in the Bentonite clay peaks intensities could be associated with the interface between TiO_2NPs . Moreover, strong peaks were observed in the 2θ range 25◦–75◦ ,which agreed with TiO_2 NPs. In particular, the several strong peaks detected at nearly 25◦,37◦ ,48◦, 54◦, 55◦ 63◦ indicated TiO_2NPs .The XRD of SA-Bn-TiO_2 shows the crystalline peaks at 25◦, 37◦, 48 ◦, and 54◦, which confirm the presence of phase of TiO_2 NPs [95]. The XRD patterns of SA-Bn-TiO_2 NPs showed all the peaks observed of TiO_2 which confirm the incorporation of TiO_2 within SA-Bn-TiO_2 NPs hydrogel matrix . with a little bit of reduced intensity and the peaks became slightly wider because of the coating of amorphous hydrogel shell. X-ray diffraction patterns of both SA-Bn and its nano composite with TiO_2 shown in Figure 3-8,which indicates that SA-Bn is amorphous but its SA-Bn-TiO_2NPs seems to be nano-crystalline materials that are clear from the peaks present in the broadband in the case of a composite [96].

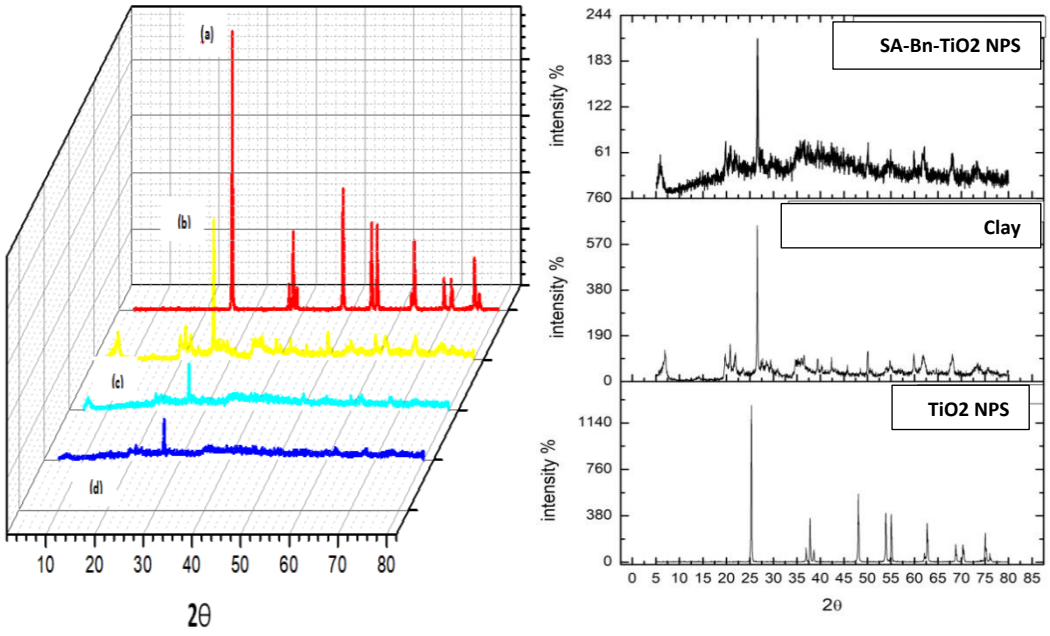

Figure 3-8. X-ray diffraction patterns for (a) TiO_2 NPs, (b) SA-Bn-TiO_2 NPs,(c) SA-Bn, d) Clay Bentonite .

3-2 Applications of Prepared SA-Bn-TiO2 NPs

3-2-1 Effect of Contact Time

Contact time is very important factor affecting the efficiency of adsorption. To study the removal of three pollutants (CR, AMX, CPH) using absorbense SA-Bn-TiO_2NPs analysis is carried out using the previously determined optimum value of pH(6.6), mass dosage (0.05g) and initial concentration(100mg/L) [97]. In this batch study samples were taken at different interval ranging from 2 to 120 minutes. The maximum adsorption occurs within 60 minutes (Figure 3-9) due a large number of surface sites are available for adsorption but after sometime,. the remaining surface sites are difficult to be occupied. The optimized value of agitation time is 60 minutes after which the adsorption becomes constant [98, 99].

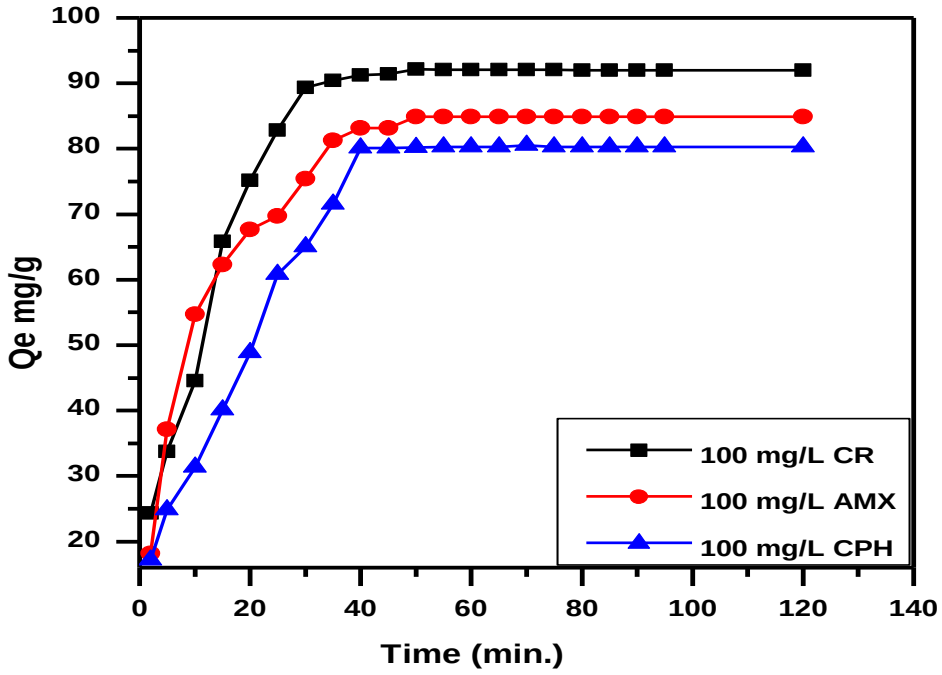

Figure (3-9) Effect of contact time on adsorption capacity for removal of Three pollutant (CR,AMX, CPH) by SA-Bn-TiO_2 NPs at pH 6.6, Temp. 30 ^{o}C and mass adsorbent 0.05 g .

3-2-2 Adsorbent Dose:

The effect of the amount of the adsorbents was necessary to observe the minimum possible amount, which shows the maximum adsorption stoichiometric. The amounts of the adsorbent was varied from 0.02 to 0.1 g/100 mL of SA-Bn-TiO_2 NPs. The results are illustrated in Table (3-1) and shown in Figures (3-10),(3-11) and (3- 12).

Table (3-1): Effect of adsorbent dose on the removal percentage of three pollutant on to SA-Bn-TiO_2 NPs .

WT	CR			AMX			CPH		
	C_e/ mg/L	Q_e/ $mg.g^{-1}$	E%	C_e/ mg/L	Q_e/ $mg.g^{-1}$	E%	C_e/ mg/L	Q_e/ $mg.g^{-1}$	E%
0.02	41.7938	291.035	58.206	57.189	214.051	42.810	40.49	297.549	59.509
0.03	17.2008	275.699	82.709	34.086	219.712	65.913	34.901	216.993	65.098
0.05	7.90076	184.198	92.099	15.120	169.758	84.879	19.705	160.588	80.294
0.08	5.3587	118.301	94.641	12.258	109.676	87.741	15.490	105.637	84.509
0.1	2.0839	97.916	97.916	9.258	90.741	90.741	8.925	91.075	91.075

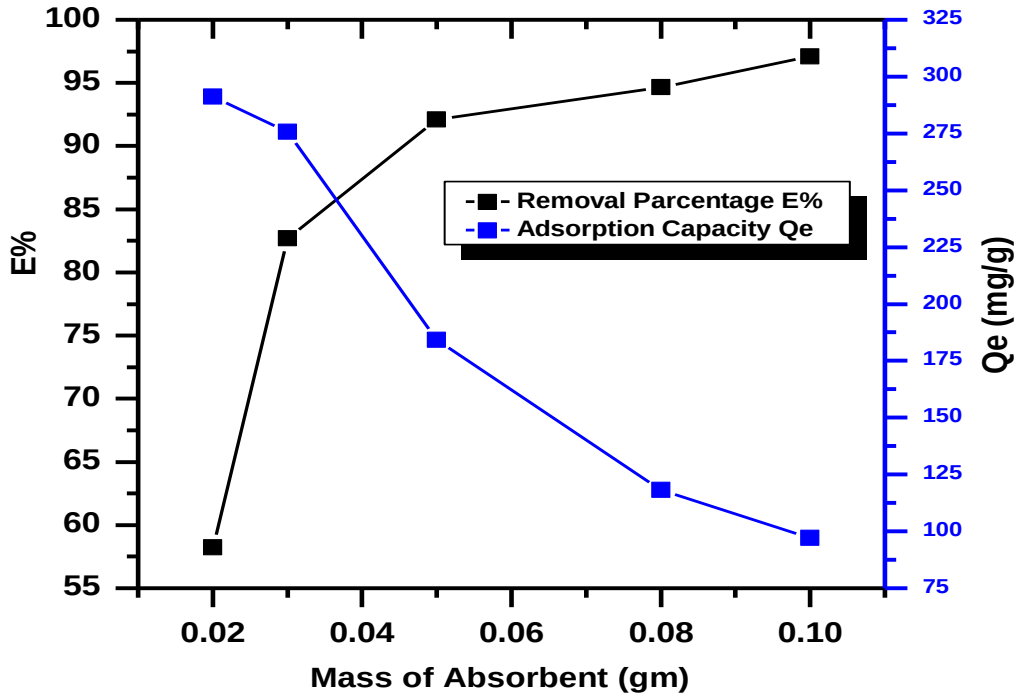

Figure (3-10): Effect of the mass amount of adsorbent SA-Bn-TiO_2 NPs on the percent removal and amount of adsorbed CR dye, initial concentration = 100 $mg.L^{-1}$, Temp. = 30°C, contact time 1hr., pH=6.6.

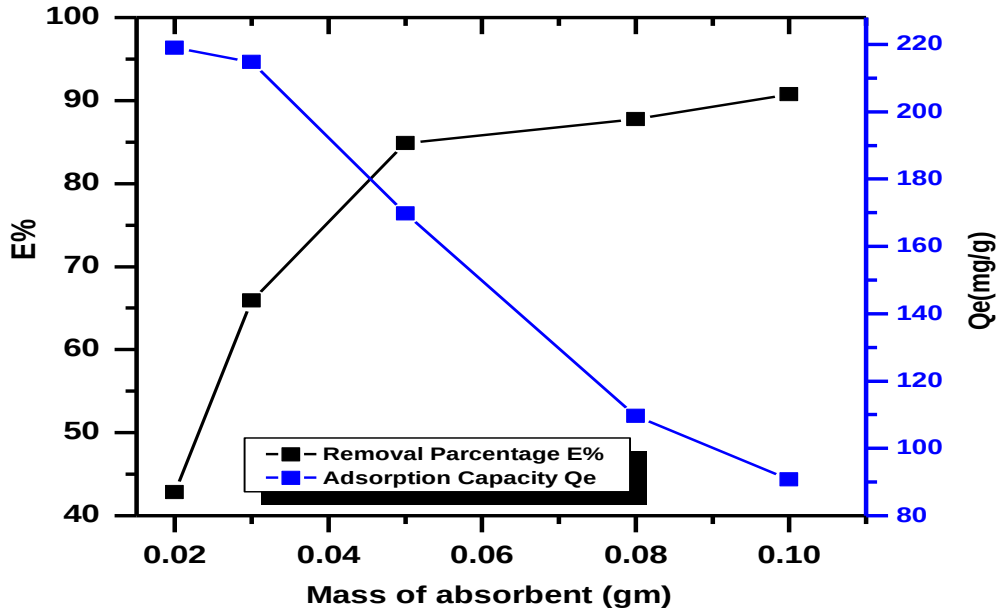

Figure (3-11): Effect of the mass amount of adsorbent SA-Bn-TiO_2 NPs on the percent removal and amount of adsorbed AMX drug, initial concentration = 100 $mg.L^{-1}$, Temp. = 30°C, contact time 1hr., pH=6.6.

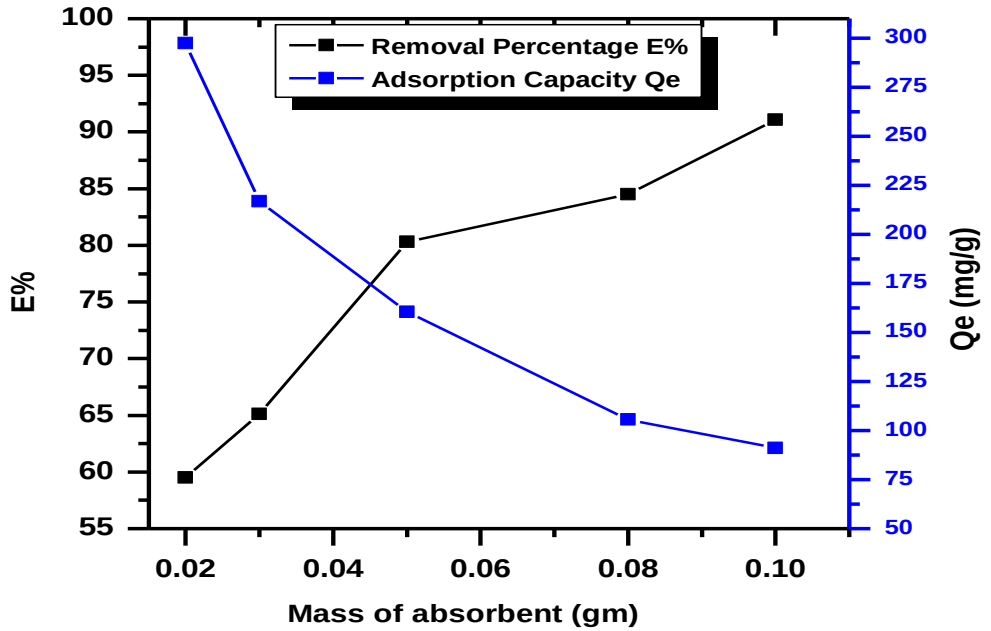

Figure (3-12): Effect of the mass amount of adsorbent SA-Bn-TiO2 NPs on the percent removal and amount of adsorbed CPH, initial concentration = 100 $mg.L^{-1}$, Temp. = 30°C, contact time 1hr., pH=6.6.

An increase in the removal percentage of the pollutants(CR, AMX, CPH) removal with adsorbent mass was related to increases in the adsorbent surface areas, enhancing the number of adsorption sites available for adsorption as reported already in other cases. The increase in removal of pollutants(CR, AMx, CPH) with adsorbent dose due to the introduction of more binding sites for adsorption [100, 101]. The primary factor explaining this characteristic is that adsorption sites remain unsaturated during the adsorption reaction whereas the number of sites available for adsorption site increases by increasing the adsorbent dose [64, 102].

3-2-3 Effect of pH

The effect of pH on the adsorption of three pollutant onto SA-Bn-TiO_2 NPs was studied at a pH range of (3-10) in the presence of initial concentrations (100 $mg.L^{-1}$). Results are given in Table (3-6) and shown in Figures 3-13 , 1-14 and 3-15.

Table (3-2): Effect of solution pH on adsorption three pollutant (CR, AMX, CPH) by SA-Bn-TiO_2 NPs

pH	CR			AMX			CPH		
	C_e/ mg/L	Q_e/ $mg.g^{-1}$	E%	C_e/ mg/L	Q_e/ $mg.g^{-1}$	E%	C_e/ mg/L	Q_e/ $mg.g^{-1}$	E%
3	51.946	96.106	48.053	71.844	53.103	28.155	61.274	77.45	38.721
4	7.9007	184.198	92.099	51.327	97.344	48.672	45.882	108.23	54.119
6	5.862	188.278	94.137	51.293	169.41	84.706	19.703	160.58	80.298
8	4.916	190.167	95.083	12.8103	174.37	87.189	13.039	173.92	86.965
10	2.816	194.366	97.183	5.362	189.27	94.637	6.666	186.66	93.336

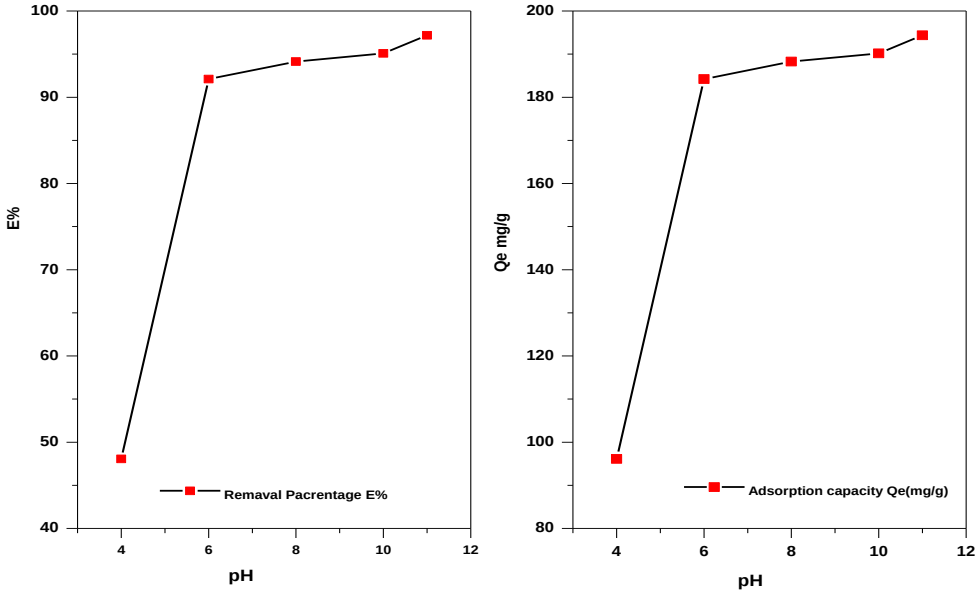

Figure (3-13): Effect of solution pH on the adsorption of CR dye on SA-Bn-TiO_2 NPs. (Exp. Condition: Temp. = 30°C, contact time 1 hr).

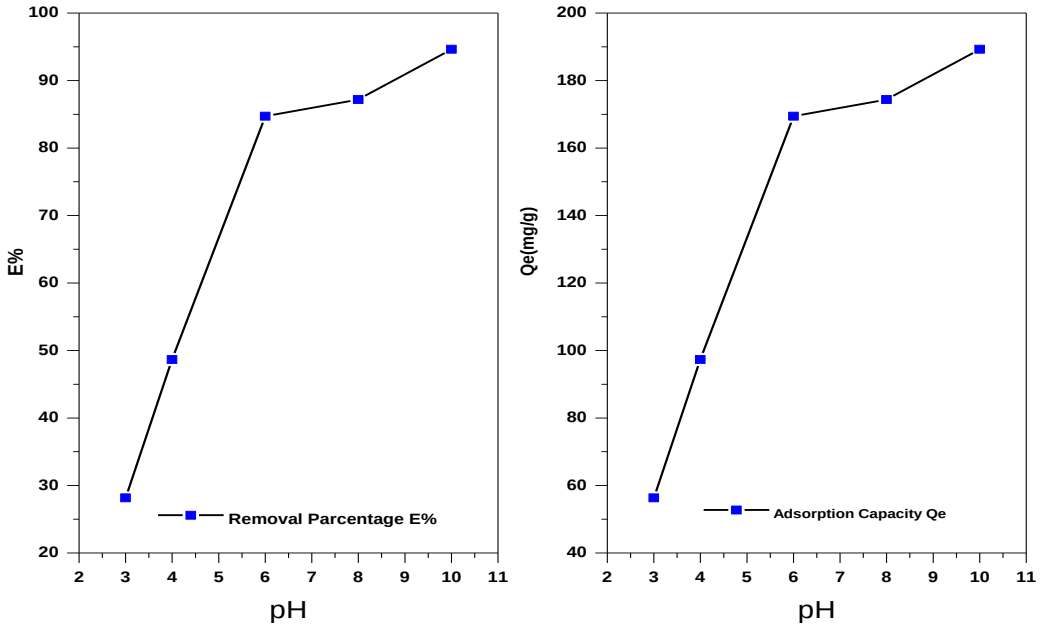

Figure (3-14): Effect of solution pH on the adsorption of AMX drug on SA-Bn-TiO_2 NPs. (Exp. Condition: Temp. = 30°C, contact time 1 hr).

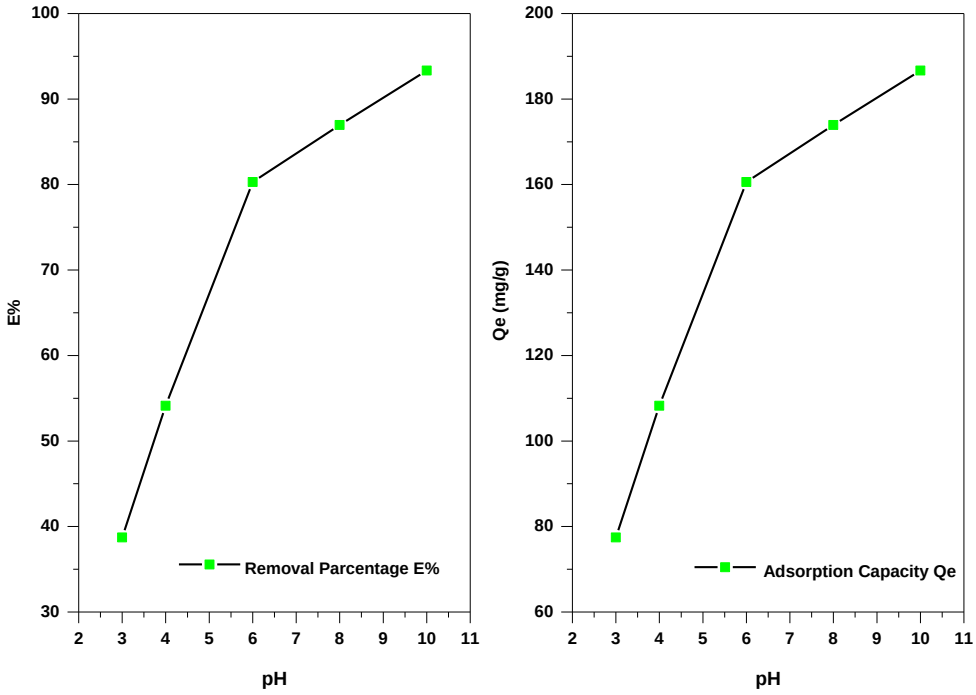

Figure (3-15): Effect of solution pH on the adsorption of CPH on SA-Bn-TiO2 NPs. (Exp. Condition: Temp. = 30°C, contact time 1 hr).

The equilibrium sorption capacity of three pollutants (CR, AMX, CPH) on SA-Bn-TiO_2 NPs very little in the pH 3 , the adsorption capacity of pH 3 SA-Bn-TiO_2 NPs equal (96.106 mg/g, 56.310 mg/g, 77.45mg/g) at the same order, which suggests that SA-Bn-TiO2 NPs are excellent adsorbents for pollutant removal from large volumes of aqueous solutions[103, 104]. When the pH is greater than 6 the sorption capacity of three pollutant on SA-Bn-TiO_2 NPs increases with increasing pH values as appear in Figure (3-13 to 3-15), the removal of three pollutants from aqueous solution by SA-Bn-TiO_2 NPs is highly pH-dependent. The results show maximum adsorption of three pollutants between pH(6-10). the adsorption capacity (qe) increase with increasing pH. Lower adsorption at acidic pH is probably due to the presence of excess H^+ ions

competing with the cation groups on the three pollutants for adsorption sites . At higher pH, the surface may get positively charged, which enhances the negatively charged three pollutants anion through electrostatic forces of attraction [105, 106].

3-2-4 Effect of temperature

To determine whether the ongoing adsorption process was endothermic or exothermic. The adsorption isotherms were determined for various pollutants-adsorbent systems. The removal of CR,AMX and CPH has been studied at different temperature (10-40 ^{o}C) in the presence of various initial concentrations (10-100 mg.L^{-1}) results are illustrated in Tables (3-3,3-4 & 3-5), and presented in Figures (3-16, 3-17 & 3-18) .

Table (3-3)Adsorption isotherm for adsorption of CR dye on the SA-Bn-TiO_2 NPs at different temperatures. (pH 6.6, mass adsorbent 0.05 gm/ 100 ml, contact time 1hr).

C_0 mg.L^{-1}	10 ^{o}C			20 ^{o}C			30 ^{o}C			40^{o}C		
	C_e mg.L^{-1}	Q_e mg.g^{-1}	E %	C_e mg.L^{-1}	Q_e mg.g^{-1}	E %	C_e mg.L^{-1}	Q_e mg.g^{-1}	E%	C_e mg.L^{-1}	Q_e mg.g^{-1}	E%
10	0.778	18.442	92.213	0.618	18.763	93.81	0.358	19.282	96.41	0.275	19.44	97.24
20	1.7099	36.580	91.450	1.374	37.251	93.12	0.961	38.076	95.19	0.786	38.42	96.06
40	3.5832	72.833	91.041	3.573	72.854	91.06	1.971	76.056	95.07	1.709	76.58	95.72
50	6.2061	87.587	90.587	4.511	90.977	90.97	2.891	94.213	94.21	2.488	95.02	95.02
60	7.053	105.89	88.244	6.206	107.58	89.65	3.832	112.33	93.61	3.236	133.52	94.60
70	8.135	122.65	88.011	7.432	132.73	89.45	4.456	122.54	93.034	3.043	122.54	94.34
80	9.656	140.68	87.92	8.755	142.48	89.05	6.114	147.77	92.35	4.427	151.14	94.26
100	11.183	177.63	86.65	10.419	179.16	88.58	7.900	184.18	92.09	6.645	186.7	93.35

Table (3-4)Adsorption isotherm for adsorption of AMX drug on the SA-Bn-TiO2 NPs at different temperatures. (pH 6.6, mass adsorbent 0.05 gm/ 100 ml, contact time 1hr).

C_0 mg.L^{-1}	10 °C			20 °C			30 °C			40°C		
	C_e mg.L^{-1}	Q_e mg.g^{-1}	E %	C_e mg.L^{-1}	Q_e mg.g^{-1}	E %	C_e mg.L^{-1}	Q_e mg.g^{-1}	E%	C_e mg.L^{-1}	Q_e mg.g^{-1}	E%
10	0.9655	18.068	90.34	0.579	18.84	94.20	0.1896	19.62	98.10	0.068	19.86	99.31
20	2.103	35.793	89.48	1.534	36.93	92.32	1.155	37.68	94.22	0.965	38.06	95.17
40	5.172	69.655	87.06	3.637	72.72	90.90	2.672	74.65	93.31	1.931	76.13	95.07
50	7.448	85.103	85.10	5.534	88.93	88.93	5.362	89.27	89.27	3.258	93.48	93.48
60	11.224	97.551	81.29	7.413	105.17	87.64	7.275	105.4	87.87	5.172	109.6	91.37
70	13.609	112.79	80.56	9.965	120.06	85.38	9.362	`121.2	86.62	8.034	123.9	88.52
80	16.844	126.31	78.94	11.689	136.62	84.28	11.275	137.44	85.90	10.15	139.6	87.30
100	21.51	175.10	78.51	18.913	162.16	81.08	15.12	169.75	84.87	11.39	181.2	86.21

Table (3-5)Adsorption isotherm for adsorption of CPH on the SA-Bn-TiO2 NPs at different temperatures. (pH 6.6, mass adsorbent 0.05 gm/ 100 ml, contact time 1hr).

C_0 mg.L^{-1}	10 °C			20 °C			30 °C			40°C		
	C_e mg.L^{-1}	Q_e mg.g^{-1}	E%	C_e mg.L^{-1}	Q_e mg.g^{-1}	E %	C_e mg.L^{-1}	Q_e mg.g^{-1}	E%	C_e mg.L^{-1}	Q_e mg.g^{-1}	E%
10	0.588	18.823	94.11	0.3921	19.215	96.07	0.0980	19.80	99.019	0.1960	19.607	98.039
20	5	30	75	3.333	33.333	90.45	1.1078	37.78	94.46	0.7941	38.411	96.029
40	6.666	66.666	83.33	5.4901	69.019	87.26	3.284	73.43	91.789	1.2304	77.539	95.876
50	7.549	84.901	84.90	6.6666	86.666	86.66	5.480	89.03	89.039	3.735	92.529	92.523
60	12.15	96.686	79.73	9.5098	100.986	84.15	7.745	104.5	87.091	5.5784	108.84	90.529
70	12.15	111.176	79.41	13.039	113.92	81.37	11.078	117.8	84.173	8.8235	122.35	87.394
80	14.41	124.902	78.06	15.392	129.215	80.75	14.215	131.6	82.234	13.529	132.94	83.085
100	17.5	157.843	77.88	20.098	159.803	79.90	19.705	160.5	80.294	18.627	162.74	81.373

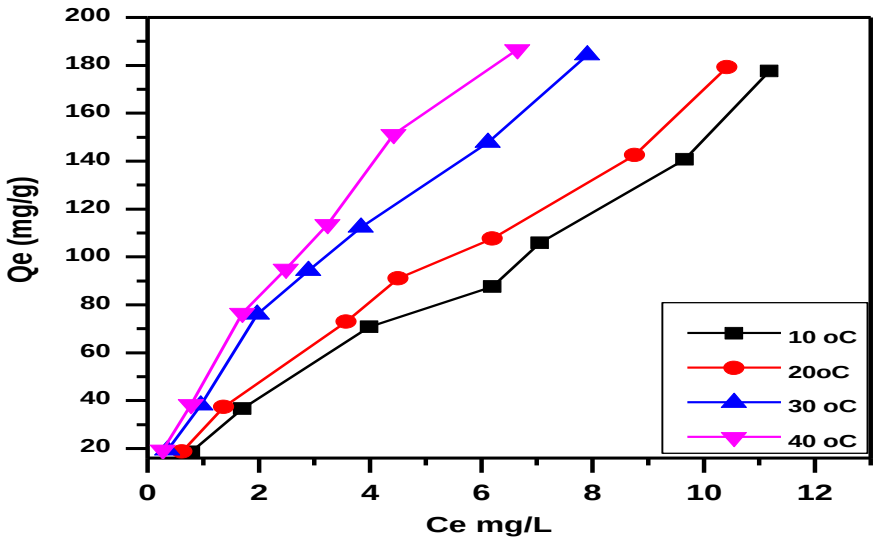

Figure (3-16) Effect of temperature on the adsorption of CR dye on the surface of SA-Bn-TiO2 NPs . (pH 6.6, mass adsorbent 0.05 gm/ 100 ml).

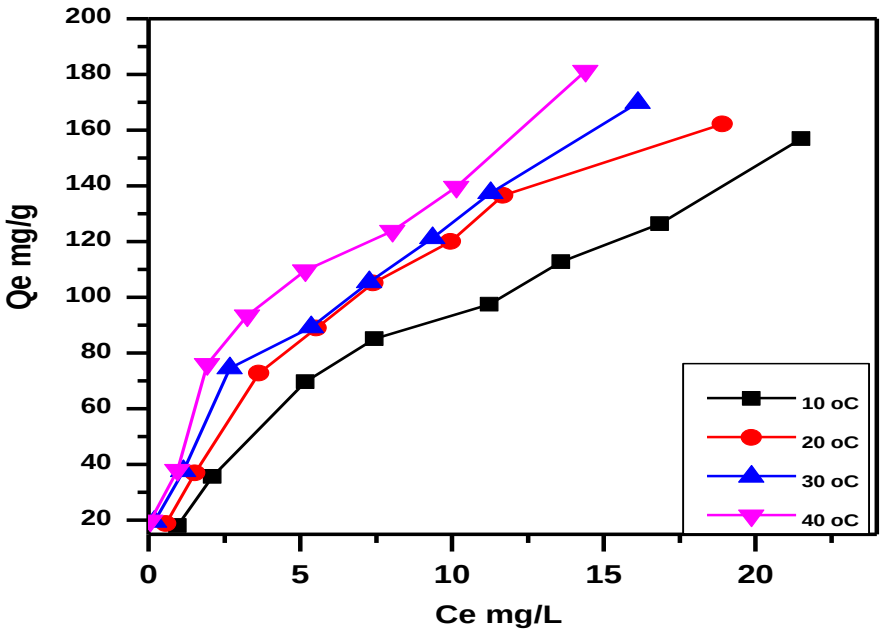

Figure (3-17) Effect of temperature on the adsorption of AMX drug on the surface of SA-Bn-TiO2 NPs . (pH 6.6, mass adsorbent 0.05 gm/ 100 ml) .

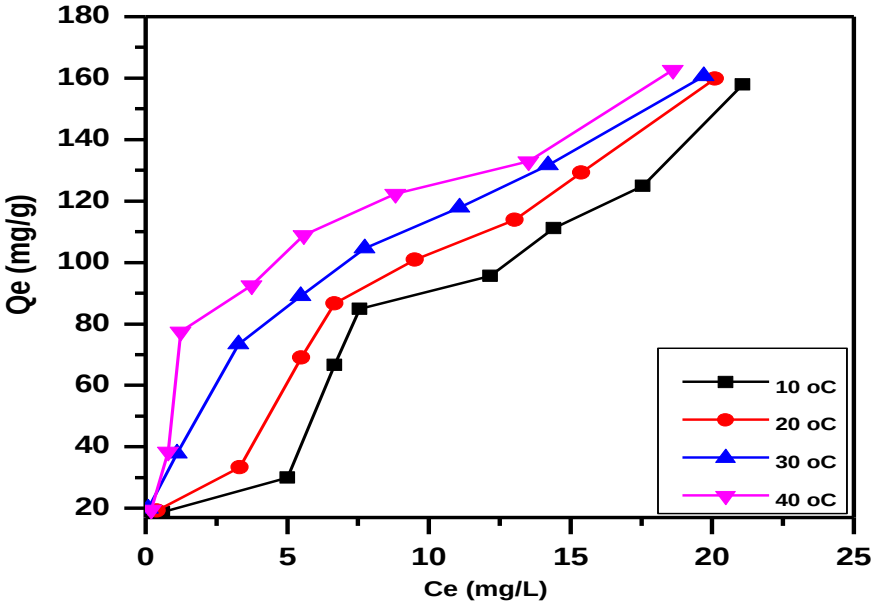

Figure (3-18) Effect of temperature on the adsorption of CPH on the surface of SA-Bn-TiO2 NPs . (pH 6.6, mass adsorbent 0.05 gm/ 100 ml) .

The result shows that the equilibrium adsorption capacity of CR , AMX and CPH wear increased while increasing the solution temperature for all initial concentrations. As generally observed from Figures. (3.16-3.18), the uptake capacity of SA-Bn-TiO_2 NPs increases with increasing temperature, due to the enhanced magnitude of the reverse (desorption) step in the mechanism. This is possibly due to the endothermic effect of the surroundings during the adsorption process [107].

The study of the temperature effect on adsorption will also help in the calculation of the basic thermodynamic functions such as Gibbs free energy (ΔG), change enthalpy (ΔH), and change entropy (ΔS) of the adsorption process [108]. The equilibrium constant (K_e) of the adsorption process at each temperature, was calculated from the equations (3-1) [109]:

$$K_e = \frac{(Q_{max}) * Wt\ (0.05\ gm)}{(C_e) * V(0.1L)} \times 1000 \qquad (3-1)$$

Where Q_{max} is the amount adsorbed in ($mg.gm^{-1}$), C_e is the equilibrium concentration of the adsorbent expressed in ($mg.L^{-1}$), 0.05 gm represents the weight of the SA-Bn-TiO_2 NPs adsorbent, and 0.1L represents the volume of the three pollutant (CR, AMX, CPH) solution used in the adsorption process [64]. The change in the free energy could be determined from the equation (3-2) :[64]

$$\Delta G = -RT \ln K_e \qquad 3-2$$

Where ΔG: Gibbs free energy ($J.K^{-1}.mol.^{-1}$), R is the gas constant (8.314 $J.K^{-1}.mole^{-1}$), T is the absolute temperature in Kelvin.

The enthalpy of adsorption may be obtained from the following equation (3-3) [43]:

$$\ln X_m = -\frac{\Delta H}{RT} + Cons. \qquad 3-3$$

When $X_{m:}$ is the maximum value of adsorption at a certain value of equilibrium concentration (C_e). Table (3-6) ,(3-7) and (3-8) gives X_m values at different temperatures for (CR, AMX and CPH) at the seam order . Plotting $\ln X_m$ versus (1/T) should produce a straight line with a slope -ΔH/R as shown in Figures (3-19 ,3-20 & 3-21) The value of ΔH and ΔS can be calculated from the slope and intercept respectively [110].

Table (3-6) Maximum adsorption quantity Xm values of CR dye onto SA-Bn-TiO_2 NPs surfaces at different temperatures.

T(K)	1000/T(K^{-1})	C_e = 6.5	
		X_m	ln X_m
283	3.5335	95	4.5538
293	3.4129	112	4.7184
303	3.3003	159	5.0689
313	3.1948	185	5.2203

Table (3-7) Maximum adsorption quantity Xm values of AMX drug onto SA-Bn-TiO_2 NPs surfaces at different temperatures.

T(K)	1000/T(K^{-1})	C_e = 14.3	
		X_m	ln X_m
283	3.5335	115	4.7449
293	3.4129	145	4.9767
203	3.3003	155	5.0434
313	3.3194	180	5.1929

Table (3-8) Maximum adsorption quantity Xm values of CPH onto SA-Bn-TiO_2 NPs surfaces at different temperatures.

T(K)	1000/T(K^{-1})	C_e = 19	
		X_m	ln X_m
283	3.5335	135	4.9052
293	3.4129	150	5.0106
303	3.3003	155	5.0434
313	3.3194	160	5.0751

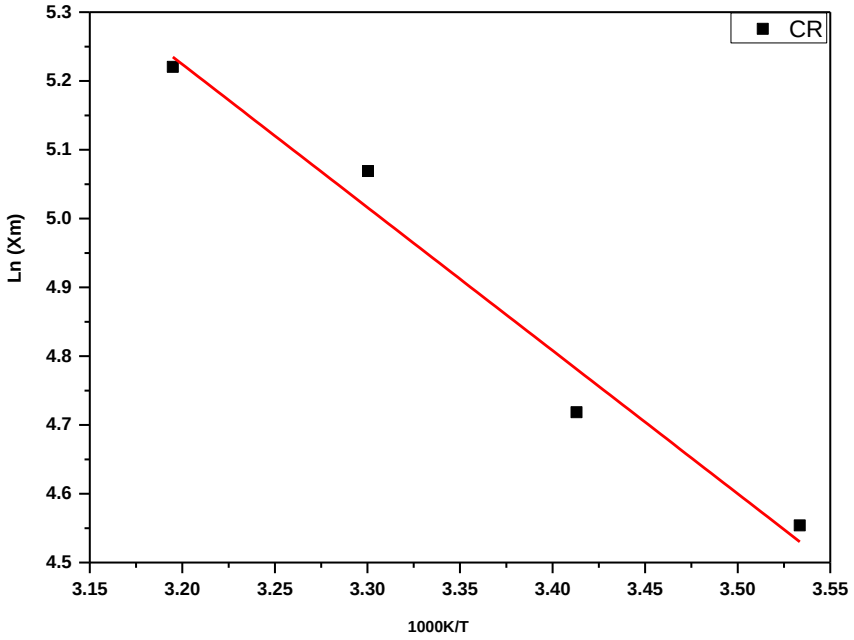

Figure (3-19) Plot ln X_m against the absolute temperature. of the adsorption (CR dye) onto SA-Bn-TiO_2 NPs .

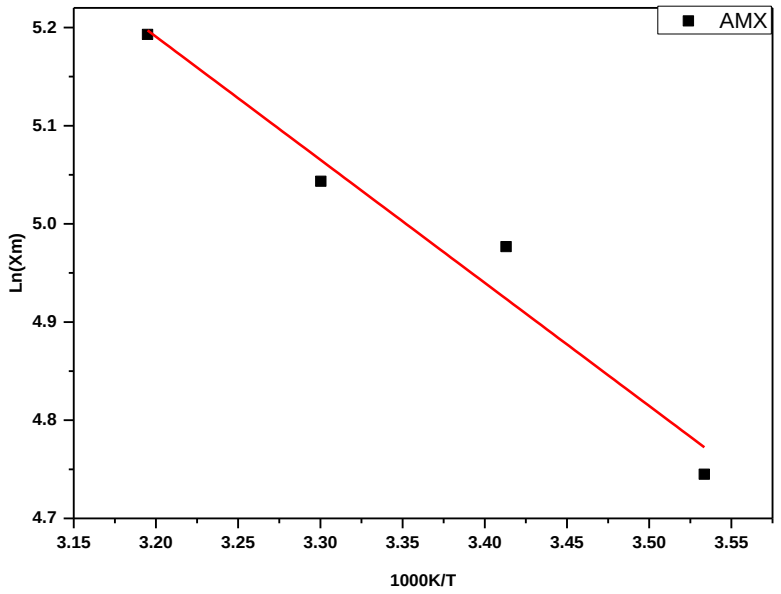

Figure (3-20) Plot ln X_m against the absolute temperature. of the adsorption (AMX drug) onto SA-Bn-TiO_2 NPs .

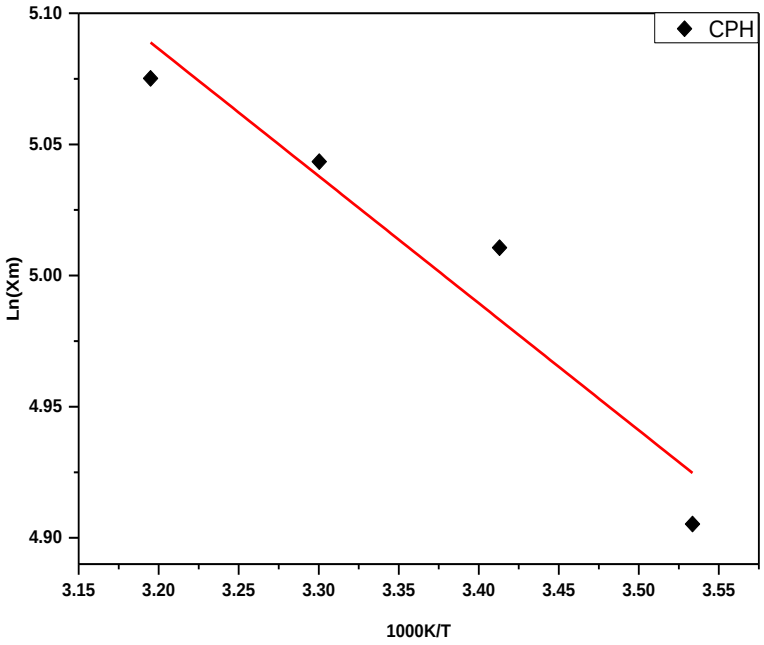

Figure (3-21) Plot ln X_m against the absolute temperature. of the adsorption (CPH) onto SA-Bn-TiO_2 NPs .

The quantitative thermodynamic data of CR and AMX and CPH on the adsorbent surfaces Bn-TiO_2 NPs are presented in Table 3.9. The Table 3.9 shows the ΔH values of CR and AMX and CPH are positive indicating that the adsorption process is endothermic reaction. All process of adsorption considered spontaneous from the negative value of ΔG. While, ΔS have positive value for CR and AMX and CPH that refer the interaction of molecules caused random of the total system [111, 112].

From results in Table 3.9, the enthalpy change ΔH and entropy change ΔS for adsorption are assumed to be temperature independent The enthalpy of the adsorption ΔH is a measure of the energy barrier that must be overcome by reacting molecules [113, 114]..

Table 3.9: Thermodynamic functions ΔG, ΔS and, ΔH of CR, AMX and CPH adsorbed on the SA-Bn-TiO_2 NPs .

SA-Bn-TiO2 NPs adsorbent/ CR adsorbate				
Thermodynamics parameters / T/K	K_e	ΔG/ kJ.mol^{-1}	ΔH/ kJ.mol^{-1}	ΔS/ J.K^{-1}.mol^{-1}
283	14615.38	-22.563	17.298	98.786
293	17230.77	-23.761		
303	24461.54	-25.455		
313	28461.54	-26.689		
SA-Bn-TiO2 NPs adsorbent/ AMX adsorbate				
Thermodynamics parameters / T/K	K_e	ΔG/ kJ.mol^{-1}	ΔH/ kJ.mol^{-1}	ΔS/ J.K^{-1}.mol^{-1}
283	8041.95	-21.157	10.424	76.563
293	22307.69	-24.390		
303	23846.15	-25.391		
313	27692.31	-26.618		
SA-Bn-TiO2 NPs adsorbent/ CPH adsorbate				
Thermodynamics parameters / T/K	K_e	ΔG/ kJ.mol^{-1}	ΔH/ kJ.mol^{-1}	ΔS/ J.K^{-1}.mol^{-1}
283	7105.263	-20.8666	4.029	55.1816
293	7894.737	-21.8606		
303	8157.895	-22.6893		
313	8421.055	-23.5207		

3-3 A Comparative adsorption between different surfaces to removal pollutant :

A Comparative study between (Titanium dioxide (TiO_2), Sodium alginate- Bentonite (SA-Bn), Sodium alginate- Bentonite- Titanium dioxide (SA-Bn-TiO_2 NPs)) surfaces as Adsorbents wear carried out. A sample of 100 mL of (CR, AMX, CPH) concentration(100 $mg.L^{-1}$) are used in this study, then added to a conical flask (Erlenmeyer) in the presence of 0.05g from prepared (TiO_2 NPs, SA-Bn , SA-Bn-TiO2 NPs), and put in a shaker water bath for 1 hr., after that the supernatant was separated by centrifuge and measured the remaining concentration by using UV-Visible spectrophotometer at the λmax nm [115, 116] .

The best results of the percentage of removal (E%) for (CR, AMX, CPH) the order increasing: (SA-Bn-TiO2 NPs) > (SA-Bn), > TiO_2NPs shows in Figure (3-22), (3-23),(3-24) .

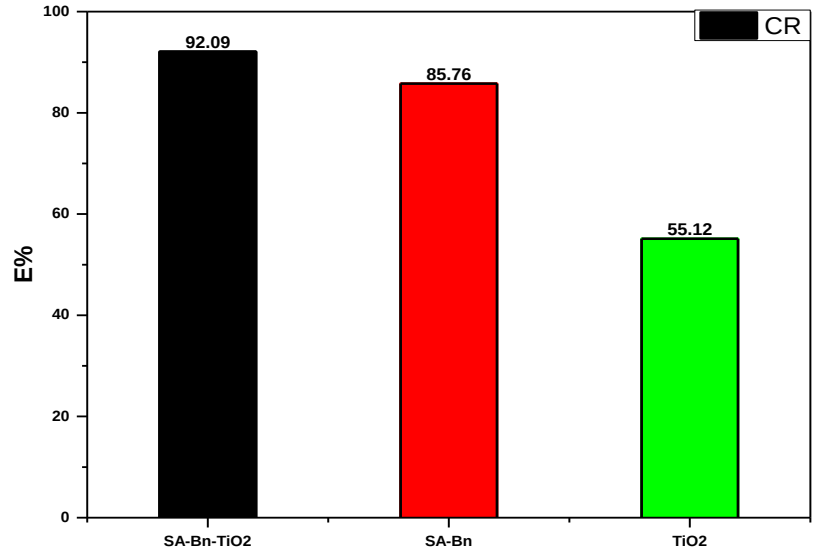

Figure (3-22): Effect comparative between (SA-Bn-TiO_2 NPs) , (SA-Bn), TiO_2NPs onto CR dye .(Exp. Condition: mass of absorbent 0.05 g, conc. 100 $mg.L^{-1}$ Temp. = 30°C, contact time 1 hr, and pH of solution 6.6) .

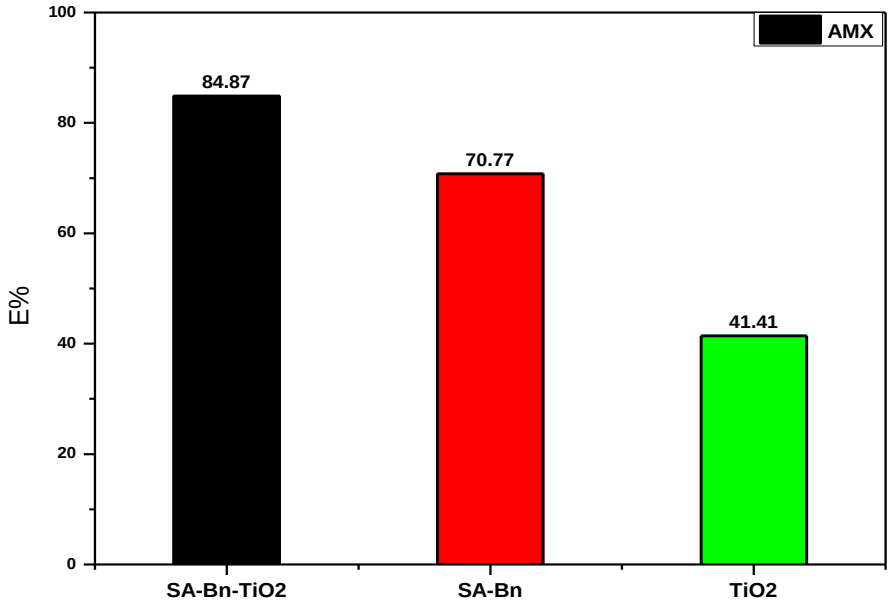

Figure (3-23): Effect comparative between (SA-Bn-TiO2 NPs) , (SA-Bn), TiO_2NPs onto AMX drug .(Exp. Condition: mass of absorbent 0.05 g, conc. 100 $mg.L^{-1}$ Temp. = 30°C, contact time 1 hr, and pH of solution 6.6) .

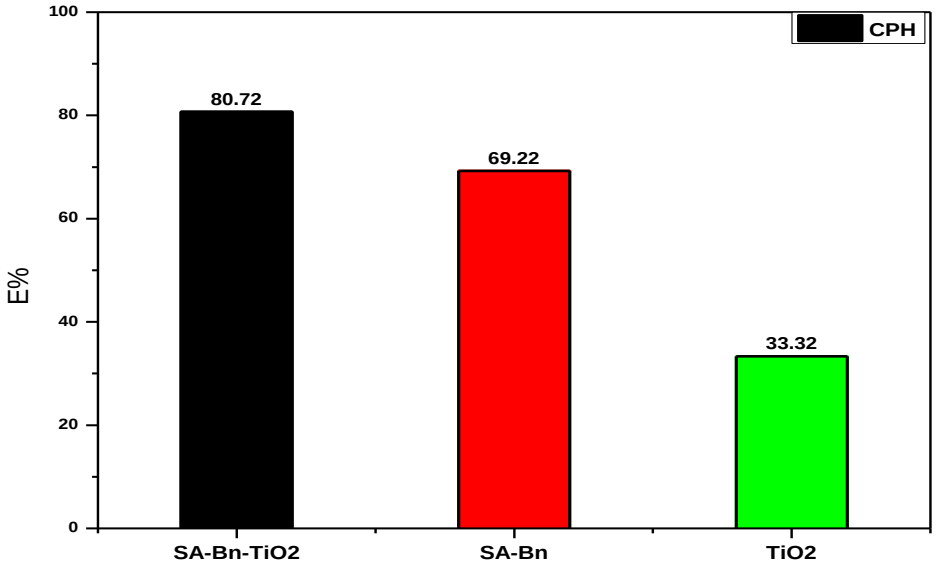

Figure (3-24): Effect comparative between (SA-Bn-TiO_2 NPs) ,(SA-Bn), TiO_2NPs onto AMX drug .(Exp. Condition: mass of absorbent 0.05 g, conc. 100 $mg.L^{-1}$ Temp. = 30°C, contact time 1 hr, and pH of solution 6.6) .

3-4 Removal of Pollutants by Using SA-Bn-TiO2 NPs

A laboratory sample 100 mL of pollutants (drugs , dyes and phenolic compound) with a refry concentration were using in this study, then added to a conical flask (Erlenmeyer) in the presence of 0.05 g from prepared SA-Bn-TiO_2 NPs , after that the mixture were putting in a Shaker water bath for 1 hr, after that the supernatant were separated by centrifuge and measured the remaining concentration by using UV-Visible spectrophotometer at the λmax 495 nm, 272nm and 270 nm for CR , AMX and CPH at the same order [116, 117] the result shows in figure (3-25), figure (3-26).and figure (3-27).

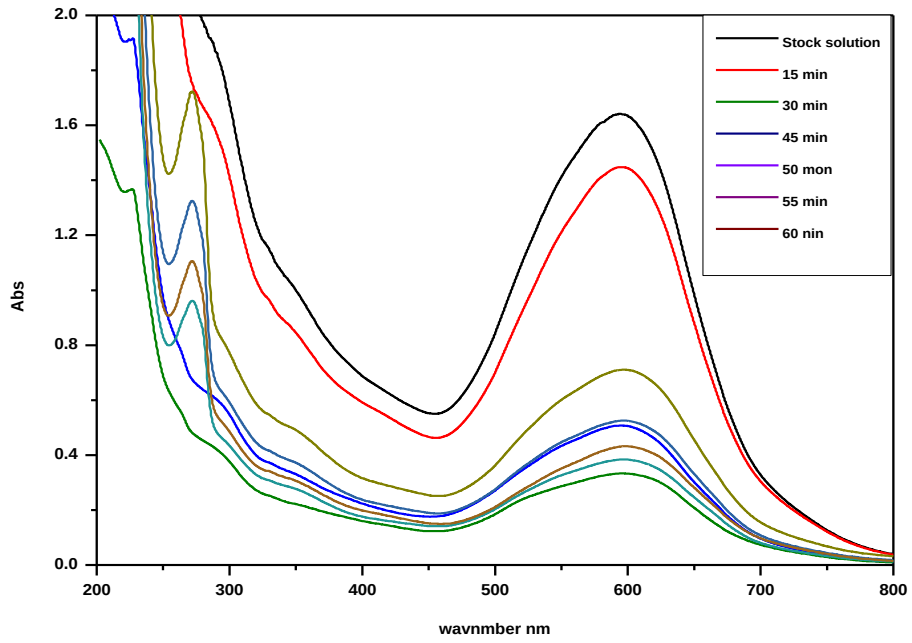

Figure (3-25): Spectra of removal several pollutant (dyes , drug and phenolic compound) by Using SA-Bn-TiO_2 NPs (Exp. Condition: Temp. = 30°C, contact time 1 h, and pH of solution 6.6).

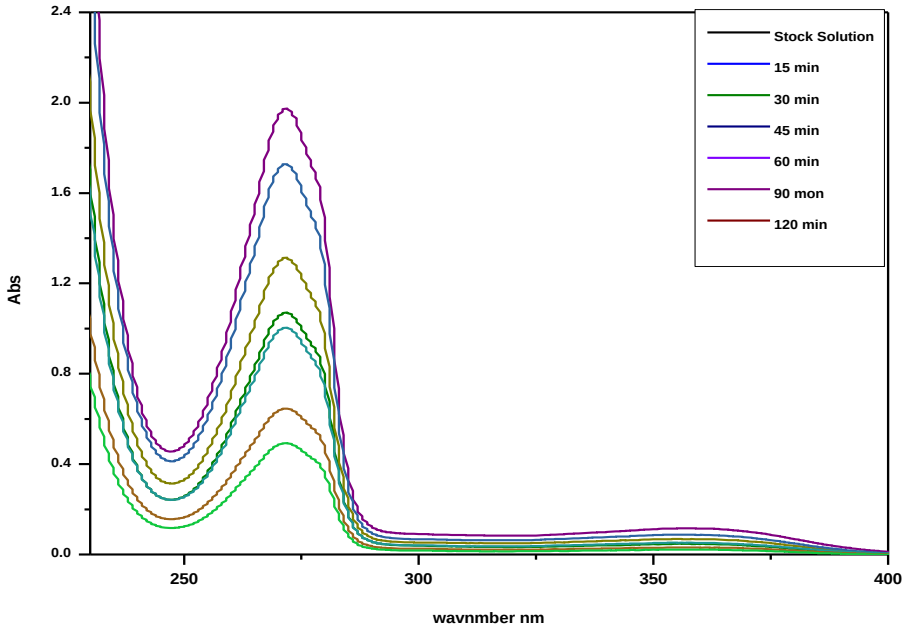

Figure (3-26): Spectra of removal several drug by Using SA-Bn-TiO_2 NPs (Exp. Condition: Temp. = 30°C, contact time 1 h, and pH of solution 6.6).

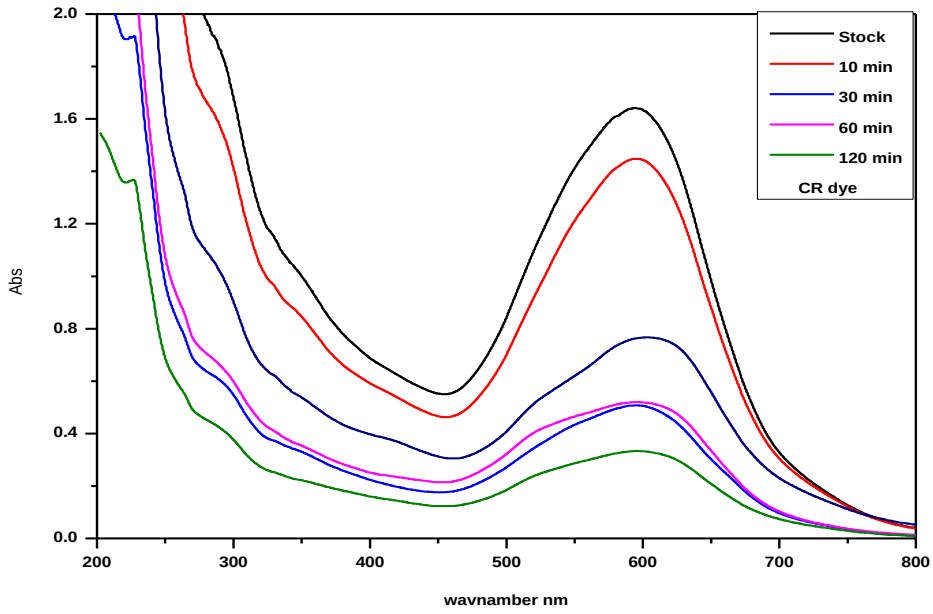

Figure (3-27): Spectra of removal several dyes by Using SA-Bn-TiO_2 NPs (Exp. Condition: Temp. = 30°C, contact time 1 h, and pH of solution 6.6).

3-5 Regeneration of SA-Bn-TiO2 NPs

The regeneration of hydrogels ,after sorption, is one of the significant economic factors for the treatment process. It helps in elucidating the mechanism of pollutants (CR,AMX, CPH) removal from pollutant-loaded adsorbent, regeneration mechanism and recycling of spent adsorbents, which in turn may reduce operational cost and protect the environment from secondary pollution. pollutants (CR ,AMX, CPH) desorption studies were carried out using different desorption agents at different concentration (0.01, 0.05, 0.1 N) such as H_2SO4, NaOH, H_3PO_4 , HCl , HNO_3, ethanol , methanol and water [118, 119]. The SA-Bn-TiO_2 NPs was regeneration with 100% by using water as shown in Table (3-10), (3-11) and (3-12) .

Table(3-10): Comparative of desorption efficiency of several type solution for the CR dye onto surface of SA-Bn-TiO2 NPs .

Regeneration and Desorption (0.01N)	E%	**Regeneration and Desorption** (0.05 N)	E%	**Regeneration and Desorption**(0.1 N)	E%
fresh	92.09	Fresh	92.09	Fresh	92.09
water	92.09	water	92.09	water	92.09
Ethanol	80.12	Ethanol	88.87	Ethanol	90.11
H_3PO_4	82.23	H_3PO_4	80.22	H_3PO_4	77.98
HCl	78.77	HCl	70.77	HCl	66.65
H_2SO_4	75.66	H_2SO_4	68.11	H_2SO_4	55.54
HNO_3	66.9	HNO_3	59.65	HNO_3	40.03
Methanol	60.11	Methanol	57,56	Methanol	39.11
NaOH	52.11	NaOH	40.2	NaOH	32.65

Table 3-11: Comparative of desorption efficiency of several type solution for the AMX drug onto surface of SA-Bn-TiO_2 NPs .

Regeneration and Desorption (0.01N)	E%	**Regeneration and Desorption** (0.05 N)	E%	**Regeneration and Desorption**(0.1 N)	E%
fresh	84.87	Fresh	84.87	Fresh	84.87
water	84.87	water	84.87	water	84.87
Ethanol	80.22	Ethanol	82.87	Ethanol	83.11
H_3PO_4	77.34	H_3PO_4	75.87	H_3PO_4	66.67
HCl	70.77	HCl	67.87	HCl	60.09
H_2SO_4	65.77	H_2SO_4	56.76	H_2SO_4	50.45
HNO_3	60.55	HNO_3	49.98	HNO_3	42.87
Methanol	55.11	Methanol	44.56	Methanol	35.01
NaOH	50.11	NaOH	42.44	NaOH	33.3

Table(3-12): Comparative of desorption efficiency of several type solution for the CPH onto surface of SA-Bn-TiO_2 NPs .

Regeneration and Desorption (0.01N)	E%	**Regeneration and Desorption** (0.05 N)	E%	**Regeneration and Desorption**(0.1 N)	E%
fresh	80.29	Fresh	80.29	Fresh	80.29
water	80.29	water	80.29	water	80.29
Ethanol	75.12	Ethanol	78.57	Ethanol	80.11
H_3PO_4	72.76	H_3PO_4	62.87	H_3PO_4	59.99
HCl	66.87	HCl	53.87	HCl	47.09
H_2SO_4	59.98	H_2SO_4	45.98	H_2SO_4	38.87
HNO_3	50.87	HNO_3	37.87	HNO_3	30.87
Methanol	47.11	Methanol	35.55	Methanol	29.77
NaOH	44.65	NaOH	30.65	NaOH	22.98

The performance and reuse of SA-Bn-TiO_2 NPs by using water in the (CR,AMX,CPH) adsorption process were investigated up to 6 steps under optimal conditions (Figure 3-28 to 3-30). After the 4 cycle of using SA-Bn-TiO_2NPs , the efficiency is still significant (>80%) and this shows SA-Bn-TiO_2 NPs is probable renewable adsorber [120, 121]. By increasing the number of stages of hydrogel adsorber application, the efficiency of the process has slightly decreased, which can be linked to various factors like damage to active sites on the adsorbent saturation of active sites and breakdown of hydrogel polymer network during the continuous adsorption-desorption cycles which destroyed the structure of SA-Bn-TiO_2 NPs particles and reduced the removal efficiency [89, 122].

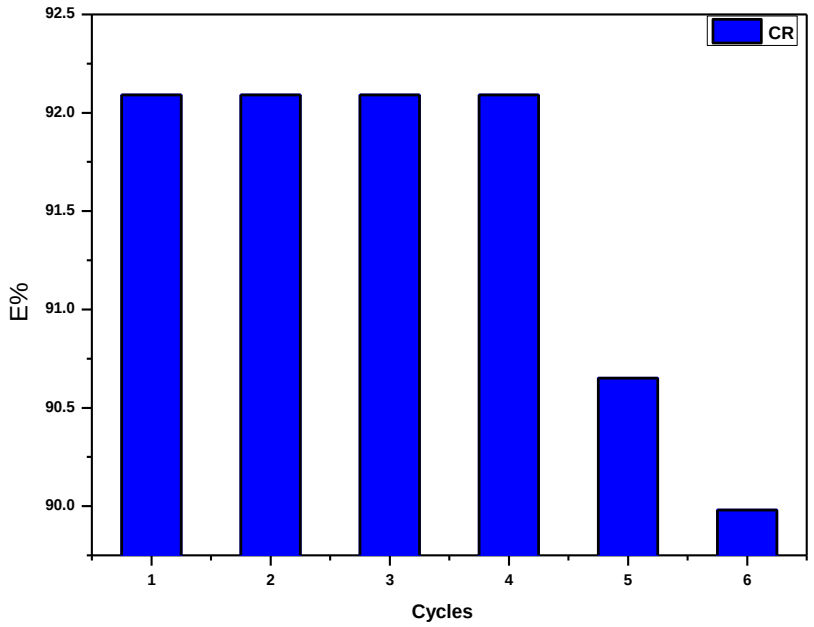

Figure 3-28: multi-cycle use of SA-Bn-TiO_2 NPs for CR dye adsorption using water as desorption medium.

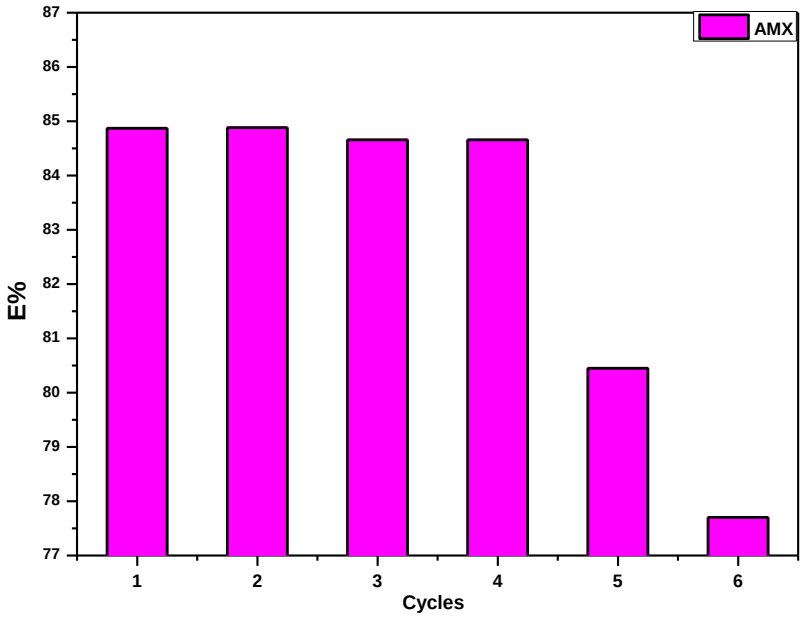

Figure 3-29: multi-cycle use of SA-Bn-TiO_2 NPs for AMX drug adsorption using water as desorption medium.

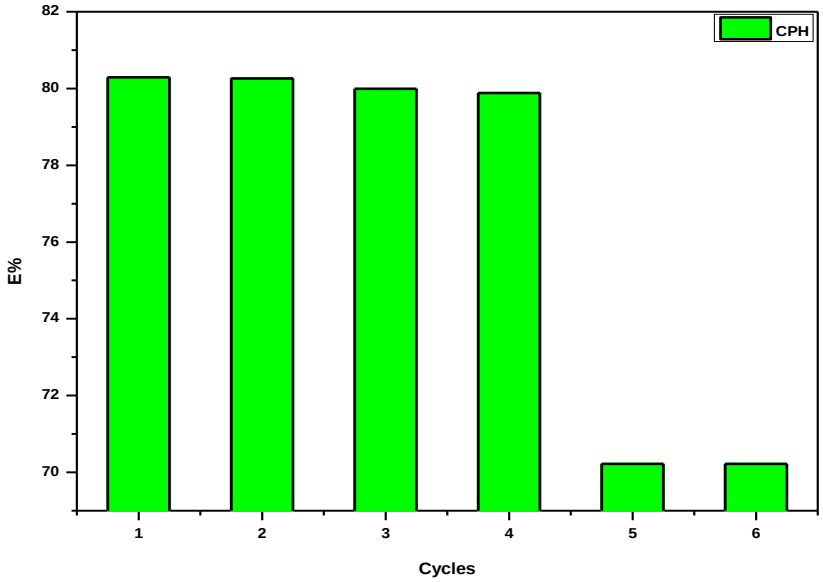

Figure 3-30: multi-cycle use of SA-Bn-TiO_2 NPs for CPH adsorption using water as desorption medium.

3-6 Effect pH on Release Ratio of Amoxillen Drug In Vitro

The release of amoxicillin was studied in conditions similar to the human body in terms of acidity and temperature. It was found that the speed of amoxicillin release was higher when the acidity function (pH=7.5), and this is due to the degree of swelling of the hydrogel and the dissolution of amoxicillin depends on the acidity function. The speed of release of amoxicillin in the alkaline medium as a result of the increase in the rate of swelling more than in the acidic medium [55]. As for the acid function (pH=1.2), the concentration of (H^+) increases, which competes with the unlinked amino group, and thus the percentage of hydrogel swelling decreases, and thus the percentage of drug release decreases. The initial burst release of 42% and 25% , in the first 1 h was observed for AMX. The cumulative release of AMX in 3 h was 68%, 44% from pH=7.5 and pH 1.2 at the same order[55, 123] , as shown in figure 3-31 .

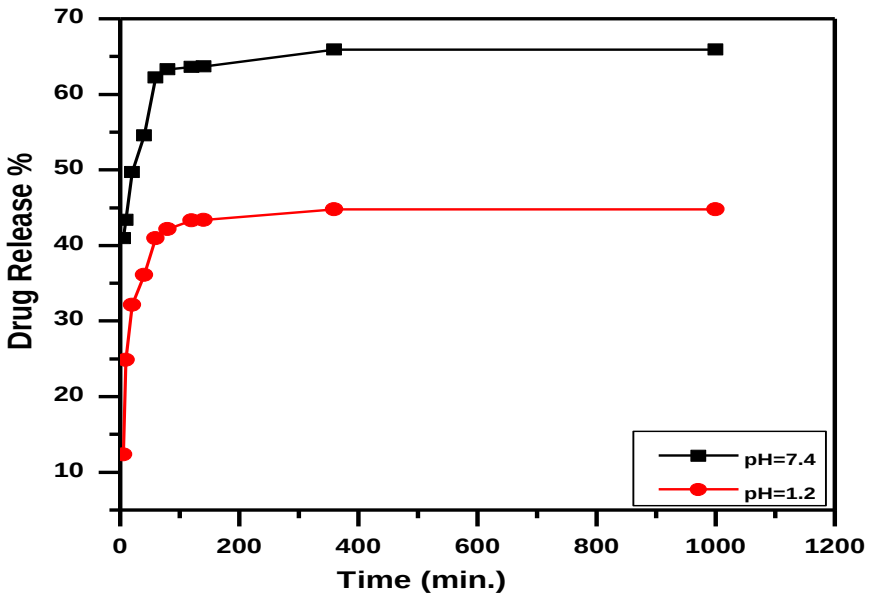

Figure 3-31. Drug Release profiles of AMX from the SA-Bn-TiO2 NPs in(pH 1.2) and (pH 7.4) at 37± 0.5 °C .

3-7 Adsorption Isotherms

3-7-1 Freundlich Isotherm:

The Freundlich isotherm is defined through the following equation 3-4 [124].

$$q_e = K_f C_e^{1/n} \qquad (3-4)$$

qe: Amount adsorbed per unit weight of adsorbent at equilibrium (mg/g), (mol/g), Ce: Equilibrium concentration of adsorbate in solution after adsorption ($mg.L^{-1}$), (mol/L), K_f: Empirical Freundlich constant or capacity factor (L/mg) or the dye quantity adsorbed for unit equilibrium concentration, 1/n: Freundlich exponent, if the value of n is equal to unity, the adsorption is linear; if below to unity, then adsorption process is chemical and if the value is above unity, then adsorption is a physical process [125, 126].

3-7-2 Langmuir Isotherm:

The Langmuir isotherm is mostly used for pollutants adsorption from liquid solutions. The nature of the adsorption process was derived by Langmuir alternative equation 3-5 [51]

$$q_e = \frac{q_m K_L C_e}{1 + K_L C_e} \qquad (3-5)$$

qe: amount adsorbed per unit weight of adsorbent at equilibrium (mg/g), Ce: equilibrium concentration of adsorbent in solution after adsorption ($mg.L^{-1}$), qm: Empirical Langmuir constant which represents maximum adsorption capacity (mg/g) of the total number of surface sites per mass of adsorbent and it may vary among different compounds because of differences in adsorbate sizes, K_L: empirical Langmuir constant (L/mg) or the equilibrium constant of the adsorption reaction [127].

The coefficients of determination (R^2) and isotherm parameters from the nonlinear regressive method were listed in Table (3-14). A comparison of nonlinear fitted curves from experimental data and two different isotherms at 30 ^oC .

A plot of q_e versus C_e Figures (3-32 , 3-33 &3-34) where the values of K_F and 1/n are obtained from the intercept and slope of the linear regressions (Table 3-13 to 3-15).

the correlation coefficient, R^2 values for the Freundlich model at tempracher 30 ^oC are (R^2=0.9998) , (R^2=0.9879) and (R^2=0.9988) of CR, AMX and CPH onto SA-Bn-TiO2 NPs respectively [128, 129].

Table 3-13: different parameters isotherm models for the adsorption study of CR dye on to SA-Bn-TiO2 NPs .

SA-Bn-TiO_2 NPs			
Freundlich	K_f	44.368	±2.241
	1/n	0.683	±0.0292
	R^2	0.9998	
Langmuir	q_m (mg/g)	262.972	±40.432
	K_L (L/mg)	0.1219	±0.0221
	R^2	0.9911	

Table 3-14: different parameters isotherm models for the adsorption study of AMX drug on to SA-Bn-TiO_2 NPs .

SA-Bn-TiO_2 NPs			
Freundlich	K_f	37.826	±3.331
	1/n	0.5377	0.0384±
	R^2	0.9879	
Langmuir	q_m (mg/g)	237.737	±39.977
	K_L (L/mg)	0.1277	±0.0459
	R^2	0.9449	

Table 3-15: different parameters isotherm models for the adsorption study of CPH on to SA-Bn-TiO_2 NPs .

SA-Bn-TiO_2 NPs			
Freundlich	K_f	41.138	2.278
	1/n	0.448	±0.0022
	R^2	0.9988	
Langmuir	q_m (mg/g)	195.570	±21.137
	K_L (L/mg)	0.1629	0.0453±
	R^2	0.9535	

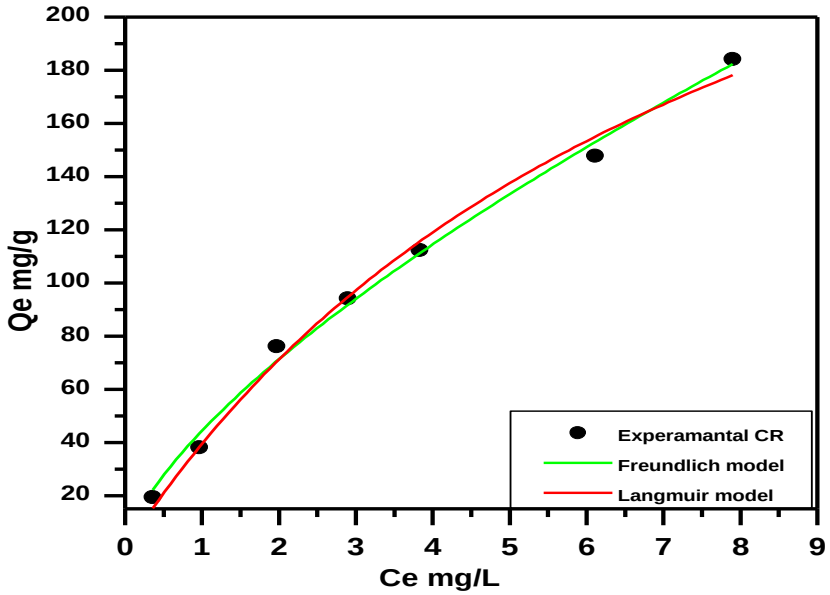

Figure 3-32: Several adsorptions models nonlinear fit of adsorption CR dye onto SA-Bn-TiO_2 at temperatures 30 oC , conc. = 100 mg. L^{-1}, pH of solution 6.6 and weight of surface 0.05 g/100ml).

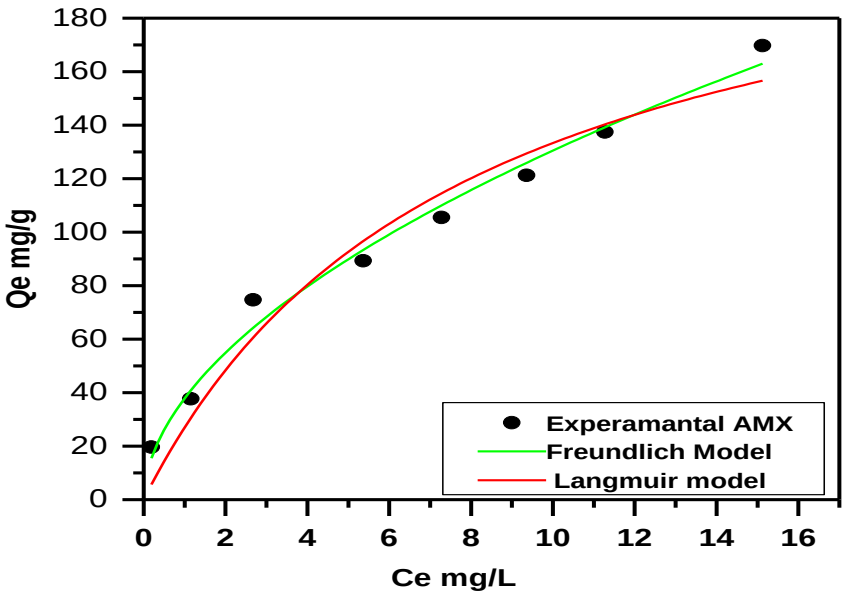

Figure 3-33: Several adsorptions models nonlinear fit of adsorption AMX drug onto SA-Bn-TiO_2 at temperatures 30 oC , conc. = 100 mg. L^{-1}, pH of solution 6.6 and weight of surface 0.05 g/100ml).

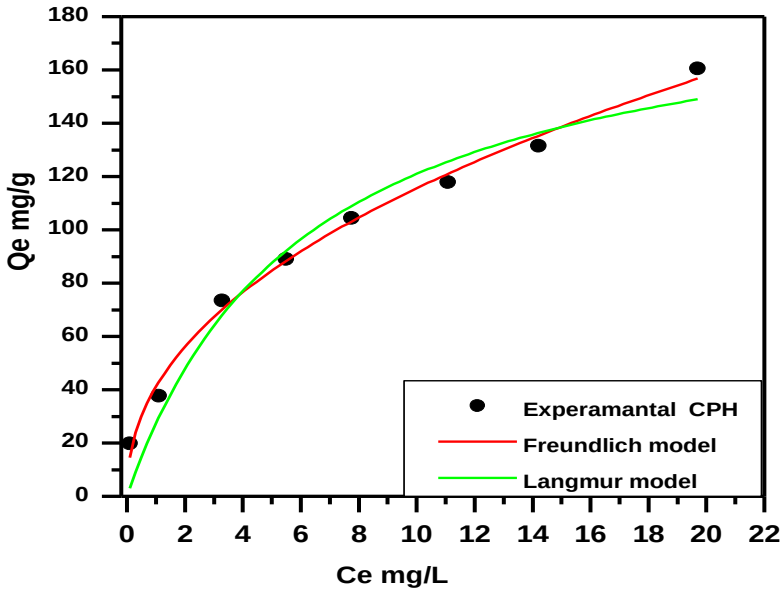

Figure 3-34: Several adsorptions models nonlinear fit of adsorption CPH onto SA-Bn-TiO_2 at temperatures 30 oC , conc. = 100 mg. L^{-1}, pH of solution 6.6 and weight of surface 0.05 g/100ml).

3-8 Kinetic study

The mechanism of adsorbate–adsorbent interaction is best described by studying the rate expression for dye adsorption on SA-Bn-TiO_2 NPs; this can be shown by examining the effect of time on the adsorption process and fitting the experimental findings to different conventional models. The agreed function for model suitability for good prediction of experimental data at different times , which is validated by a low relative error among the orchid and experimental adsorption potential [43]. The rate expression can be calculated by analyzing the adsorption data with three different kinetic models: Lagergren first-order ,pseudo-second-order , and Chemisorption [77] . The fitting results are seen in Figure (3-35 to 3-37) and Table)(3-16 to 3-18). A simple kinetic description of adsorption (pseudo-first-order equation) is as follows :

$q_t=q_e[1-\exp(k_f t)]$ (3-6)

where qt is the total amount of adsorbate adsorbed at time t (mg^{-1}), qe is the equilibrium adsorption potential (mg g^{-1}), kf is the pseudo-first-order rate constant (min^{-1}), and t is the contact time (min).

Lagergren's usability deviates from its linear form, according to the results. This means that the new kinetic model is inadequate for forecasting pseudo-first order sorption kinetics on SA-Bn-TiO_2 NPs. We wanted to apply the experimental data to models because the first-order kinetic model failed to represent the sorption effects [50].

The following is an example of a pseudo-second-order equation based on adsorption equilibrium capacity:

$$qt=\frac{K2qe2t}{1+K2qet} \qquad (3\text{-}7)$$

k_2 and qe were estimated from qt versus t; Figure (3-35 to 3-37) and Table (3-16 to 3-18) shows the pseudo-second-order plot; it can be seen that the sorption data maintains its linear profile over the entire period; however, higher values of correlation coefficients and qe determined using the pseudo-second-order model were more compatible with the experimental data [52, 113].

Both of these findings indicate that the model can be used to describe adsorption data over time. Furthermore, the model supports the theory that the sorption process is caused by chemisorption.

The non-linear structure of the Elovich (Chemisorption kinetic formula) [49] model equation is usually written as:

$$qt=\frac{1}{\beta}1\beta\ln(\alpha\beta)+\frac{1}{\beta}\ln t \qquad (3-8)$$

The kinetic data from the Elovich model .The nonlinear plots of qt versus t for initial concentrations demonstrated good consistency between the experimental and calculated qe values. Furthermore, the pseudo-second-order kinetic model has higher correlation coefficients than the Chemisorption model. As a result, the adsorption is best suited to the pseudo-second-order model than the Chemisorption kinetic model. Adsorption kinetics are associated with the intraparticle diffusion concept.

The gap in dye adsorption on an SA-Bn-TiO_2 NPs with shaking time (0–60 min) and initial concentration 100 mg/L is visualized in Figure 3-35 to 3-37 . Although dye adsorption was initially very high, the rate of adsorption slowed over time and gradually reached a constant value, (equilibrium time). As the dye concentration rose, this process was gradually repeated. The initial faster rate may be due to the adsorbents' exposed surface region being available [15, 110, 126].

Table 3-16 : Pseudo first-order, pseudo-second-order, and Elovich including correlation coefficients for (CR dye) adsorption onto SA-Bn-TiO_2 NPs.

Type	Parameters	**Value**	**Stand. Error**	***R*2**
Pseudo-First-order	q*e* (mg g^{-1})	192.8917	0.9519	0.9975
	k*f* (min^{-1})	0.0844	0.0045	
pseudo-second-order	q*e* (mg g^{-1})	104.335	2.4101	0.9466
	ks (gmg^{-1} min^{-1})	0.1188	0.0148	
Elovich	α (mg g^{-1} min^{-1})	44.011	3.7601	0.8717
	β (g min^{-1})	1.8810	0.3040	

Table 3-17 : Pseudo first-order, pseudo-second-order, and Elovich including correlation coefficients for (AMX drug) adsorption onto SA-Bn-TiO_2 NPs

.

Type	Parameters	**Value**	**Stand. Error**	***R*2**
Pseudo-First-order	q*e* (mg g^{-1})	165.3333	0.7577	0.9998
	k*f* (min^{-1})	0.0937	0.0047	
pseudo-second-order	q*e* (mg g^{-1})	93.8769	1.0135	0.9856
	ks (gmg^{-1} min^{-1})	0.1363	0.0085	
Elovich	α (mg g^{-1} min^{-1})	39.7754	1.9068	0.9558
	β (g min^{-1})	1.9460	0.1797	

Table 3-18 : Pseudo first-order, pseudo-second-order, and Elovich including correlation coefficients for (CPH) adsorption onto SA-Bn-TiO2 NPs.

Type	Parameters	**Value**	**Stand. Error**	***R*2**
Pseudo-First-order	q*e* (mg g^{-1})	160.6858	1.4335	0.9865
	k*f* (min^{-1})	0.05389	0.0037	
pseudo-second-order	q*e* (mg g^{-1})	98.253	3.5667	0.9437
	ks (gmg^{-1} min^{-1})	0.0636	0.0090	
Elovich	α (mg g^{-1} min^{-1})	42.935	4.6214	0.8100
	β (g min^{-1})	1.4146	0.2460	

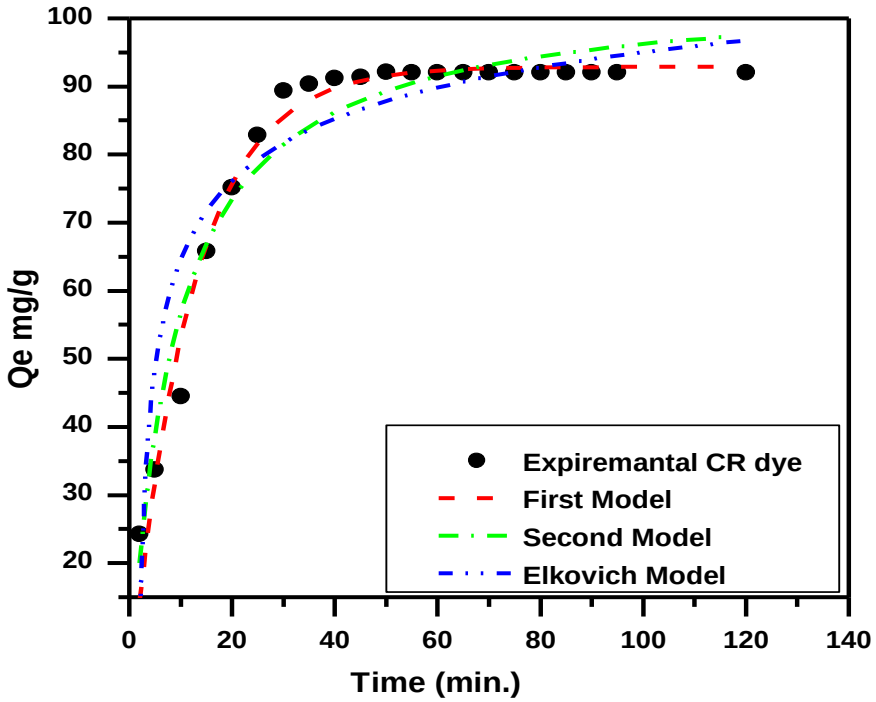

Figure 3-35 . Adsorption rate curve models fitted to experimental CR dye adsorption on the surface of SA-Bn-TiO_2 NPs a) first-order kinetic; b) second-order kinetic; and c) Elkovich kinetic (pH 6.6, Temp. 30 oC , mass dosage 0.05 g).

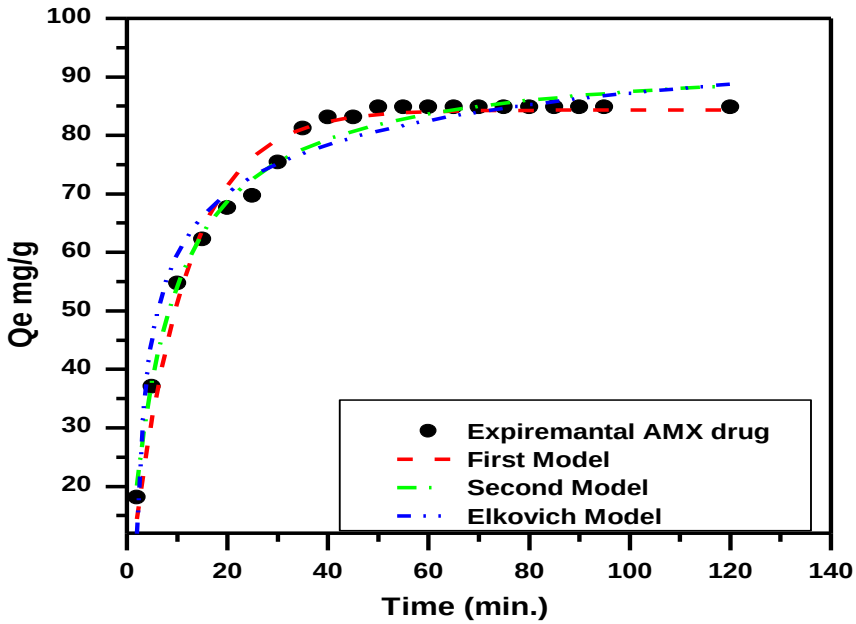

Figure 3-36 . Adsorption rate curve models fitted to experimental AMX drug adsorption on the surface of SA-Bn-TiO_2 NPs a) first-order kinetic; b) second-order kinetic; and c) Elkovich kinetic (pH 6.6, Temp. 30 oC , mass dosage 0.05 g).

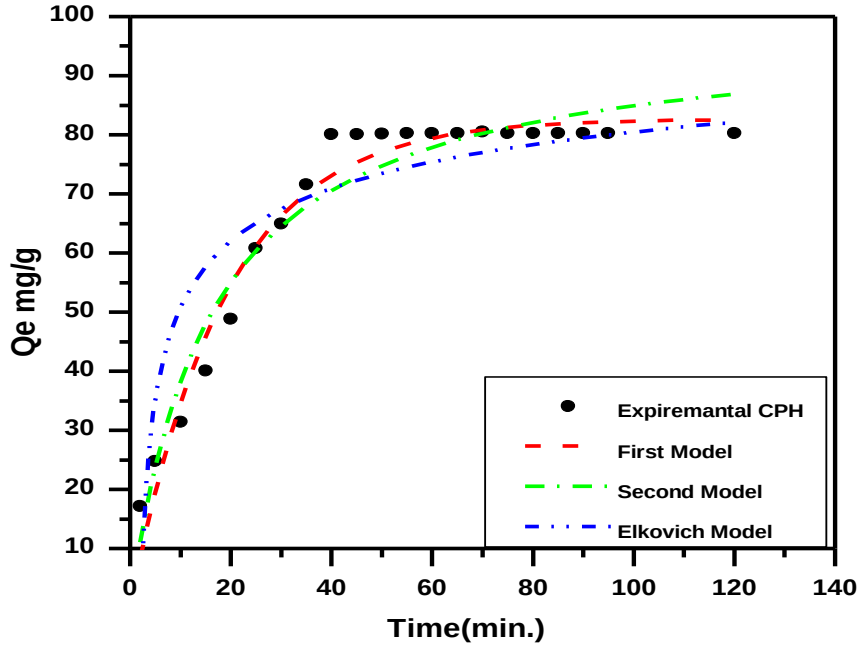

Figure 3-37: Adsorption rate curve models fitted to experimental CPH adsorption on the surface of SA-Bn-TiO_2 NPs a) first-order kinetic; b) second-order kinetic; and c) Elkovich kinetic (pH 6.6, Temp. 30 oC , mass dosage 0.05 g).

3-9 Biological Activity

In this study, the two types of bacteria were Gram-positive bacteria (*staphylococcus aureus and Staphylococcus epidermidi*) and Gram-negative bacteria (*klebsiella spp and E coli*), using four isolates depending on the method of disc diffusion, where two concentrations (0.1gm), (0.2 gm) from the four surfaces (SA-Bn-TiO_2 NPs), (SA-Bn) were used.), (TiO_2 NPs), (clay), the results showed that the surface SA-Bn-TiO2 NPs and SA-Bn- have antibacterial activity against the Gram-negative bacteria compared to the gram-positive bacteria with an inhibition area (20 mm),. More than TiO_2 NPs and clay. where the results showed that it has very little antibacterial activity against two types of bacteria [130] as shown in the Figure 3-38 .

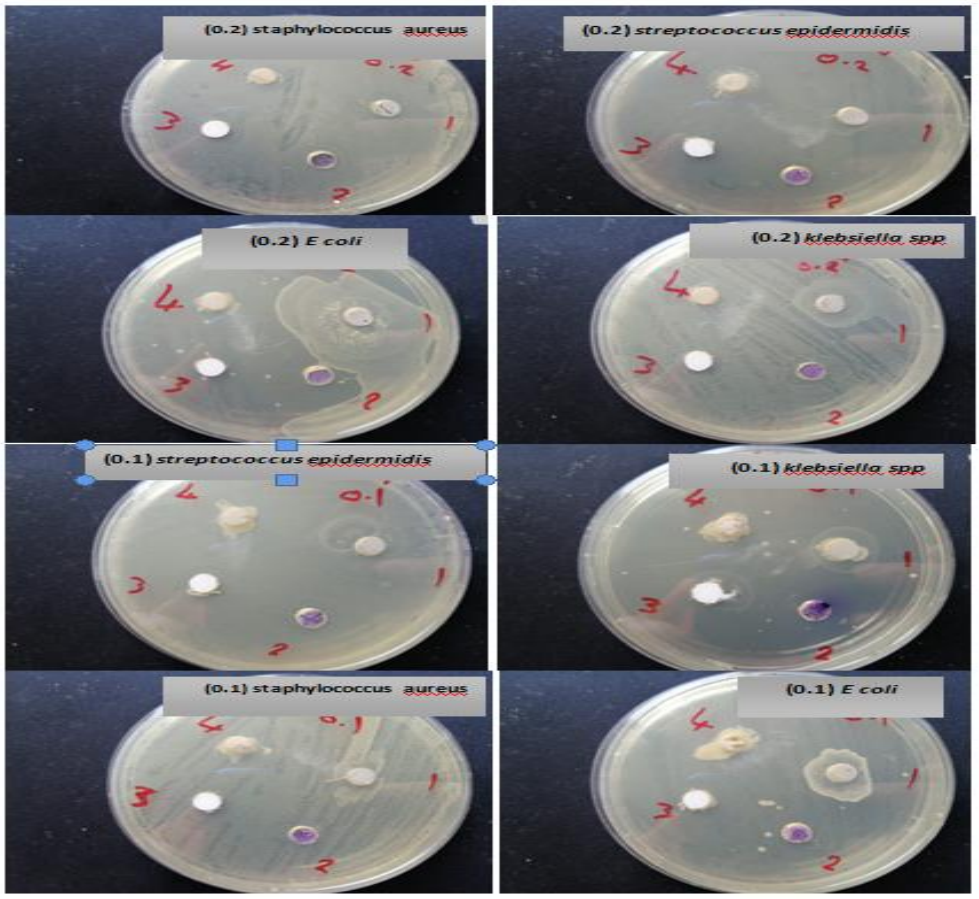

Figure 3-38: Anti-bacterial activities of the (1) SA-Bn-TiO_2 NPs , (2) SA-Bn, (3) TiO_2 NPT , (4) Clay using disc diffusion method.

The results shown in Figure 3-39 and Figure 3-40 are the inhibition regions of the four compounds at weight (0.1g), (0.2g) (SA-Bn-TiO2 NPs , SA-Bn , TiO_2NPs , Clay), which were given that Compound (Ag-Clay /TiO2 NPs) has antibacterial activity, (20 mm) against negative bacteria (*E coli*), (15 mm) against (*klebsiella spp*), (11 mm, 8 mm) against bacteria *E coli , klebsiella spp*), meaning that it had a higher effect on Gram-negative bacteria than on Gram-positive bacteria, respectively[130-132]. .

The compound SA-Bn compound has antibacterial activity against E coli (7 mm), against *klebsiella spp* (6mm), has no activity against (*Staphylococcus aureus*), (*strp. epigene*) . That is, it had an effect on Gram-negative bacteria and had a low effect on Gram-positive bacteria. The compound (TiO_2 NPs) and (clay) have very low antibacterial activity for Gram-negative and Gram-positive bacteria[133] .

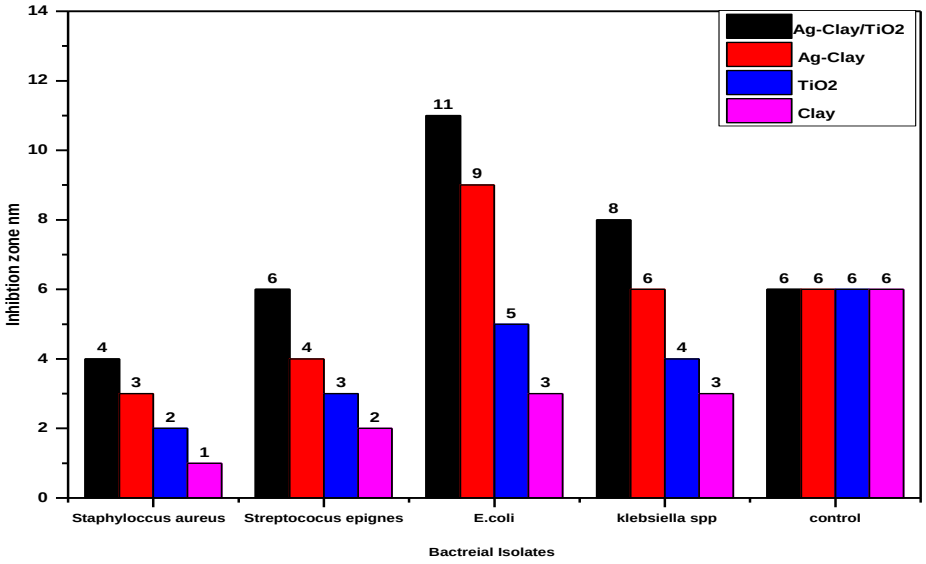

Figure 3-39: Effect of inhibition zones against pathogenic bacteria isolates at 0.1 g .

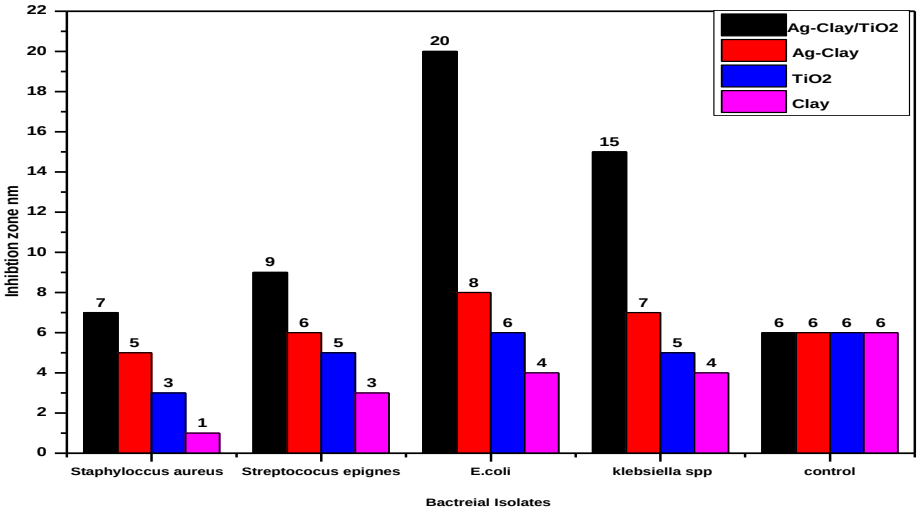

Figure 3-40: Effect of inhibition zones against pathogenic bacteria isolates at 0.2 g .

Surface efficacy in Mice healing

Figure (3-41) shows the stages of recovery of wounded mice, as (0.1 gm)was treated from the surface SA-Bn-TiO_2 NPs, where mice were incised in the animal house at Al-Qadisiyah University, College of Science, and the results were obtained as shown in Figure (3-41)

On the first day, mice were clearly injured on the first day of wounding, and they were treated with about (0.1 gm) from the surface SA-Bn-TiO_2 NPs as shown in image (A)

On the second day, a clear improvement was observed in the treatment of Mice, where the rate of healing and improvement of wounds was at the beginning, as shown in image (B) .

On the third day, an improvement was observed in the mice, where the rate of healing and improvement of mice was very clear, with some redness in the skin surrounding the mice as shown in image (C) .

On the four and five day, the clear results in image showed a clear healing of the mice and the return of the skin to its natural pink color, a clear evidence of the surface's efficiency in mice healing, as shown in image (D, E)

On the seven day, according to the results shown in image (F), there is a complete healing of the mice and the return of the skin to its natural color. This is due to the fact that SA-Bn-TiO2 NPs has a high effective efficiency in treating and healing mice. It is considered environmentally friendly, non-toxic and also considered an anti-inflammatory. In addition, there is a biocompatibility with mammalian cells [134-136].

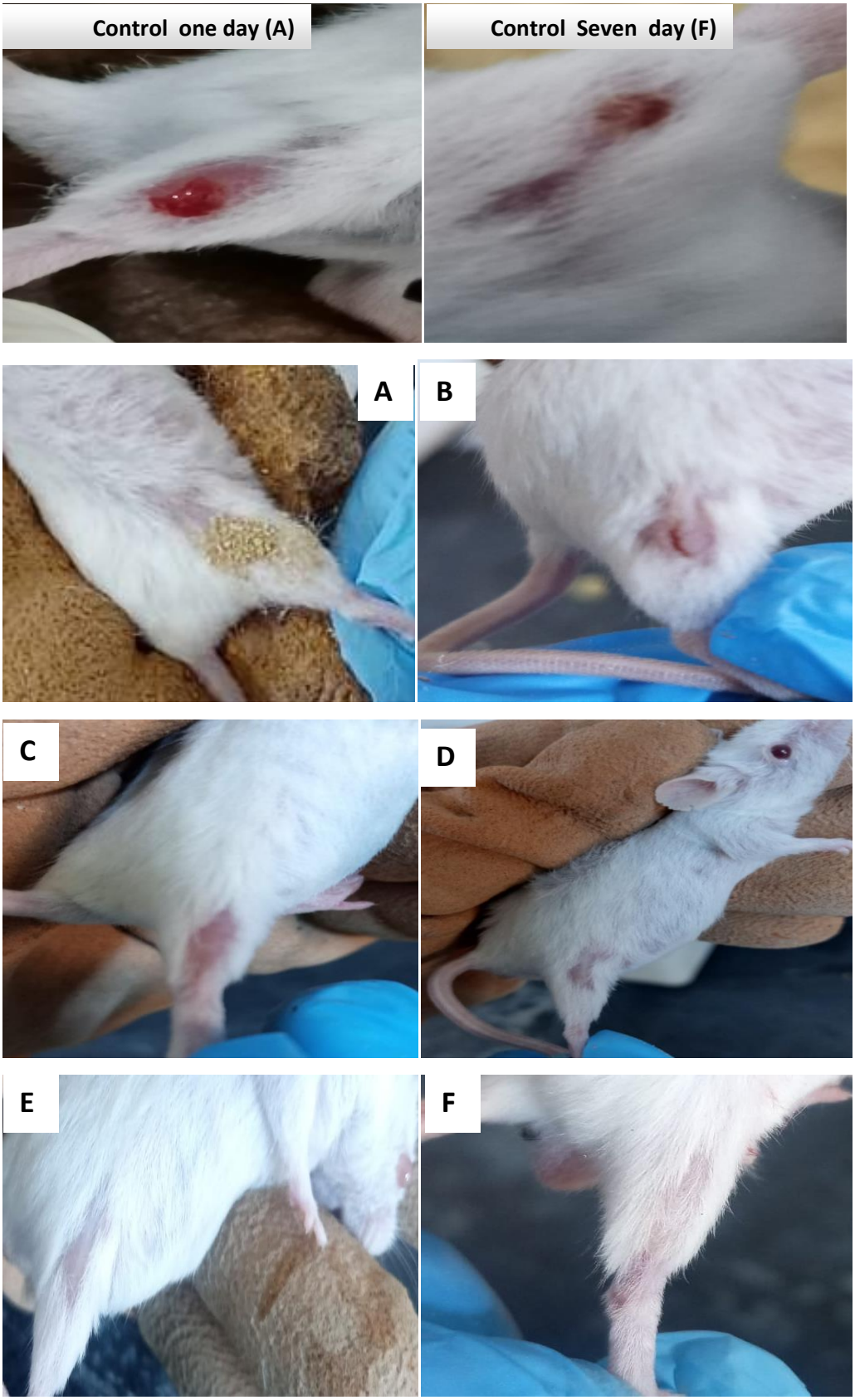

Figure 3-41: Effect of the surface SA-Bn-TiO_2 NPs .on the wound healing of mice during seven days

Conclusions:

Studies have been conducted to gain an understanding and generic knowledge of the equilibrium aspects of adsorption of different adsorbents, SA-Bn-TiO_2 NPs surfaces. Removal of three pollutants Congo red CR dye , Amoxicillin drug AMX , 4-chlorophenol CPH) from aqueous solutions by adsorption with SA-Bn-TiO_2 NPs , SA-Bn and TiO2 NPs surfaces have been experimentally determined. The best results have been found in pH 6.6, temperature 30 oC, and adsorbent dosage 0.05 gm of SA-Bn-TiO_2 NPs for both studying adsorption capacity and removal percentage" and the following observations are made:

1. The adsorption capacity and percentage of three pollutant removal increase with increasing contact time, surface area, and temperature solution. But adsorption capacity has decreased with the increase of adsorbent dosage.
2. The optimum contact time for equilibrium to be achieved is found to be 1 hr. It is basically due to saturation of the active site which does not allow further adsorption to take place.
3. For Three pollutant on adsorbent surfaces, maximum adsorption was found to be at base medium . Adsorption was found to increase with an increase in the pH of the solution.
4. The negative value of ΔG confirms the spontaneous nature adsorption process. The positive value of ΔS showed the increased randomness at the solid-solution interface during adsorption and the positive value of ΔH indicated the adsorption process was endothermic.
5. The interaction between dose and initial concentration showed a significant effect on the adsorption process. Adsorbent showed fits

better to Freundlich isotherm which suggests that adsorption is heterogeneous.

6. The adsorption efficiency for removal of three pollutant (SA-Bn-TiO_2 NPs surface was found better than the SA-Bn and TiO2 NPs.

7. Removal of real aqueous pollutants(dyes , drugs , phenols) by using SA-Bn-TiO2 NPs to give low absorbance (0.0001) by using UV-Visible spectrophotometer for at a chosen wavelength for 60 minutes .
8. The chemisorption, pseudo-first-order, and pseudo-second-order kinetic models were applied to test the experimental data. The pseudo-first-order exhibited the best fit for the kinetic studies.
9. The release values of Amoxilluin drug from the hydrogel are in the hypothetical bowel fluid (pH= 7.5).
10. The SA-Bn-TiO_2 NPs was regeneration with 100% can be desorbed in water in the three pollutant(CR,AMX and CPH) adsorption process was investigated up to 4 steps under optimal conditions .
11. SA-Bn-TiO_2 NPs had high antibacterial activity, That is, it had a higher effect on the Gram- negative bacteria than on the Gram-positive bacteria, respectively .The SA-Bn hydrogel That is, it had an effect on the Gram- negative bacteria and had low effect on the Gram- positive bacteria .The compound (ZnO NPs) had very low antibacterial activity for Gram-negative and Gram-positive bacteria.
12. In two to seven days, according to the results, there is complete healing of the mice and the return of the skin to its natural color.

Future Works:

A study of the adsorption of three pollutants using SA-Bn-TiO_2 NPs work needs to be done to further understand the science behind the adsorption processes.

1-The possibility of using these surfaces SA-Bn-TiO_2 NPs and SA-Bn to remove many contaminants such as heavy elements.

2-Preparing new surfaces that are inexpensive, environmentally friendly, and the possibility of replacing titanium dioxide with Zinc oxide .

3-Synthesizing new polymeric complexes adsorbent on the Activated carbon , CNT and GO surfaces .

4-Studying the possibility of loading the surface with more than one drug so that does not interfere or contradict medically and comparison between the method of loading the drug used in this study and other methods of loading.

5-Completing the study of drug release inside the body of an organism (in vivo) and following up on changes by drawing blood from the body.

6- Study of biological activity on fungi and other types of bacteria .

Reference

Reference

1. Mahdi, A.B., Aljeboree, A.M., Alkaim, A.F., *Adsorption and removal of pollutants (Dyes) from wastewater using different types of low-cost adsorbents: A review.* Journal of Chemical Health Risks, 2021. **11**(2): p. 203-212.
2. Heloise Beatriz Quesada, A.T.A.B., Luís Fernando Cusioli,Daiana Seibert,Charleston de Oliveira Bezerra,Ros^angela Bergamasco,, *Surface water pollution by pharmaceuticals and an alternative of removal by low-cost adsorbents: A review.* Chemosphere 2021. **222**: p. 766e780.
3. Aljeboree, A.M., Alrazzak, N.A., Alqaraguly, M.B., Jasim, L.S., Alkaim, A.F., *Adsorption of pollutants by using low-cost (Environment-Friendly): Equilibrium, kinetics and thermodynamic studies: A review.* Systematic Reviews in Pharmacy, 2021. **11**(12): p. 1988-1997.
4. Martínez-Huitle, C.A., Brillas, E., *Decontamination of wastewaters containing synthetic organic dyes by electrochemical methods: A general review.* . Appl. Catal. B Environ.,, 2019. **87**: p. 105-145.
5. Mohib Ullah, R.N., Muslim Khan,Waliullah Khan,Mohib Shah,Sahib Gul Afridi,Amir Zada1, *The effective removal of heavy metals from water by activated carbon adsorbents of Albizia lebbeck and Melia azedarach seed shells* Soil and Water Research, 2020. **15**(1): p. 30-37.
6. Gamoudi, S. and E. Srasra, *Adsorption of organic dyes by HDPy+-modified clay: effect of molecular structure on the adsorption.* Journal of Molecular Structure, 2019.
7. Arif Chowdhury, S.K., Afaq Ahmad Khan, M. Ravi Chandra, and Sahid Hussain, *Activated carbon loaded with Ni-Co-S nanoparticle*

for SuperiorAdsorption Capacity of Antibiotics and Dye from Wastewater: Kinetics and Isotherms. Journal Pre-proof, 2020. **20**: p. https://doi.org/10.1016/j.colsurfa.2020.125868.

8. Chen J.P., C.M.L., Zhang B., *Effects of competitive ions, humic acid, and pH on removal of ammonium and phosphorous from the synthetic industrial effluent by ion exchange resins.* Waste. Manage., 2012. **22** p. 711-719.
9. Amer M. J. Alshamri, A.M.A., Mohammed B. Alqaragully, Ayad F. Alkaim, *Removal of toxic textile dyes from aqueous solution through adsorption onto coconut husk waste: Thermodynamic and isotherm studie.* Caspian J. Environ. Sci. , 2021.
10. Mohamad A Salleh , D.K.M., Wan A Karim , Azni I Salleh, *Cationic and anionic dye adsorption by agricultural solid wastes:A comprehensive review.* Desalination, 2020. **280**: p. 1-13.
11. Aseel M. Aljeboree, N.A.A., Mohammed B. Alqaraguly,Makarim A. Mahdi, Layth S. Jasim, Ayad F. Alkaim, *Adsorption Of Pollutants By Using Low-Cost (Environment-Friendly): Equilibrium, Kinetics And Thermodynamic Studies: A Review.* Sys Rev Pharm 2020. **11**(12): p. 1988-1997.
12. Leudjo Taka, E.F.-K., K. Pillay, X. Yangkou Mbiand, *Metal nanoparticles decorated phosphorylated carbon nanotube/cyclodextrin nanosponge for trichloroethylene and Congo red dye adsorption from wastewater.* Journal of Environmental Chemical Engineering, 2020. **8**: p. 103602.
13. Anny Leudjo Taka, E.F.-K., Kriveshni Pillay and Xavier Yangkou Mbianda, *Descriptive data on trichloroethylene and Congo red dye adsorption from wastewater using bio nanosponge phosphorylated-carbon nanotube/nanoparticles polyurethane*

composite. Journal of Environmental Chemical Engineering, 2021. **12**(1): p. https://doi.org/10.1016/j.jece.2019.103602.

14. Khawla S Abd-Alrassol, Q.A.Q., Maitham A Ali , Ali K AL-Salman *The development of analytical methods to determine metoclopramide-hydrochloric acid in the standard raw and it compared with pharmaceuticals.* Int. J. Res. Pharm. Sci., 2019. **10**(4): p. 1-14.
15. Arif Chowdhury, S.K., Afaq Ahmad Khan, M. Ravi Chandra, and Sahid Hussain, *Activated carbon loaded with Ni-Co-S nanoparticle for Superior Adsorption Capacity of Antibiotics and Dye from Wastewater: Kinetics and Isotherms.* Journal Pre-proof, 2020. **1**: p. https://doi.org/10.1016/j.colsurfa.2020.125868.
16. Azuma, T., K. Otomo, M. Kunitou, M. Shimizu, K. Hosomaru, S. Mikata, Y. Mino, and T. Hayashi, *Removal of pharmaceuticals in water by introduction of ozonated microbubbles.* . Separation and Purification Technology, , 2019. **212**: p. 483-489.
17. Yazidi A Atrous, M.E.S., Felycia S Lotfi , Smadji E Suryadi , Alessandro B Petriciolet , Luiz D Guilherme , Ben L Abdelmottaleb, *Adsorption of amoxicillin and tetracycline on activated carbon prepared from durian shell in single and binary systems: Experimental study and modeling analysis.* Chemical Engineering Journal, 2020. **379**: p. 122320.
18. Moussavi, G., Alahabadi, Ahamd,Yaghmaeian, Kamyar,Eskandari, Mahboube, *Preparation, characterization and adsorption potential of the NH4Cl-induced activated carbon for the removal of amoxicillin antibiotic from water.* Chemical Engineering Journal, 2020. **217**: p. 119-128.
19. Karimi-Maleh, H., Tahernejad-Javazmi, Fahimeh, Gupta, Vinod Kumar, Ahmar, Hamid, Asadi, Malek Hossein, *A novel biosensor*

for liquid phase determination of glutathione and amoxicillin in biological and pharmaceutical samples using a ZnO/CNTs nanocomposite/catechol derivative modified electrode. Journal of Molecular Liquids, 2020. **196**: p. 258-263.

20. Maximino, M.D.C., Carlos J. L.; Oliveira, Osvaldo N.; Alessio, Priscila, *Synergy in the interaction of amoxicillin and methylene blue with dipalmitoyl phosphatidyl choline (DPPC) monolayers.* Applied Surface Science, 2019. **476**: p. 493-500.
21. Jun, L.Y., Yon, Lau Sie,Mubarak, N. M.,Bing, Chua Han,Pan, Sharadwata,Danquah, Michael K.,Abdullah, E. C.,Khalid, Mohammad, *An overview of immobilized enzyme technologies for dye and phenolic removal from wastewater.* Journal of Environmental Chemical Engineering, 2019. **7**(2): p. 102961.
22. Peixoto M Carla , D.M.A., Maria N Jos , Calhelha C Ricardo ,Barros P Lillian ,Ferreira C Isabel *Grape pomace as a source of phenolic compounds and diverse bioactive properties.* Food Chemistry, 2019. **253**: p. 132-138.
23. Arruda S Henrique , S.E.K., Pereira A Gustavo , Angolini C Fernando ,Eberlin M Meireles, Angela A Pastore, *Effects of high-intensity ultrasound process parameters on the phenolic compounds recovery from araticum peel.* Ultrasonics Sonochemistry, 2019. **50**: p. 82-95.
24. Gulin Selda Pozan, A.K., *Significant enhancement of photo catalytic activity over bifunctional ZnO-TiO2 catalysts for 4-chlorophenol degradation.* Chemosphere, 2014. **105**: p. 152-159.
25. C.V. Lazaratou, D.V.V., D. Papoulis, *The role of clays, clay minerals and clay-based materials for nitrate removal from water systems : a review.* Appl. Clay Sci. Rep., 2020. **185**: p. 105377.

26. GRIM, R.E., J.B. DROSTE, and W.F. BRADLEY, *A mixed-layer clay mineral associated with an evaporite*, in *Clays and Clay Minerals*. 1960. p. 228-236.
27. McGraw-Hill, R.E.G., *Applied Clay Mineralogy.* Science, 1962. **136**(3519): p. 870-871.
28. Bananezhad, B.I., Mohammad Reza;Ghonchepour, Ehsan;Mostafavi, Hamid;Tikdari, Ahmad Momeni;Rafiei, Hamid Reza, *Bentonite clay as an efficient substrate for the synthesis of the super stable and recoverable magnetic nanocomposite of palladium (Fe3O4/Bentonite-Pd).* Polyhedron, 2019. **162**: p. 192-200.
29. Mousa, M.E., Nicholas D.;Oreffo, Richard O. C.;Dawson, Jonathan I., *Clay nanoparticles for regenerative medicine and biomaterial design: A review of clay bioactivity.* Biomaterials, 2020. **159**: p. 204-214.
30. Santos, S.C.R.O., A.F.M.; Boaventura, R.A.R., *Bentonitic clay as adsorbent for the decolourisation of dyehouse effluents.* J. Clean. Prod. , 2019. **126**: p. 667-67.
31. Jaskaran Dhiman , S.O.P., Eman ElSayed, Ramanbhai M. Patel,Christopher Nzediegwu, Ali Mawof, *Heavy metal uptake by wastewater irrigated potato plants grown on contaminated soil treated with hydrogel based amendments.* Environmental Technology & Innovation, 2020. **19**: p. 100952.
32. Nompumelelo Malatji, E.M., Kwena D Modibane, Kabelo E Ramohlola,Thabiso C Maponya,Gobeng R Monama , Mpitloane J Hato, *Removal of methylene blue from wastewater using hydrogel nanocomposites: A review.* Nanomaterials and Technologies for Environmental Applications 2021. **11**: p. 1-27.

33. Makhado E, P.S.R.J.M.a., *synthesis of xanthan gum-cl-poly (acrylic acid) based reduced graphene oxide hydrogel composite for adsorption of methylene blue and methyl violet from aqueous solution.* Int J Biol Macromol 2018. **119**: p. 255-269.
34. Mohammed A. Jawad, A.J.K., Nadher D. Radia, *Role of Sodium Alginate-g-poly (Acrylic acid-fumaric acid) Hydrogel for Removal of Pharmaceutical Paracetamol from Aqueous Solutions by Adsorption* International Journal of Pharmaceutical Quality Assurance, 2021. **12**(3): p. 202-205.
35. Nompumelelo A Malatji, E.B.M., Kwena D Modibane,Kabelo E Ramohlola,Thabiso C Maponya,Gobeng R Monama,Mpitloane J Hato, *Removal of methylene blue from wastewater using hydrogel nanocomposites: A review.* Nanomaterials and Nanotechnology, 2021. **11**: p. 1-27.
36. Ahmed, E.M., *Hydrogel: Preparation, characterization, and applications: A review.* Journal of Advanced Research, 2019. **6**(2): p. 105-121.
37. Anaya-Esparza LM, Villagran-de la Mora Z, and Ruvalcaba-Gómez JM, *Use of Titanium Dioxide (TiO2) Nano particles as reinforcement agent of polysaccharide-based materials.* . Processes 2020. **11**(8): p. 1395.
38. Kangwansupamonkon W, Klaikaew N, and Kiatkamjornwong S, *Green synthesis of titanium dioxide/acrylamide-based hydrogel composite, self degradation and environmental applications.* Eur Polym J, 2019. **107**: p. 118-131.
39. Han S, Wang T, and Li B *Preparation of a hydroxyethyl titanium dioxide-carboxymethyl cellulose hydrogel cage and its effect on the removal of methylene blue.* J Appl Polym Sci, 2018. **134**(23): p. 44925.

40. Mittal H and Ray S, *A study on the adsorption of methylene blue onto gum ghatti/TiO2 nanoparticles-based hydrogel nanocomposite.* Int J Biol Macromol 2019. **88**: p. 66-80.
41. Ba Ryong An, G.-D.L., Dae Hee Son, Seung Ho Lee and Seong Soo Park, *Thermochromic Property of Tungsten Doped VO2 Prepared by Hydrothermal Method.* Journal of the Korean Industrial and Engineering Chemistry, 2019. **24**(6): p. 611-615.
42. Otromke, M.W., Robin J.;Sauer, Jrg, *Hydrothermal base catalyzed depolymerization and conversion of technical lignin : An introductory review.* Carbon Resources Conversion, 2019. **2**(1): p. 59-71.
43. Abdalghaffar M Osman, A.H.H., Tawfik A.Saleh, *Simultaneous adsorption of dye and toxic metal ions using an interfacially polymerized silica/polyamide nanocomposite: Kinetic and thermodynamic studies.* Journal of Molecular Liquids, 2020. **314**(15): p. 113640.
44. Ahmed Medhat , H.H.E.-M., Amr Abdelghany ,Nabil M. Abdel Menem,Patrice Raynau,Yasser M. Moustaf,Mohamed A. Elsayed,Amr A. Nada, *Efficiently activated carbons from corn cob for methylene blue adsorption.* Applied Surface Science Advances, 2021. **2**: p. 100037.
45. Aseel M. Aljeboree, H.Y.A.-G., Ali T. Bader,Ayad F. Alkaim, *ADSORPTION OF TEXTILE DYES IN THE PRESENCE EITHER CLAY OR ACTIVATED CARBON AS A TECHNOLOGICAL MODELS: A REVIEW.* Journal of Critical Reviews, 2020. **7**(5).
46. Tariq J. AlMusawi, N.M., Mahmoud Taghavi, Samaneh Mohebi, Davoud Balarak, *Activated carbon derived from Azolla fliculoides fern: a high adsorption capacity adsorbent for residual ampicillin in pharmaceutical wastewater.* Biomass Conversion and

Biorefnery 2021. **1**: p. https://doi.org/10.1007/s13399-021-01962-4.

47. Aseel M Aljeboree, R.A.M., Makarim A. Mahdi, Layth S. Jasim, Ayad F. Alkaim, *Synthesis, Characterization of P(CH/AA-co-AM) and Adsorptive Removal of Pb (II) ions from Aqueous Solution: Thermodynamic Study.* NeuroQuantology 2021. **19**(7): p. 137-143.
48. Salleh, M., Mahmoud, D.K.,Karim, W.A., Idris, A., *Cationic and anionic dye adsorption by agricultural solid wastes: A comprehensive review.* . Desalination, 2021. **280**(1-3): p. 1-13.
49. Abbas, N.K.L., S. Jasim *Synthesis and Characterization of Poly (CH/AA-co-AM) Composite: Adsorption and Thermodynamic Studies of Benzocaine on from Aqueous Solutions* International Journal of Drug Delivery Technology 2019. **9**(4): p. 558-562.
50. Saeed U J, A.A.K., Saad M, Iftikhar A, Guohua S, Cheng-Meng C, Rashid A, *Removal of azo dye from aqueous solution by a low-cost activated carbon prepared from coal: adsorption kinetics, isotherms study, and DFT simulation.* Environmental Science and Pollution Research, 2020. **1**: p. https://doi.org/10.1007/s11356-020-11344-4.
51. Langmuir, I., *The adsorption of gases on plane surfaces of glass, mica and platinum.* Journal of the American Chemical society, 1918. **40**(9): p. 1361-1403.
52. Del Mar Orta, M., Martn, Julia,Medina-Carrasco, Santiago,Santos, Juan Luis,Aparicio, Irene,Alonso, Esteban, *Adsorption of propranolol onto montmorillonite: Kinetic, isotherm and pH studies.* Applied Clay Science, 2019. **173**: p. 107-114.
53. Freundlich, H., *Over the adsorption in solution.* J. Phys. Chem, 1906. **57**(385471): p. 1100-1107.

54. Singh, A.K., Chandra, Ram, *Pollutants released from the pulp paper industry: Aquatic toxicity and their health hazards.* Aquatic Toxicology, 2019. **211**: p. 202-216.
55. Bhavesh D. Kevadiya, G.V.J., Haresh M. Mody, Hari C. Bajaj *Biopolymer–clay hydrogel composites as drug carrier: Host–guest intercalation and in vitro release study of lidocaine hydrochloride.* Applied Clay Science 2021. **52**: p. 364-367.
56. Jolanta Sarowsk , B.F.K., Agnieszka Jama Kmiecik, Magdalena Frej Madrzak, *Virulence factors, prevalence and potential transmission of extraintestinal pathogenic Escherichia coli isolated from diferent sources: recent reports.* Gut Pathogens, 2019. **10**: p. 1-11.
57. Clement Yaw Efah, T.S., Shaohua Liu ,Yongjun Wu, *Klebsiella pneumoniae: an increasing threat to public health.* Ann Clin Microbiol Antimicrob 2020. **19**: p. 1.
58. V, N., *Streptococcal beta-hemolysins: genetics and role in disease pathogenesis.* Trends Microbiol 2020. **10**: p. 575-580.
59. Katz AR, M.D., *Severe streptococcal infections in historical perspective.* . Clin Infect Dis 2019. **12**: p. 14:298-307.
60. Aziz RK, K.M., *Rise and persistence of global M1T1 clone of Streptococcus pyogenes.* . Emerg Infect Dis, 2018. **14**: p. 1511-1517.
61. Kwinn LA, N.V., *How group A Streptococcus circumvents host phagocyte defenses.* . Future Microbiol 2019. **2**: p. 75-84.
62. Nelly Janira Avire , H.W., Kirstin Ross *A Review of Streptococcus pyogenes: Public Health Risk Factors, Prevention and Control.* pyogenes, 2021. **10**: p. 248.
63. Aljeboree, A.M.R., Nadher D;Jasim, Layth Sameer ;Alwarthan, Abdulrahman A.;Khadhim, Mustafa M.;Washeel Salman, Abbas

;Alkaim, Ayad F., *Synthesis of a new nanocomposite with the core TiO2/hydrogel: Brilliant green dye adsorption, isotherms, kinetics, and DFT studies.* Journal of Industrial and Engineering Chemistry, 2022. **109**: p. 475 - 485.

64. Huda Salim Al-Niaeem , A.A., Whidad Hanoosh, *Preparation of Semi IPNs-Hydrogel Composite for Removing Congo Red and Bismarck Brown Y from Wastewater: Kinetic and Thermodynamic Study.* Egypt. J. Chem., 2022. **56**(1): p. 19 - 34.
65. Ali M. El Shafey, M.K.A.-L., H.M. Abd El-Salam, *The facile synthesis of poly(acrylate/acrylamide) titanium dioxide nanocomposite for groundwater ammonia removal.* Desalination and Water Treatment, 2021. **212** p. 61-70.
66. Mariana Alves Leite Dutra , N.d.N.M., Men de Sá Moreira de Souza Filho ,Rosangela de Carvalho Balaban, *Phenol removal from wastewater using eco-friendly hybrid hydrogels.* Applied polymer 2021. **2**: p. 1-19.
67. Mohammad T. ALSamman, J.S., *Recent advances on biobased hydrogels based on chitosan and alginate for the adsorption of dyes and metal ions from water.* Arabian Journal of Chemistry, 2021. **2**: p. https://doi.org/10.1016/j.arabjc.2021.103455.
68. Gaofeng Pan , K.-I.K., Yutaka Yamad, *Application of hydrogel for the removal of pollutant phenol in water.* Journal of the Chinese Institute of Chemical Engineers 2021. **39** p. 361-366.
69. Mariana Alves Leite Dutra, N.d.N.M., Men de Sá Moreira de Souza Filho, Rosangela de Carvalho Balaban,, *Phenol removal from wastewater using eco-friendly hybrid hydrogels.* Applied polymer 2020. **2**: p. 1-22.
70. Akeem Adeyemi Oladipo, M.G., *Enhanced removal of crystal violet by low cost alginate/acid activated bentonite composite*

beads: Optimization and modelling using non-linear regression technique. journal of Water Process Engineering, 2019. **2**: p. 43-52.

71. Ju-Zhen Yi , L.-M.Z., *Removal of methylene blue dye from aqueous solution by adsorption onto sodium humate/polyacrylamide/clay hybrid hydrogels.* Bioresource Technology 2018. **99**: p. 2182-2186.
72. Thakur, S., *Synthesis, characterization and adsorption studies of an acrylic acid-grafted sodium alginate-based TiO2 hydrogel nanocomposite.* Adsorption Science & Technology, 2017. **0**: p. 1-20.
73. Lamin Sanyang , K.G., Ruziah Zainudin, *SORPTION OF PHENOL FROM WASTEWATER BY HYDROGEL-BIOCHAR COMPOSITE.* International Journal of Engineering and Technology, 2013. **10**(1): p. 38-49.
74. Abdelhahi Ely, M.B., Mohamed Ould Sid'Ahmed Ould Kankou, Jean-Philippe Basly, *Copper and nitrophenol removal by low cost alginate/Mauritanian clay composite beads.* Chemical Engineering Journal, 2011. **178**: p. 168-174.
75. Hany El-Hamshary , S.E.-S., Manal F. Abou Taleb , Nabil A. El-Kelesh *Removal of phenolic compounds using (2-hydroxyethyl methacrylate/acrylamidopyridine) hydrogel prepared by gamma radiation.* Separation and Purification Technology 2007. **57**: p. 329-337.
76. A. H. Al-muhtaseb and T.Magee, *Moisture Sorption Isotherm Characteristics of Food Products: A Review.* Food Bioprod. Process., 2021. **1**: p. 1-22.
77. Aseel M. Aljeboree , A.B.M., *Synthesis highly active surface of ZnO/AC nanocomposite for removal of pollutants from aqueous solutions: thermodynamic and kinetic study.* Applied Nanoscience,

2021: p. https://link.springer.com/article/10.1007%2Fs13204-021-01946-w.

78. Bouhssira N, A.S., Tomasella E, Cellier J, Mosbah A, Aida M S *Influence of annealing temperature on the properties of ZnO thin films deposited by thermal evaporation* Appl. Surf. Sci. , 2020. **252**: p. 55-94.
79. Jenkins, R. and R.L. Snyder, *Introduction to X-ray Powder Diffractometry, Volume 138.* Chemical analysis, a series of monographs on analytical chemistry and its applications, 1996.
80. Aljeboree, A.M., et al., *Photocatalytic of pharmaceutical tetracycline (TCS) by zinc oxide (ZnO).* Journal of Critical Reviews. **7**(7): p. 960-962.
81. Rangaraju , A. and K. Chaitanya, *Spectrophotometric determination of lamotrignine using oxidative coupling reaction in Pharmaceutical dosage forms.* Journal of Innovation in Pharmaceutical Sciences, 2018. **2**(2): p. 49-52.
82. Ashour, S. and R. Bayram, *Selective and validated kinetic spectrophotometric method for the determination of irbesartan in pure and pharmaceutical formulations.* Annales Pharmaceutiques Fran¦§aises, 2019. **77**(2): p. 101-111.
83. Metrani, R., G.K. Jayaprakasha, and B.S. Patil, *Optimized method for the quantification of pyruvic acid in onions by microplate reader and confirmation by high resolution mass spectra.* Food Chemistry, 2018. **242**: p. 451-458.
84. Abdoon, F.M., Yahyaa, S Y., *Validated spectrophotometric approach for determination of salbutamol sulfate in pure and pharmaceutical dosage forms using oxidative coupling reaction.* Journal of King Saud University - Science, 2018. **1**: p. https://doi.org/10.1016/j.jksus.2018.11.002.

85. Peter Cass , W.K., Eliana Pereeia, Natalie P. Holmes, Tim Hughes, *Preparation of hydrogels via ultrasonic polymerization.* Ultrasonics Sonochemistry 2010. **17**: p. 326-332.
86. Hanieh Gharehbakhsh , H.A.P., Mohammad Reza Toosi ,Amir Hessam Hassani , Elham Moniri *Adsorptive removal of toluenediamine from aqueous solution by polysulfone/graphene oxide/TiO2 membrane functionalized by allylamine.* Chemical Data Collections, 2022. **37**: p. 100800.
87. Zhao Ying, C.Y., Zhao Jian, Tong Zongrui, Jin Shaohua, *Preparation of SA-g-(PAA-co-PDMC) polyampholytic superabsorbent polymer and its application to the anionic dye adsorption removal from effluents.Ultrasonics Sonochemistry* 2020. **25**: p. 12-18.
88. Soulaima Chkirid , N.Z., Redouane Achour , Hicham Hassoune , Adil Lacheha, Abou el kacem Qaiss, Rachid Bouhfid, *Highly synergic adsorption/photocatalytic efficiency of Alginate/Bentonite impregnated TiO2 beads for wastewater treatment* Journal of Photochemistry and Photobiology A: Chemistry, 2021. **412**: p. 113215.
89. Hemant Mittal , A.A.A., Pranay P. Morajkar , Saeed M. Alhassan, *Graphene oxide crosslinked hydrogel nanocomposites of xanthan gum for the adsorption of crystal violet dye.* ournal of Molecular Liquids 2021. **323**: p. 115034.
90. Mittal H. , R.S., *A study on the adsorption of methylene blue onto gum ghatti/TiO2 nanoparticles-based hydrogel nanocomposite.* Int J Biol Macromol 2019. **88**: p. 66-80.
91. Y. Guo, H.S.W., C.L. He, L.J. Qiu, X.B. Cao Langmuir, 2009. **25**: p. 4678-4684.

92. H.M. Xiong, Y.X., Q.G. Ren, Y.Y. Xia Journal of the American Chemical Society, 2008. **130**: p. 7522-7523.
93. X. Zhou, Y.Z.L., T. Peng, W. Xie, X.J. Zhao Materials Letters, 2009. **63**: p. 1747-1749.
94. Zhou, M., He, J., *Uniform hamburger-like mesoporous carbon-incorporated ZnO nanoarchitectures: One-pot solvothermal synthesis, high adsorption and visible-light photocatalytic decolorization of dyes.* Applied Catalysis B: Environmental, 2013. **138**: p. 1-8.
95. Hanieh Gharehbakhsh , H.A.P., Mohammad Reza Toosi , Amir Hessam Hassani , Elham Moniri *Adsorptive removal of toluenediamine from aqueous solution by polysulfone/graphene oxide/TiO2 membrane functionalized by allylamine* Chemical Data Collections, 2022. **37**: p. 100800.
96. Inas A. Ahmed , M.K.S., Eder C. Lima , Michael A. Badawi , Zichao S. Liaa , Adrián B. Petriciolet , Ioannis A. Anastopoulos *Outstanding Performance of a New Exfoliated Clay Impregnated with Rutile TiO2 Nanoparticles Composite for Dyes Adsorption: Experimental and Theoretical Studies.* Coatings, 2022. **12**: p. 22.
97. Zheng, M.C., K.; Chen, M.; Zhu, Y.; Zhang, L.; Zheng, B. , *pH-responsive poly(gellan gum-co-acrylamide-co-acrylic acid) hydrogel: Synthesis, and its application for organic dye removal.* Int. J. Biol. Macromol. , 2020. **153**: p. 573-582.
98. Hossein Esmaeili, R.F., Dariush Jafari , Mohammad Aghil Rezaei *Effect of interfering ions on phosphate removal from aqueous media using magnesium oxide@ferric molybdate nanocomposite.* Korean Journal of Chemical Engineering 2021. **37**: p. 804-814.
99. León, G., Saura, F., Hidalgo, A.M.; Miguel, B. , *Activated Olive Stones as a Low-Cost and Environmentally Friendly Adsorbent for*

Removing Cephalosporin C from Aqueous Solutions. Int. J. Environ. Res. Public Health 2021. **18**: p. 4489.

100. Yasin, A.S., Kim D.H, and Lee K., *One-pot synthesis of activated carbon decorated with ZnO nanoparticles for capacitive deionization application.* Journal of Alloys and Compounds, 2021. **870**: p. 159422.
101. Aljeboree, A.M., Al-Baitai, A.Y., Abdalhadi, S.M., Alkaim, A.F., *Investigation study of removing methyl violet dye from aqueous solutions using corn-cob as a source of activated carbon.* Egyptian Journal of Chemistry 2021. **64**(6): p. 2873-2878.
102. Qiuyan Luo, T.R., Zihua Lei , Yifeng Huang , Yong Huang , Dong Xu ,Caichao Wan , Xin Guo , Yiqiang W, *Non-toxic chitosan-based hydrogel with strong adsorption and sensitive detection abilities for tetracycline* Chemical Engineering Journal 2022. **427**: p. 131738.
103. Wenyan Jiang, L.Z., Xiaoming Guo, Mei Yang, Yiwen Lu, Yijun Wang, Yousen Zheng & Guangtao Wei, *Adsorption of cationic dye from water using an iron oxide/activated carbon magnetic composites prepared from sugarcane bagasse by microwave method.* Environmental Technology, 2019. **2**: p. DOI: 10.1080/09593330.
104. Mohammed A. Jawad, Z.I.A.M., Aseel M. Aljeboree, Ayad F. Alkaim, *Removal of Cationic Dyes (Crystal Violet) by Using Low-cost Surface as an Ecofriendly Surface.* International Journal of Pharmaceutical Quality Assurance, 2021. **12**(3): p. 196-201.
105. Makarim A. Mahdi, A.M.A., Layth S. Jasim, Ayad F. Alkaim, *Synthesis, Characterization and Adsorption Studies of a Graphene Oxide/Polyacrylic Acid Nanocomposite Hydrogel.* NeuroQuantology 2021. **19**(9): p. 46-54.

106. Yu, F., Li, Yong,Han, Sheng,Ma, Jie, *Adsorptive removal of antibiotics from aqueous solution using carbon materials.* Chemosphere, 2019. **153**: p. 365-385.
107. Amer M. Alshamri, A.M.A., Mohammed B. Alqaragully, Ayad F. Alkaim, *Removal of toxic textile dyes from aqueous solution through adsorption onto coconut husk waste: Thermodynamic and isotherm studies.* Caspian J. Environ. Sci. , 2021. **19**(3): p. 513~522
108. Yahya A. Faleh , N.D.R., *Removal of Metformin hydrochloride from Aqueous Solutions by using Carboxymethyl cellulose-g-poly(acrylic acid-co-acrylamide) Hydrogel: Adsorption and Thermodynamic Studies.* IOP Conf. Series: Earth and Environmental Science 2021. **790**: p. 012062.
109. A. F. AlKaim, A. N. AlShirifi, and A. H. AlDujaili, *Kinetic study of adsorption of phenol on the novel polymer prepared AUFP from aqueous solution.* National Journal of Chemistry, 2007. **27**: p. 428-455.
110. Nasseh, N., Barikbin, Behnam,Taghavi, Lobat,Nasseri, Mohammad Ali, *Adsorption of metronidazole antibiotic using a new magnetic nanocomposite from simulated wastewater (isotherm, kinetic and thermodynamic studies).* Composites Part B: Engineering, 2019. **159**: p. 146-156.
111. Abdalghaffar M. , O.A.H., Tawfik A.S *Simultaneous adsorption of dye and toxic metal ions using an interfacially polymerized silica/polyamide nanocomposite: Kinetic and thermodynamic studies.* Journal of Molecular Liquids, 2020. **314**(15): p. 113640.
112. Adheem, H.M., Jasim, L.S., *Preparation and Characterization of a three-component hydrogel composite and study of kinetic and thermodynamic applications of adsorption of some positive and*

negative dyes from their aqueous solutions. IOP Conference Series: Materials Science and Engineering, 2020. **928**(5): p. 052027.

113. Shumei Zhao, Y.Z., Xinyi Wan, Shuangjiang He, Xulin Yang, Jiaxin Hu, Guiyuan Zhang, *Selective and efficient adsorption of anionic dyes by core/shell magnetic MWCNTs nano-hybrid constructed through facial polydopamine tailored graft polymerization: Insight of adsorptionmechanism, kinetic, isotherm and thermodynamic study.* Journal of Molecular Liquids 2020. **319**: p. 1-6.
114. Sakin, O.A., H. M. ;Belal , H. M.;Arbi,M, *Adsorption thermodynamics of cationic dyes (methylene blue and crystal violet) to a natural clay mineral from aqueous solution between 293.15 and 323.15 K.* Arabian Journal of Chemistry, 2019. **11**(5): p. 615-623.
115. Aljeboree, A.M., et al., *THE EFFECT OF DIFFERENT PARAMETERS ON THE REMOVAL OF VITAMIN B12 DRUG (AS A MODEL BIOCHEMICAL POLLUTANTS) BY AC/ CLAY.* ***Biochem. Cell. Arch.*** , 2019. **19**(1): p. 755-759.
116. Xiong, J., et al., *Hexagonal boron nitride adsorbent: Synthesis, performance tailoring and applications.* Journal of Energy Chemistry, 2020. **40**: p. 99-111.
117. Shoaib Nawa , M.S., Romana Khan, Nadia Riaz, Ummara Waheed ,Irum Shahzadi , Asmat Ali, *Ultrasound-Assisted Hydrogen Peroxide and Iron Sulfate Mediated Fenton Process as an Efficient Advanced Oxidation Process for the Removal of Congo Red Dye.* Pol. J. Environ. Stud, 2022. **31**(3): p. 1-13.
118. Zhang, G., Feizbakhshan, Mohammad,Zheng, Shuilin,Hashisho, Zaher,Sun, Zhiming,Liu, Yangyu, *Effects of properties of minerals*

adsorbents for the adsorption and desorption of volatile organic compounds (VOC). Applied Clay Science, 2019. **173**: p. 88-96.

119. Hoppen, M.I., Carvalho, K. Q.,Ferreira, R. C.,Passig, F. H.,Pereira, I. C., Rizzo-Domingues, R. C. P.,Lenzi, M. K.,Bottini, R. C. R., *Adsorption and desorption of acetylsalicylic acid onto activated carbon of babassu coconut mesocarp.* Journal of Environmental Chemical Engineering, 2019. **7**(1): p. 102862.
120. Al-Bayati, R.A., *Adsorption-desorption isotherm of one of antidibetic drug from aqueous solutions on some pharmaceutical adsorbents.* Eur. J. Sci. Res., 2020. **40**: p. 580-588.
121. Sevda Pashaei-Fakhri , S.J.P., Rauf Foroutan ,Nasser Arsalani , Bahman Ramavandi, *Crystal violet dye sorption over acrylamide/graphene oxide bonded sodium alginate nanocomposite hydrogel, 2021*. Chemosphere **270**: p. 129419.
122. Sukul, P., Lamsh, Marc,Zhlke, Sebastian,Spiteller, Michael, *Sorption and desorption of sulfadiazine in soil and soil-manure systems.* Chemosphere, 2019. **73**(8): p. 1344-1350.
123. Aguzzi, C., Capra, P.,Bonferoni, C.,Cerezo, P.,Salcedo, I.,Snchez, R.,Caramella, C.,Viseras, C., *Chitosanâ silicate biocomposites to be used in modified drug release of 5-aminosalicylic acid (5-ASA).* Applied Clay Science, 2020. **50**(1): p. 106-111.
124. Freundlich H, W., *The Adsorption of cis- and trans-Azobenzene* J Am Chem Soc, 1939. **61**: p. 2228-2230.
125. Yongde Liu, Y.C., Yahui Shi, Dongjin Wan, Jing Chen, Shuhu Xiao, *Adsorption of toxic dye Eosin Y from aqueous solution by clay/carbon composite derived from spent bleaching earth. Journal of Hazardous Materials,*, 2019. **1**: p. 4656-5544.

126. Kim, Y.-S., Kim, Jin-Hyun, *Isotherm, kinetic and thermodynamic studies on the adsorption of paclitaxel onto Sylopute.* The Journal of Chemical Thermodynamics, 2019. **130**: p. 104-113.
127. Zaheer, Z., Al-Asfar, Aisha,Aazam, Elham Shafik, *Adsorption of methyl red on biogenic Ag@Fe nanocomposite adsorbent: Isotherms, kinetics and mechanisms.* Journal of Molecular Liquids, 2019. **283**: p. 287-298.
128. Nadavala Siva Kumar , M.A., Anesh Manjaly Poulose , Madala Suguna and Mansour I. Al-Hazza, *Equilibrium and Kinetic Studies of Biosorptive Removal of 2,4,6-Trichlorophenol from Aqueous Solutions Using Untreated Agro-Waste Pine Cone Biomass.* processes, 2019. **1**: p. 22-33.
129. E. Alipanahpour Dil , M.G., A.M. Ghaedi , A. Asfaram, A. Goudarzi , S. Hajati , M. Soylak, Shilpi Agarwal, Vinod Kumar Gupt *Modeling of quaternary dyes adsorption onto ZnO-NR-AC artificial 3 neural network: Analysis by derivative spectrophotometry* Journal of Industrial and Engineering Chemistry 2015. **1**: p. 22.
130. Asmaa H. Hammadi, S.A.H., Lena Fadhil Al-Jibouri, Falah H. Hussien, *Synthesis, Characterization and Biological Activity of Zinc Oxide Nanoparticles (ZnO NPs).* Sys Rev Pharm 2020. **11**(5): p. 431 439.
131. Adam, A.M.A., *Structural, thermal, morphological and biological studies of proton-transfer complexes formed from 4-aminoantipyrine with quinol and picric acid.* Spectrochimica Acta Part A: Molecular and Biomolecular Spectroscopy, 2010. **104**: p. 1-13.

132. R.V. Mundra, X.W., J. Sauer, J.S. Dordick, R.S. Kane, *Nanotubes in biological applications.* Curr. Opin. Biotechnol.,, 2014. **28**: p. 25-32.
133. Mukha IP, E.A., Smirnova NP, Mikhienkova AI, Korchak GI, Gorchev VF, *Antimicrobial activity of stable silver nanoparticles of a certain size.* Appl Biochem Microbio, 2019. **49** p. 199-206.
134. Dehui Xu, S.W., Bing Li, Miao Qi, Rui Feng, Qiaosong Li, Hao Zhang, Hailan Chen, and Michael G Kong, *Effects of Plasma-Activated Water on Skin Wound Healing in Mice.* Microorganisms, 2020. **7**(8): p. 1091.
135. Evelina Vågesjö, E.Ö., Anneleen Mortier, Hava Lofton, Fredrik Huss, Paul Proost, Stefan Roos, Mia Phillipsona,, *Accelerated wound healing in mice by on-site production and delivery of CXCL12 by transformed lactic acid bacteria.* National Center for Biotechnology Information, 2018. **7**(8): p. 1-9.
136. Samia Afrin , M.S., Papia Haque , Md. Sazedul Islam , Shafiul Hossain ,Taslim Ur Rashid , Tanvir Ahmed , Makoto Takafuji , Mohammed Mizanur Rahman *Advanced CNC/PEG/PDMAA Semi-IPN Hydrogel for Drug Delivery Management in Wound Healing.* Gels, 2022. **8**: p. 340.

الخلاصة

في هذا العمل ، تم تصميم طريقه بسيطة ومستقره و صديقه للبيئة ، من خلال تحضير سطح ماز بمواصفات جديدة مكون من حبيبات مصنوعة من الطين والبولمر الحيوي من خلال تفاعل الربط المتبادل . تم تصنيعها من خلال دمج الطين في ألجينات الصوديوم (طين البنتونيت / خرز الجينات) متبوعًا بالتشريب TiO_2NPs و ($CaCl_2$.6H2O) لامتزاز ثلاثة ملوثات (صبغة الكونغو الحمراء CR ، دواء الاموكسلين AMX ، و ٤- كلورو فينول CPH). تم تحضير جزيئات TiO2 النانوية بالتحلل المائي الحراري (الطريقة الحرارية المائية) باستخدام ثنائي هيدروكسيد التيتانيوم (IV) مكرر (أمونيوم لاكتات) (TALH) وهيدروكسيد الأمونيوم (NH4OH).

تم فحص شكل وبنية حبات هيدروجيل SA-Bn-TiO_2 NPs باستخدام التحليل الطيفي للأشعة فوق البنفسجية المرئية (UV-Vis) ، مطيافية الاشعه تحت الحمراء (FT-IR) ، التحليل الحراري الوزني (TGA) ، المجهر الكتروني الماسح ذو المجال المنبعث (FESEM) ، المجهر الإلكتروني النافذ (TEM) ، الأشعة السينية المشتتة للطاقة (EDX) حيود الاشعه السينيه (XRD).

تضمنت التجارب العملية حساب الطول الموجي الأعظم ودراسة الظروف المثلى لتأثير معاملات الامتزاز وتشمل : تأثير زمن التلامس ، تأثير جرعة الممتزات ، تأثير محلول الأس الهيدروجيني ، تأثير محلول درجة الحرارة ، تجارب تجديد الممتزات (الامتصاص) ، مقارنة بين الأسطح المختلفة لإزالة ثلاثة ملوثات ، وإزالة الملوثات المائية الحقيقية ، وتحميل دواء الاموكسيلوين (AMX) ، وإطلاق الدواء في المختبر ، والاختبار البكتيري للنشاط البيولوجي ، وعلاج جروح الفئران باستخدام سطح محضر من SA-Bn-TiO2 NPs.

تظهر نتائج دراسة الامتزاز أن نسبة الإزالة تزداد مع زيادة وزن السطح. وزمن الاتزان. القيمة المثلى لزمن الاتزان هي ساعة واحدة. وبعد ذلك يصبح الامتزاز ثابتا. تم تحقيق أفضل النتائج لنسبة الإزالة في الرقم الهيدروجيني (pH=6.6) ، ولكن في الرقم الهيدروجيني pH=4 هناك كمية صغيرة جدًا من الإزالة ؛ كما تم تقديم نماذج ايزوثيرم Freundlich و Langmuir. لقد وجد أن جميع النتائج تتبع نموذج موديل Freundlich في وجود ثلاثة ملوثات .

مقارنة بين أسطح ($SA-Bn-TiO_2$ NPs و SA-Bn و TiO_2 NPs) كمواد مازه. أفضل نتائج لنسبة الازاله (E٪) لثلاثة ملوثات (صبغة كونغو الحمراء CR ، دواء الاموكسلين AMX و ٤ كلوروفينول CPH) مرتبة بالترتيب (SA-Bn-TiO2 NPs> SA-Bn> TiO2 NPs) ، حيت كانت نتائج النسبة المئوية للإزالة (E٪) لـ $SA-Bn-TiO_2$ NPs، 92.45 ٪ ، و 87.58٪ و 82.56% لـ CR و AMX و CPH بنفس الترتيب.

تمت دراسة حركيات الامتزاز لثلاثة ملوثات بتراكيز مختلفه على SA-Bn-TiO2 NPs باستخدام ثلاثة نماذج حركية. تصنيف النماذج الحركية وفقًا لمحاكاة دراسة الامتزاز هو تصنيف Psuedo-second order> Chemisorption> Psuedo-First order. وتشير العوامل الديناميكية الحرارية المحسوبة إلى أنها عملية ماصة للحرارة وتلقائية.

تم دراسة إعادة التدوير وتنشيط السطح المحضر للحصول على أداء افضل لإعادة التدوير للمركب المحضر. بناءً على النتائج ، يمكن أن يكون $SA-Bn-TiO_2$NPs كماده فعاله وصديقة للبيئة من حيث التكلفة وفعالة لإزالة الملوثات. تم إجراء الدراسات باستخدام العديد من عوامل بتركيزات مختلفة (0.1 N , 0.01, 0.01).) مثل H_2SO_4 و NaOH و H_3PO_4 و HCl و HNO_3 والإيثانول والأسيتون والماء. تم تجديد $SA-Bn-TiO_2$NPs بنسبة ١٠٠٪ باستخدام الماء.

تمت دراسة تحرر دواء الأموكسيسيلين في ظروف مشابهة لجسم الإنسان من حيث الحامضيه ودرجة الحرارة. تم ملاحظة إطلاق دواء بنسبة (62٪ , 42٪) في أول ساعة بالنسبة لـ AMX. كان االتحرر التراكمي لـ AMX في ٣ ساعات (68٪ , 44٪) من pH = 7.5 و pH 1.2 بنفس الترتيب.

أظهرت النتائج أن السطح $SA-Bn-TiO_2$ NPs و SA-Bn لهما نشاط مضاد للجراثيم ضد البكتيريا سالبة الكرام مقارنة بالبكتيريا موجبة الكرام مع منطقة تثبيط (٢٠ مم). أكثر من TiO2 NPs والطين حيث أظهرت النتائج أن له نشاطًا مضادًا للبكتيريا قليلًا جدًا ضد نوعين من البكتيريا.

تم دراسة علاج جروح الفئران باستخدام سطح محضر من SA-Bn-TiO2 NPs. حيث لوحظ في غضون يومين إلى سبعة أيام ، وفقًا للنتائج ، هناك شفاء كامل للفئران وعودة الجلد إلى لونه الطبيعي. هذا يرجع إلى حقيقة أن $SA-Bn-TiO_2$ NPs لها كفاءة عالية في علاج

الفئران وشفاءها. يعتبر صديقًا للبيئة وغير سام ومضاد للالتهابات. بالإضافة إلى ذلك ، هناك توافق حيوي مع خلايا الثدييات.

بسم الله الرحمن الرحيم

اقرأ باسم ربك الذي خلق (١) خلق الإنسان من علق (٢) اقرأ وربك الأكرم (٣) الذي علم بالقلم (٤) علم الإنسان ما لم يعلم (٥)

صدق الله العظيم

سورة العلق

الآيات ١ ـ ٥

جمهورية العراق
وزارة التعليم العالي والبحث العلمي
جامعة بابل/ كلية العلوم للبنات
قسم الكيمياء

دور تخليق حبيبات الالجينات /البنتونايت المشبعه ب TiO_2 النانوي كسطح ماز قابل لإعادة التدوير لإزالة الملوثات والنشاط البيولوجي

رسالة مقدمة

الى مجلس كلية العلوم للبنات-جامعه بابل

جزء من متطلبات نيل شهادة الماجستير في الكيمياء / الكيمياء التحليلية

من قبل
زينب طلال محمد سعيد الحطاب
بكالوريوس علوم كيمياء – جامعة بابل
١٩٩٩-٢٠٠٠

بإشراف

أ.م .د. اسيل مشتاق كاظم الجبوري

1444هـ

2022 م